All-aqueous compartmentalized structures by microfluidics

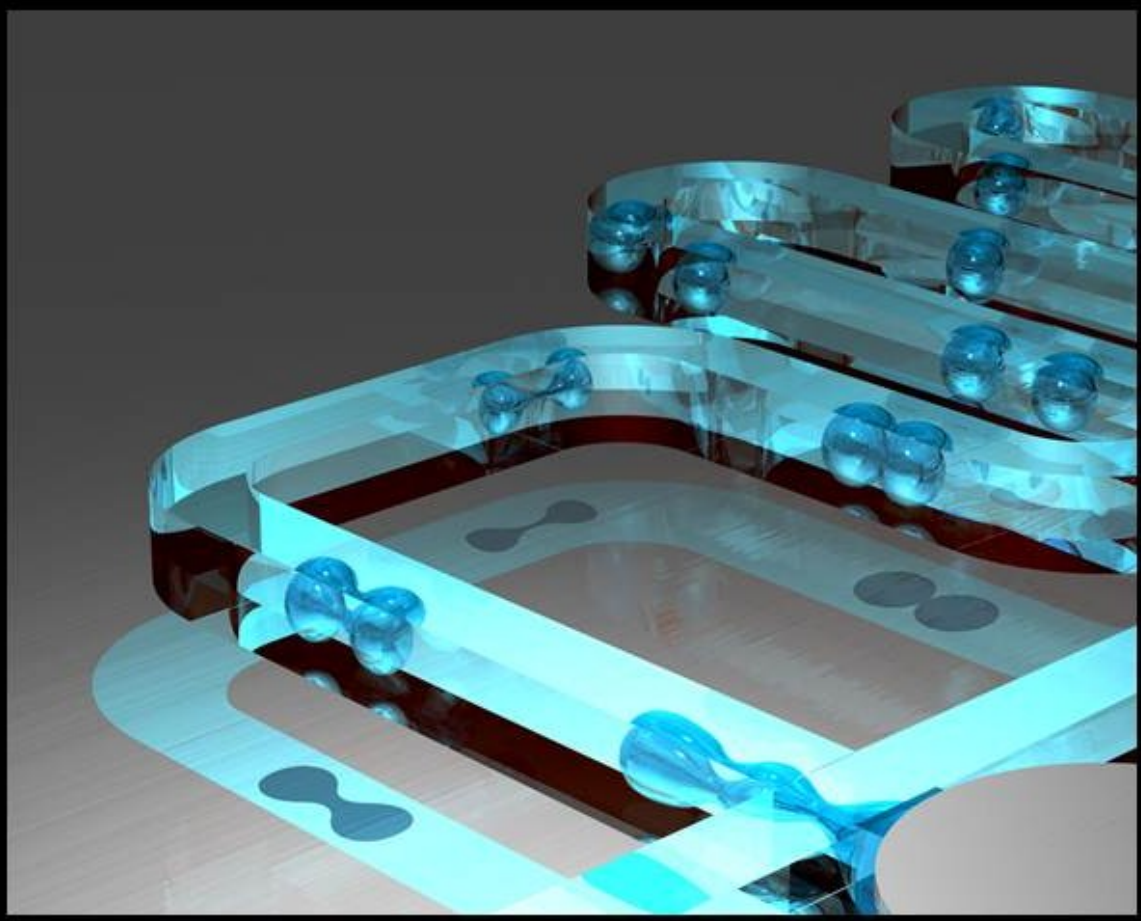

Iwona Ziemecka

All-Aqueous Compartmentalized Structures by Microfluidics

Proefschrift

ter verkrijging van de graad van doctor

aan de Technische Universiteit Delft,

op gezag van de Rector Magnificus prof. ir. K.C.A.M. Luyben,

voorzitter van het College voor Promoties,

in het openbaar te verdedigen

op dinsdag 5 februari 2013 om 12:30 uur

door

Iwona ZIEMECKA

Master of Science in Chemistry
Uniwersytet Łódzki

geboren te Łódź (Poland)

Dit proefschrift is goedgekeurd door de promotoren:
Prof. dr. J. H. van Esch
Prof. dr. ir. M. T. Kreutzer
Copromotor: dr. ir. V. van Steijn

Samenstelling promotiecommissie:

Rector Magnificus,	voorzitter
Prof. dr. J. H. van Esch	Technische Universiteit Delft, promotor
Prof. dr. M. T. Kreutzer	Technische Universiteit Delft, promotor
Dr. ir. V. van Steijn	Technische Universiteit Delft, copromotor
Prof. dr. R. P. Sijbesma	Technische Universiteit Eindhoven
Prof. dr. ir. C. R. Kleijn	Technische Universiteit Delft
Prof. dr. U. Hanefeld	Technische Universiteit Delft
Dr. S. A. Khan	National University of Singapore

The research described in this thesis was supported by NWO-VICI grant.

ISBN: 978-94-6191-593-1

Cover image reproduced by permission of Volkert van Steijn.
Back cover image reproduced by permission of Volkert van Steijn and The Royal Society of Chemistry from *Lab Chip*, 2011, **11**, 620-624, **DOI:**10.1039/C0LC00375A.

Printed in the Netherlands

Moim Rodzicom

CONTENTS

Introduction 1

1.1 Compartmentalization

Compartmentalization is omnipresent and vitally important. Its role is best illustrated by an everyday example, our house, where we use each room for a different purpose. Compartmentalization is an essential strategy to build advanced and highly organized structures. The most important example of compartmentalized organization is a natural cell. Its organization allows cells to concurrently run incompatible metabolic processes. Cells comprise many different types of compartments, starting from the outer membrane that separates their interior from the environment in which they live. This membrane is build up from phospholipids that are organized in the form of a bilayer. Lipids also form the main building block of many smaller compartments inside the cell, including the mitochondria in which cells produce ATP and the endosomes in which material is protected during intracellular trafficking. Lipid bilayers thus effectively protect the inside of the compartment from their environment and only allow specific components to enter or leave. Besides, cells also have compartments that are not enveloped by a lipid bilayer. Take for example the cytosol in which DNA, proteins, and other polymers crowed together rather than spreading uniformly. Crowding is caused by the associative interactions between the polymers, which leads to phase separation. In contrast to compartments enclosed by lipids, those compartments do not have a selective physical border and form an important and interesting class of micro structured environments. This motivates the development of methods to create such environments with a great level of precision. How to form all-aqueous compartmentalized microstructures from phase separating polymers is the topic of this thesis.

1.2 Artificial compartmentalized microstructures

Traditionally, work on biomimetic cells has focused on the use of lipids to make micron-sized compartments with and without internal structure. The most simple structure build up from phospholipids is a unilamellar vesicle, where lipids organize in a bilayer that encloses its aqueous core. The bilayer consists of two monolayers put together such that the hydrophobic tails form the inside of the bilayer and the hydrophilic heads point towards the interior and exterior. Vesicles made artificially are called liposomes. They can be unilamellar (with one bilayer) or multilamellar[1] (with multiple bilayer). Giant unilamellar vesicles (GUV) are commonly used as the membrane model system.[2-4] Besides lipids, other amphiphilic molecules also form vesicles. For example, co-block polymers form vesicles known as polymersomes. Another class of amphiphilic molecules that can be used to make compartmentalized structures is surfactants. In contrast to vesicles, liposomes, and polymersomes, they form compartments that are enclosed by a monolayer. As a consequence, they are much smaller and have different encapsulation and release properties. What all these structures unite is that they form spontaneously through self-assembly such that their size is typically sub-micron.

A wide variety of non-thermodynamically driven methods have been developed for the preparation of nano- and micro-sized compartmentalized particles. Advantages of this engineering approach over self-assembly is that they allow the formation of i) non-spherical particles, ii) particles with hybrid composition and, iii) particles with anisotropic functions. Among these techniques, lithographic and template-based methods are used most frequently.[5] Different strategies have been developed to fabricate truly 3D small size

structures.[6] Since traditional top-down approach is limited with regards to high-throughput fabrication of 3D-patterned, submillimeter length scales structures, the bottom-up strategy has been utilized as challenging alternative. Small structures are produced by self-assembly,[7] 3D lithographic patterning, self-folding (a more deterministic form of self-assembly) methods: pneumatic, external magnet, permanent magnet, electroactive swelling, thermal bimorph actuation, polyimide shrinkage, shape memory actuation, ultrasonic pulse impact, muscular actuation, thin-film stress, surface forces.[6] Photolithography-based microfluidic techniques are efficient in production of functional microparticles with complex nanostructured compartments.[8-10] Self-folding is practicable method for fabricating 3D structures and can leverage the strengths of lithography and self-assembly.

Droplets are another frequently used template for the synthesis of micro and nanoparticles. They restrict shape of the particles to sphere or shapes that result from the simple geometrical deformation of spheres. Spherical shapes are sufficient and desirable for many application and droplets can be very efficiently generated by microfluidics. Compared to bulk methods, microfluidics offers an unsurpassed control over the size, shape, and composition of droplets. Droplet microfluidics offers the precision needed for the synthesis of compartmentalized particles and is the method of choice for the work described in this thesis.

1.3 Droplet microfluidics

Droplet-based microfluidics opens the door to the continuous production of monodisperse particles. Using this method, different type of particles[11] were synthesized, including: compartmentalized particles,[1,12] Janus particles,[13,14] porous particles[15] and particles with core-shell structure.[16, 17]

So far, the field of droplet microfluidics has relied on the use of organic solvents in combination with aqueous solutions for the production of particles from emulsions. A disadvantage of the use of organic solutions is that they harm biomaterial upon encapsulation. The obvious solution is to omit the use of organic solvents and produce compartmentalized microparticles from two or more immiscible aqueous solutions, which is the aim of this work.

All-aqueous compartmentalized microparticles not only open the door to a better understanding of cells, but these advanced bio friendly materials are also expected to play an important role in fields as diverse as food, cosmetics, pharmacy, self-assembly,[18] tissue engineering,[19] photonic devices,[20] multiplexing assays,[21] and drug delivery.[22]

1.4 Thesis outline

This thesis is structured as follows: in chapter 2 we will review the literature on compartmentalized microparticles produced with microfluidics. New to the field of droplet based microfluidics is the use of aqueous two-phase systems and we will introduce basic knowledge on this topic in this chapter as well. We will also briefly describe basic theory on the Rayleigh-Plateau instability as a background to the work described in chapters 3 – 6. In chapter 3 we will explain the methods that we developed to force the formation of water-in-water droplets and to stabilize the droplets after formation by polymerization. An interesting observation from this work that triggered a follow-up study is that the aqueous thread from which the droplets form is remarkably stable, much more stable than predicted

by Rayleigh-Plateau theory for confined threads. In chapter 4, we will report the experiments performed to better understand the reason why the thread is so stable. After being able to produce water droplets in water we increased level of compartmentalization in all-aqueous system. In chapter 5 we will present the method to produce all-aqueous core-shell emulsions by microfluidics. In order to stabilize these structures we polymerized them, which is shown in chapter 6. In the last chapter, we will consider a completely different system and show directional self-assembly of hydrogel which can be also applied in creating compartmentalized structures in aqueous environment.

References

1 T. G. Leong, A. M. Zarafshar and D. H. Gracias, *Small*, 2010, **6**, 792-806

2 H.-P. M. de Hoog, M. Nallani and N. Tomczak, *Soft Matter*, **8**, 4552-4561

3 F. M. Menger and M. I. Angelova, *Acc. Chem. Res.*, 1998, **31**, 789-797

4 R. Dimova, S. Aranda, N. Bezlyepkina, V. Nikolov, K. A. Riske and R. Lipowsky, *J. Phys. Condens. Mat.*, 2006, **18**, S1151-S1176

5 A. M. Brizard and J. H. Van Esch, *Soft Matter*, 2009, **5**, 1320-1327

6 J. Yoon, K. J. Lee and J. Lahann, *J. Mater. Chem.*, 2011, **21**, 8502-8510

7 M. Fialkowski, A. Bitner and B. A. Grzybowski, *Nature Mater.*, 2005, **4**, 93-97

8 K. W. Bong, K. T. Bong, D. C. Pregibon and P. S. Doyle, *Angew. Chem. Int. Ed.*, 2010, **49**, 87-90

9 J. Kim, L. He, Y. Song, Y. Yin and S. Kwon, *Chem. Comm.*, 2012, **48**, 6091-6093

10 D. Dendukuri, D. C. Pregibon, J. Collins, T. A. Hatton and P. S. Doyle, *Nature Mater.*, 2006, **5**, 365-369

11 D. Dendukuri and P. S. Doyle, *Adv. Mater.*, 2009, **21**, 4071-4086

12 A. R. Abate and D. A. Weitz, *Small*, 2009, **5**, 2030-2032

13 S. Lone, S. H. Kim, S. W. Nam, S. Park, J. Joo and I. W. Cheong, *Chem. Comm.*, 2011, **47**, 2634-2636

14 Z. Nie, W. Li, M. Seo, S. Xu and E. Kumacheva, *J. Am. Chem. Soc.*, 2006, **128**, 9408-9412

15 C. Ye, A. Chen, P. Colombo and C. Martinez, *J. R. Soc. Interface.*, 2010, **7**, S461-S473

16 A. S. Utada, E. Lorenceau, D. R. Link, P. D. Kaplan, H. A. Stone and D. A. Weitz, *Science*, 2005, **308**, 537-541

17 S. Okushima, T. Nisisako, T. Torii and T. Higuchi, *Langmuir*, 2004, **20**, 9905-9908

18 Q. Chen, S. C. Bae and S. Granick, *Nature*, 2011, **469**, 381-384

19 Y. A. Du, E. Lo, S. Ali and A. Khademhosseini, *Proc. Natl. Acad. Sci. U. S. A.*, 2008, **105**, 9522-9527

20 V. Rastogi, S. Melle, O. G. Calderon, A. A. Garcia, M. Marquez and O. D. Velev, *Adv. Mater.*, 2008, **20**, 4263-4268

21 H. Lee, J. Kim, H. Kim, J. Kim and S. Kwon, *Nature Mater.*, 2010, **9**, 745-749

22 J. A. Champion and S. Mitragotri, *Proc. Natl. Acad. Sci. U. S. A.*, 2006, **103**, 4930-4934

Literature Survey

2

2.1 Introduction

During the last decade great developments in the field of particle synthesis resulted in spectacular variety of techniques to produce micro- and nanoparticles of different shapes, compositions, morphologies, and functionalities.[1,2] Fig. 2.1 shows an overview of many different types of particles including those with simple shapes such as rods and discs as well as particles with much more complex and exotic structures such as nanocolloidal cubes and icosahedra, striped particles, and polyvalent spheres. These particles find their use in a wide variety of fields including optic,[3,4] biology,[5] magnetism, electronic,[6-8] food,[9-11] and medicine.[12-14] Examples of applications include sensors,[15-17] catalysis,[18] displays,[19] corrosion protection,[20,21] antireflective films,[22-24] bacteriostatic surfaces[25,26] and supports for bioresistant SAMs.[27] These applications either make use of the individual particles or use them as elemental building blocks for the assembly of larger structures based on a bottom-up approach, much like Lego's®. If needed, the stability of these assemblies can be guaranteed by crosslinking[28] them after their assembly. Increasing the complexity of the assembly (dimensionality) and the complexity of the building blocks (shape of the particles) materials of well-defined structure can be obtained such as planar arrays and spherical assemblies[2] as shown in Fig. 2.2.

In this literature review, we focus on the production of microparticles with one or more internal compartments and review methods to produce them in section 2.2. After a brief overview of traditional methods in section 2.2.1, we turn our attention to microfluidic methods to produce compartmentalized particles in section 2.2.2. Microfluidics is the method of choice for the research described in this thesis, because the laminar flow in microfluidic devices allows the production of microparticles with a high level of control over their size, shape, and morphology. Special attention is paid to the field of droplet microfluidics (in section 2.2.2) as we adopt this strategy in our work. This field predominantly relies on the use of oil and water for the formation of compartmentalized microparticles from microdroplets. In this thesis we pioneer the use of immiscible aqueous solutions for the formation of compartmentalized particles rather than using oil and water. Combination of two immiscible aqueous solutions are better known as Aqueous Two Phase Systems (ATPS) or Aqueous Biphasic Systems (ABS). After providing background information on ATPS in section 2.3.1, we review their use in microfluidics and in droplets microfluidics in sections 2.3.2 and 2.3.3. In contrast to oil-water systems, the production of droplets from ATPS is a challenge. One of the reasons is that the driving force for droplet formation, i.e. the interfacial tension, is much smaller in ATPS than in oil-water systems.

Consequently, the instability needed for droplet breakup develops too slowly to ensure reproducible drop formation. This instability is known as the Rayleigh-Plateau instability and theory on this subject is briefly reviewed in the appendix.

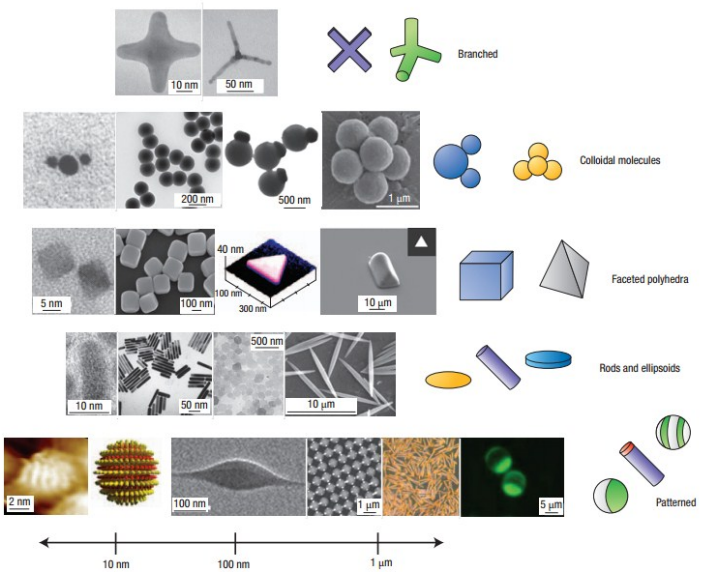

Fig. 2.1 *Overview of classes of engineered micro and nanoparticles. [Reproduced from ref. 1].*

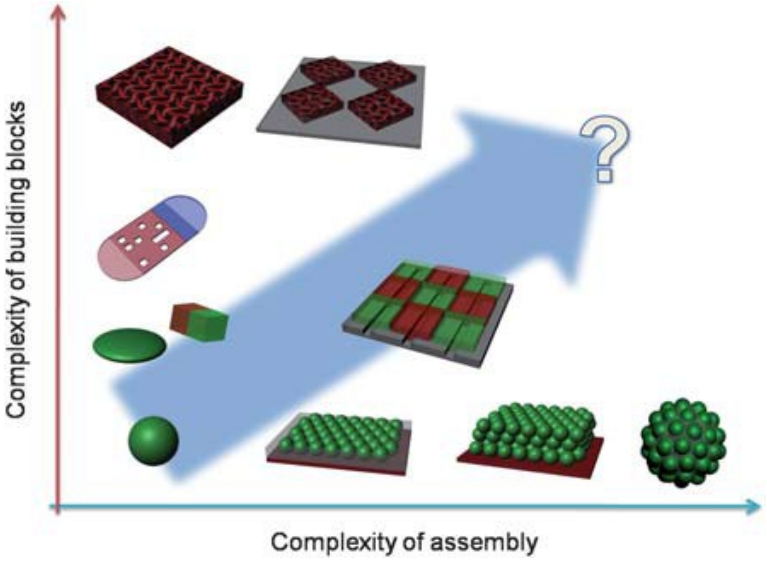

Fig. 2.2 *Schematic diagram of colloid-based biofunctional materials. The complexities in both colloidal particles and assembly schemes have been improved by creative strategies of materials synthesis and fabrication. [Reproduced from ref. 2].*

2.2 Compartmentalized micro particles (CMP)

Well-known examples of micro particles with one or more internal compartments are core-shell particles and Janus Particles. Methods to produce CMPs can generally be divided in chemical methods, physical methods, and biologically inspired methods. Among chemical methods, selective crystallization and deposition[29-32] are used most frequently, because they yield highly organized particles and are easy to process. They involve a bottom-up approach where building blocks have to be pre-designed. Examples of physical methods include the use of emulsions (electrified jetting, emulsion drying, emulsion deformation)[33] or the use of microfabrication techniques (microcontact printing, selective, surface templating, direct writing and lithography).[34,35-41] Biologically inspired methods for instance use plant extracts,[42] viruses[43] or living organisms such as fungi[44] to produce CMPs. Rather than providing a complete overview of all the different methods, we present a few examples of different types of CMPs together with the method to prepare them in section 2.2.1.

Until recently these methods were developed in segregated field of research (chemistry, physics, biology, engineering and materials science). A multidisciplinary approach such as adopted in the work described in this thesis provides a powerful method for the fabrication of new types of CMP.

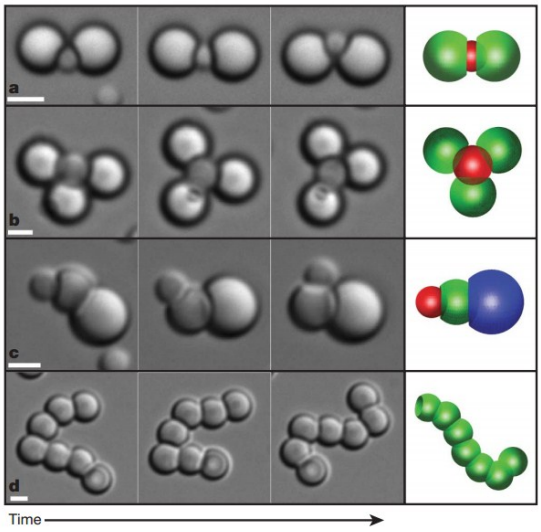

Fig. 2.3 *Time-lapse optical microscopy images (left three columns), and schematics (rightmost column), show the flexibility of lock–key bonds in various assemblies (a–d), which are confined to two dimensions by being placed on a glass microscope slide. The absence of irreversible chemical bonds between the building blocks allows these ball-in-socket joints to move freely. Scale bars 2 µm. [Reproduced from ref. 45].*

2.2.1 Examples of CMPs prepared with traditional methods

Lock-Key Principle

One of the interesting examples of a physical method to produce CMP is the use of key and lock colloids.[45] The three important components in that method are the key particles, the lock particles and the depletion interaction. Assembly of key and lock particles is based on complementary shapes. In a first step, particles with well-defined spherical cavities have to be synthesized. In the work of Saccana *et al*.[45] colloidal spheres are used as keys and monodisperse colloidal particles carrying a spherical cavity as locks. Lock-key particles can be assembled into structures with different sizes and shapes (Fig. 2.3). Binding and unbinding of particles can be controlled by temperature and solution composition.

Janus Particles

Zhang *et al.*[46] presented an interesting method to produce Janus particles and core-shell particles. They controlled the morphology of the particles via internal phase separation (evaporation of dichloromethane (DCM) from the polymer/HD/DCM-in-water emulsion droplets) followed by the extraction of the organic solvent as shown in Fig. 2.4. They obtained poly(methylmethacrylate) (PMMA) and polystyrene(PS)/PMMA particles with Janus-like morphology. The morphology depends on the organic solvent/polymer ratio and the interfacial tensions, which can be adjusted by changing the type and concentration of the emulsifier. Via adjusting the composition of the system and the corresponding interfacial tensions, they could tailor the morphology. For example using poly(vinyl pyrrolidone) (PVP) as emulsifier, they obtained PMMA hollow spheres and using SDS as emulsifier, they observed that particles changed from bowl-like particles to hemispheres and truncated spheres with the increase of SDS content.

Particles with multiple aqueous compartments

Microparticles with multiple internal compartments[1] can be produced by self-assembly. Among them are vesosomes (lipid vesicle inside lipid vesicle)[47] and giant unilamellar vesicles containing phase-separated (responsive) material.[48] Usually unilamellar vesicles are produced by non-equilibrium techniques,[49] which do not allow the encapsulation of a specific volume nor do they encapsulate other vesicles. To overcome this problem, Walker *et al.*[47] developed a method to encapsulate aggregates of vesicles in a bigger vesicle. They used molecular recognition processes (Fig. 2.5) to produce multi-

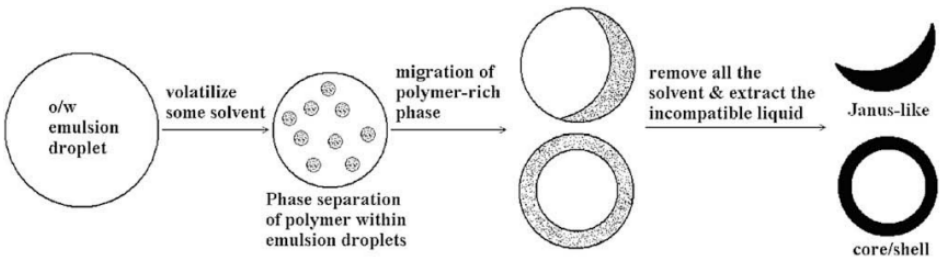

Fig. 2.4 *Scheme of the internal phase separation in the PMMA/ hexadecane/CH_2Cl_2/ aqueous phase system. [Reproduced from ref. 46].*

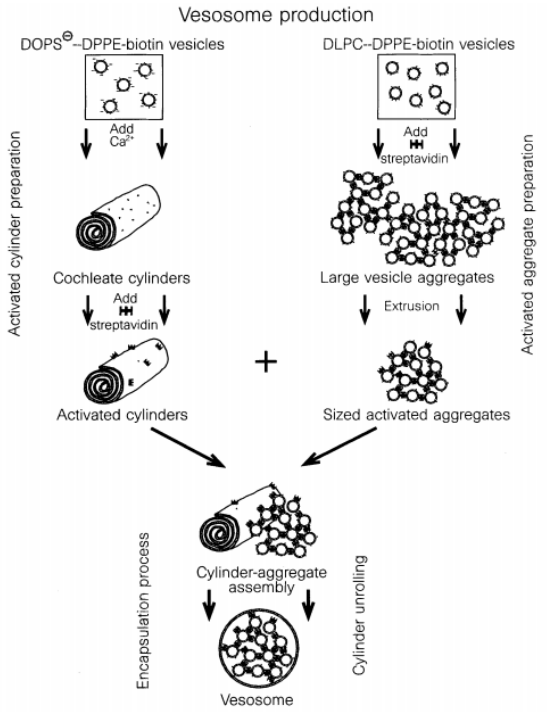

Fig. 2.5 *Vesosome production. Their construction involves two parallel processes, one being the production of vesicles aggregates, the other being the production of cochleate cylinders. Activated cylinders and sized aggregates are finally mixed. The cylinders and vesicle aggregates bind together, and the cylinder unrolls around the vesicles, attached by biotin-streptavidin linkages. [Reproduced from ref. 47].*

compartment particles of vesicles encapsulated inside a larger vesicle.

Long *et al.*[48] showed that vesicles can be prepared with encapsulation of concentrated aqueous solutions of dextran and PEG, which phase separate at low temperatures leading to compartmentalization within the vesicles. Fig. 2.6 presents the reversibility of the segregation of proteins in aqueous two-phase systems. Soybean agglutinin lectin partitions to the dextran-rich phase at T = 5 ºC (top row: dextran phase separates), spreads over the whole volume at T = 21 ºC (middle row: PEG and dextran phase mix), and recompartmentalizes again at 5 ºC (bottom row).The middle panel and right panel represent fluorescence from rhodamine tagged lipids and lectin. With this system phase segregation can be tuned as wished thanks to temperature.

Polymer capsules

Polymer capsules inside polymer capsules are other interesting example of compartmentalized structures.[50] Capsule formation is based on sequential layer-by-layer (LbL) absorption of polymers on a template via covalent or non-covalent interactions. Subsequent template dissolution leads to free-standing capsules (e.g., calcium carbonate template can be easily removed using EDTA).

Much more complex structures such as capsosomes[51] (lipid vesicles inside polymer capsules) and polymersomes in polymersomes or non-spherical polymersome

multicompartments[52] are other inspiring examples of compartmentalized structures notably because of their potential for making artificial cells.

2.2.2 Microfluidic methods

Most microfluidic methods for the production of CMPs are based on the use of droplets. Before thoroughly reviewing the different methods developed in the field of droplet microfluidics in section 2.2.2, we first discuss another important method based on flow lithography.

Flow lithography

Doyle and co-workers[34, 53] developed a new class of photolithographic methods to produce polymer-based particles. In contrast to conventional photolithography, which produces patterns on solid substrates, flows are patterned such that the particles can be immediately used on the chip or collected at the exit.

Those particles form by exposing a monomer solution, which flows through a microchannel to UV-light through a transparency mask. The features on the mask hereby define the shape of the particles.[34, 53] In Continuous Flow Lithography (CFL) particles are formed in a continuously flowing oligomer stream with a resolution down to 3 μm. To overcome the problem that throughput is limited in CFL due to the fact that the resolution of particles is comprised at high velocities, the same group invented Stop flow Lithography (SFL).[53] The difference between CFL and SFL is that in SFL a flowing stream of pre-polymer is stopped before exposed to UV light as shown Fig. 2.7. This provides improvement of resolution down to 1 μm and allows higher throughput. In both these methods features that are formed have a 2D extruded shape.

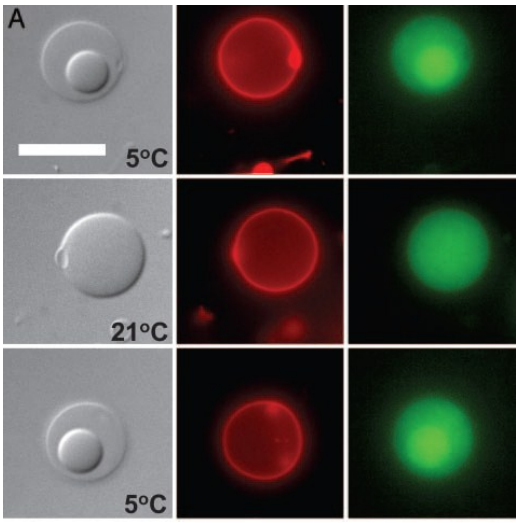

Fig. 2.6 *Vesicles with compartments made of phase separated PEG and dextran solution due to temperature change. The scale bars denote 10 μm. [Reproduced from ref. 48].*

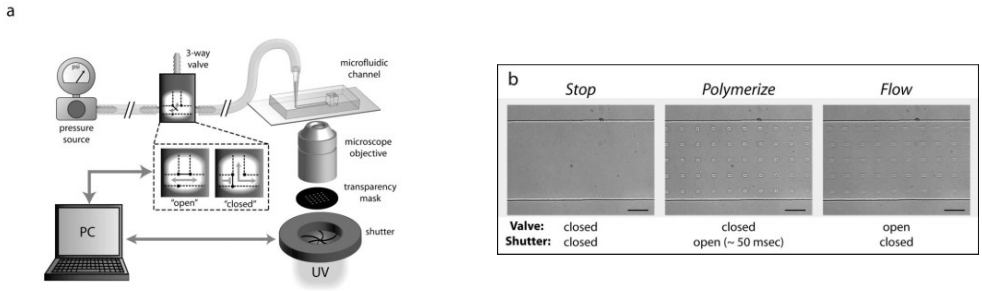

Fig. 2.7 *Stop-flow lithography setup. (a) Schematic showing the computer-controlled flow setup. Oligomer flows within a microfluidic channel are driven using a pressure profile provided by a computer controlled 3-way solenoid valve that alternates between atmospheric pressure (closed) and a specified input pressure (open). The computer also controls the exposure time provided by the shutter. (b) Microscope images showing the three states of the process. [Reproduced from ref. 53].*

To obtain the control over particle features in 3D, Stop Flow Interference Lithography (SFIL)[54] was developed. A schematic diagram of the setup used for SFIL is shown in Fig. 2.8. The microfluidic device and the phase mask were both molded in PDMS. They were sealed to each other as shown in the cross-sectional view in Fig. 2.8a. UV light passing through the phase mask, lead to the formation of a 3D structure. Fig. 2.9 presents an overview of different types of microparticles produced with the three flow lithography methods.[55]

Droplet microfluidics

Droplet microfluidics[56,57] involves the generation, manipulation, and use of

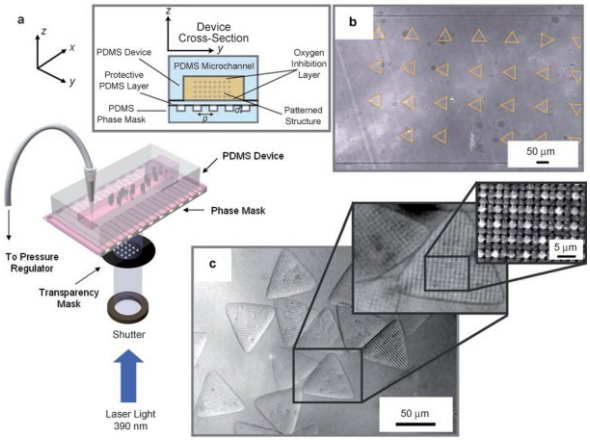

Fig. 2.8 *SFIL experimental setup. (a) Schematic drawing showing the PDMS microfluidic device integrated with a PDMS phase mask. (b) Bright field image of an array of patterned triangles of side length 60 μm formed in a 600-μm-wide and 30-μm-tall microfluidic device. (c) DIC image of the triangles shown in (b) after they have been suspended in ethanol. [Reproduced from ref. 54].*

discrete picoliter to nanoliter droplets inside microfluidic devices. One of the fields of application is material science, where droplets are used as templates for the synthesis of micro and nanoparticles. These droplets can be formed with excellent control over size, morphology, and composition due to the laminar flows. Although the use of droplets as a template yields mostly to particles with a spherical shape, methods have been developed to arrest the shape of non-spherical droplets. Such particles with non-spherical shapes are interesting, because they can for instance be used for modifying optical properties[58] or as a building block for self-assembled biomaterials.[59] Another example is drug delivery where the shape of the particles influences the release.[60]

Compartmentalized microparticles can be obtained by encapsulating different materials inside the droplets. Well known examples of such compartmentalized particles [12] include Janus particles,[61,62,63] porous particles,[64,65] and particles with core-shell structure.[66,67,68] We will review the different microfluidic methods used for the production in this section.

Importantly, the field of droplet microfluidics so far relied on the use of organic solvents in combination with aqueous solutions to form droplets. A disadvantage of the use of organic solution is that they harm biomaterial upon encapsulation. The obvious solution is to omit the use of organic solvent and produce compartmentalized microparticles from two or more immiscible aqueous solutions also known as Aqueous Two Phase Systems (ATPS). We review the first few papers that appeared in ATPS droplet microfluidics in a separate section (2.3.3).

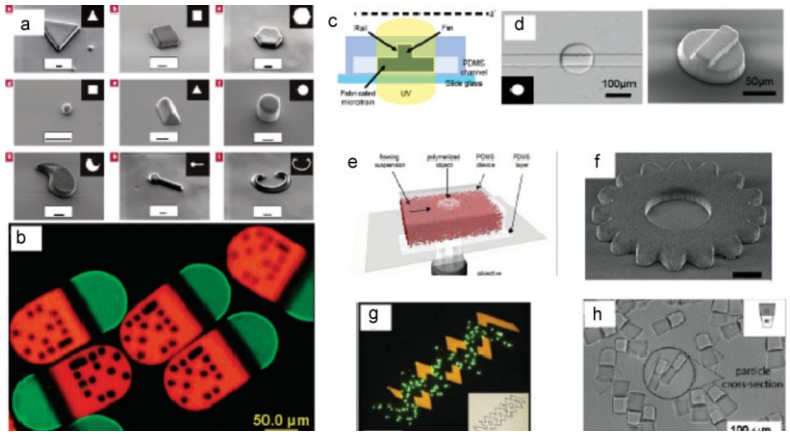

Fig. 2.9 *(a) A variety of 2D extruded shapes produced using CFL. (b) Barcoded particles used for the assembly of viruses that contain three distinct sections. (c) Schematic of a non-rectangular cross-section of a PDMS device used for the synthesis of 3D particles and (d) particles with a 3D cross section synthesized using this method. (e) SFL based synthesis of colloid granule containing microgears and (f) sintered microgear formed from the process in (e). (g) 3D particle with complex patches of fluorescent green and yellow formed using LRL. (h) Amphiphilic particles formed from two immiscible phases using CFL. [Reproduced from ref. 55].*

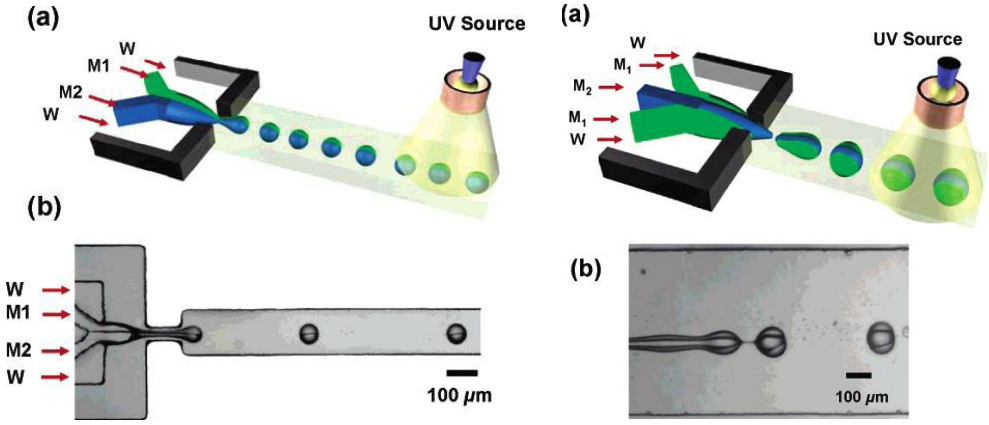

Fig. 2.10 *Left: (a) Schematic of generation of Janus droplets from immiscible monomers M1 and M2, emulsified in an aqueous solution of SDS (W).The droplets are irradiated with UV light in the downstream channel. (b) Optical microscopy image of formation of Janus droplets. Right: a) Schematic of formation of droplets with ternary structures. (b) Optical microscopy image of the generation of droplets with a ternary structure. Monomers M1 and M2 are introduced in intermediate and central channels, respectively. [Reproduced from ref. 52].*

Janus particles

Janus particles were synthesized in microfluidic devices by different groups as explained in the review by Teranashi.[69] Lone *et al.*[51] synthesized monodisperse Janus particles by UV-directed phase separation. They used homogenous photo-polymerizable water-in-oil (W/O) emulsion. In the microfluidic channel emulsion was subjected to UV irradiation, which caused phase separation of light sensitive random copolymer and production of Janus particles. Nie *et al.*[52] reported the microfluidic method of synthesis of Janus particles and ternary three-phase polymer particles with narrow size distribution in the size range from 40 to 100 μm. They produced emulsion of monomer liquid in the chip and photopolymerized in situ multiphase droplets. Fig. 2.10 shows the formation of Janus droplets (a) and droplets with ternary structures (b) from immiscible (M1, M2) liquids.[52] The biggest advantage of this technique is that the phase ratio between M1 and M2 in the

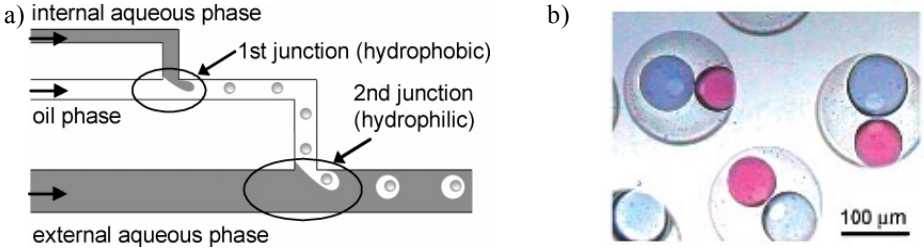

Fig. 2.11 *(a) Basic concept for preparing double emulsions (W/O/W) using T-shaped microchannels. (b) Organic droplets enclosing two different aqueous drops. [Reproduced from ref. 70].*

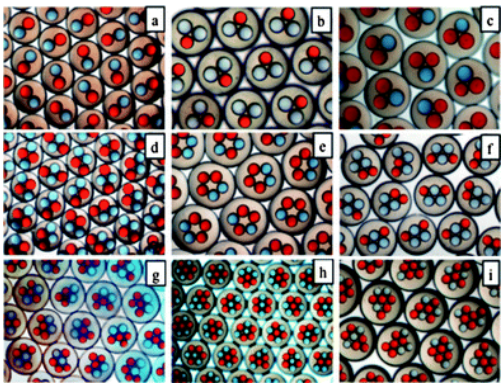

Fig. 2.12 *Combinations of monodispersed double emulsions with two different types of inner drops for configurations of: (a) two, (b and c) three, (d) four, (e and f) five, (g) six, (h) seven, and (i) eight total inner drops. [Reproduced from ref. 70].*

Janus particles can be conveniently adjusted by varying the flow rate of M1and M2. Nie *et al*. also created features with an asymmetric chemical modifications of the surface for example by introducing functional moieties in one of the monomer phases during microfluidic synthesis.

Core-shell particles

Core-shell particles can be produced from double emulsions. Okushima *et al*.[68] presented a method to produce double emulsions by two steps droplet breakup (Fig. 2.11). They used the microfluidic device with hydrophobic and hydrophilic components. Utada *et al*.[67] showed how to produce double emulsions in one step method. For this purpose, they used a microcapillary device. They obtained high control over the size of the core and the thickness of the shell by controlling the rates of flow. They adapted the classical production of well-defined double emulsions for core-shell particle by changing the properties of the fluids which make up the shell.

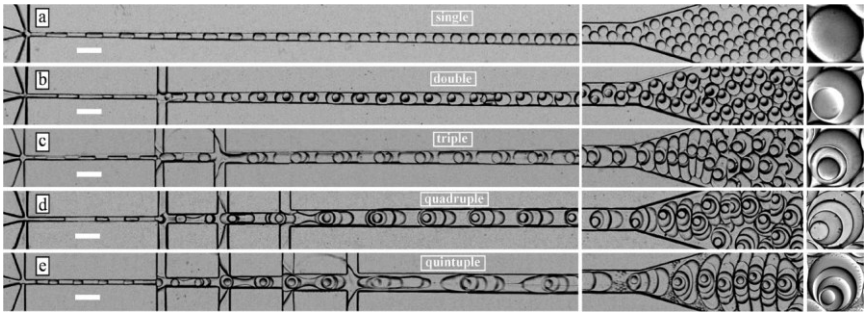

Fig. 2.13 *Drop maker arrays used to produce multiple emulsions with controlled order. Photomicrographs of (a) single, (b) double, (c) triple, (d) quadruple, and (e) quintuple emulsion drop maker arrays. The multiple emulsions produced by the arrays are shown to the right. The scale bars denote 100 μm. [Reproduced from ref. 71].*

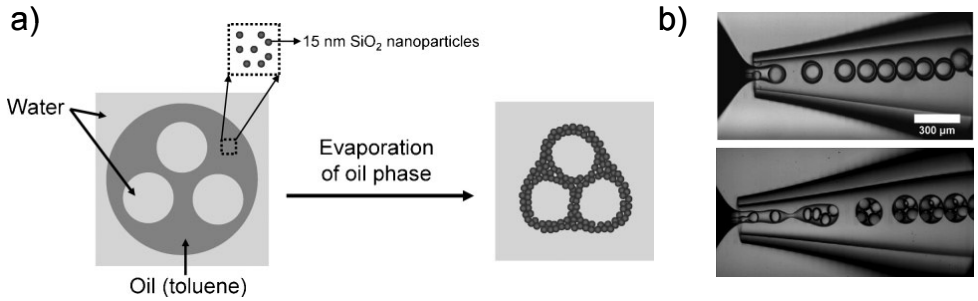

Fig. 2.14 *(a) Generation of non-spherical colloidosome from W/O/W double emulsions with multiple internal aqueous drops. Oil phase comprises toluene and 15 nm hydrophobic silica nanoparticles. (b) Generation of double emulsions with varying number of internal drops. [Reproduced from ref. 72].*

Multiple emulsions

Adams *et al.*[70] extended the work of Utada and used a single-step emulsification technique to encapsulate two, three, and four different inner drops inside double emulsions. The optical microscopy images presented in Fig. 2.11b represent monodisperse double emulsions with discrete numbers of inner drops indicating the achievement of a high level of control with this technique. They loaded precise numbers of two different types of inner aqueous drops inside oil drops for the generation of monodisperse water–oil–water double emulsions. The number of two different type of inner drops that are encapsulated can be controlled as wished (Fig. 2.12b,c).

Abate *et al.*[71] showed an elegant manner to produce double and higher order emulsion droplets. They showed that increasing number of shell-compartments requires change of wettability properties by increasing number of parts of channels within the microfluidic chip. They produced water-in-oil single emulsion in a one junction chip with

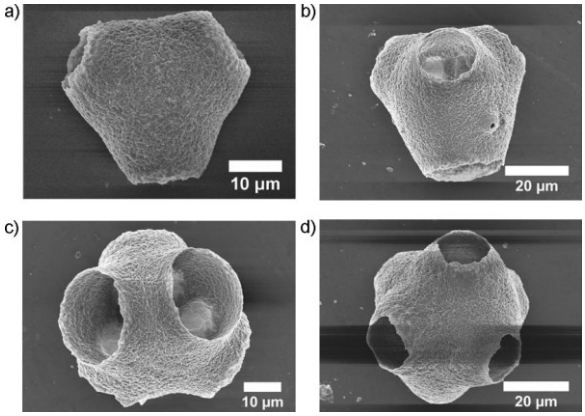

Fig. 2.15 *SEM images of non-spherical colloidosomes with 3 (a), 4 (b), 5 (c), and 6 (d) internal voids. [Reproduced from ref. 72].*

uniform hydrophobic wettability. To form a double emulsion, they used a chip with two junctions functionalized to have opposite wettability. Triple, quadruple and quintuple emulsions were generated with more complex designed chips shown on the Fig. 2.13. According to Abate *et al.*[71] generating droplets at synchronized time is crucial for production of multiple emulsions.

Non-spherical compartmentalized microparticles can also be prepared from multiple emulsions as shown by Lee and Weitz,[72] who prepared non-spherical multi compartment colloidosomes from W/O/W double emulsions in a capillary device (Fig. 2.14). They produced emulsions with a different number of internal aqueous drops in the oil drop, which were stabilized with poly(vinyl alcohol) as a surfactant. They suspended hydrophobic SiO_2 nanoparticles in the oil phase. Upon the removal of the oil these nanoparticles become the shell of the colloidosomes. They showed that the W/O interface retains its spherical shape, whereas the outer O/W interface deforms leading to the generation of non-spherical colloidosomes with multiple compartments (Fig. 2.15).

Another example of non-spherical particles involved porous particles that can be produced in microfluidics using droplets that contain gas bubbles as templates. Wan and Stone[65] presented a method to produce high volume fraction of bubbles in droplets using the microfluidic device shown in Fig.2.16a. They generated monodisperse microbubbles in a continuous water phase using a flow-focusing geometry. Further down in the channel, at the T-junction, the gas–water system was dispersed into a continuous oil phase. The parent water droplets contain a small number of gas bubbles (Fig. 2.16b). These droplets flow in a continuous oil phase and further breakup into smaller droplets with fewer bubbles but with a higher gas volume fraction (Fig. 2.16c). These kind of particles with high gas can be used for instance as pressure sensors. Also the authors expect that this technique will be useful for the fabrication of functional biomaterials such as ultrasound contrast agents and drug delivery materials.

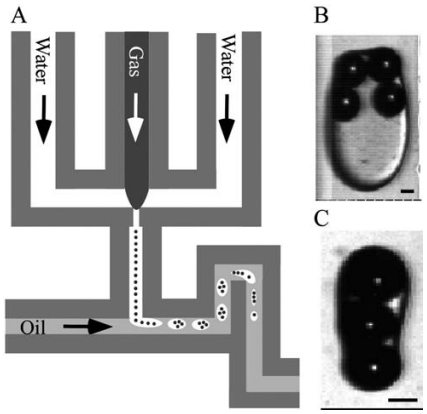

Fig. 2.16 *(a) Schematic of the microfluidic approach for generation of gas in-water-in-oil emulsions (not to scale). The typical size of the channel is 200 μm (w) x 38 μm (h), except the orifice where the width is 20 μm. (b) Image of a parent water droplet before the breakup process. (c) Image of a secondary water droplet with three encapsulated gas bubbles after the breakup process. Scale bar: 30 μm. [Reproduced from ref. 65].*

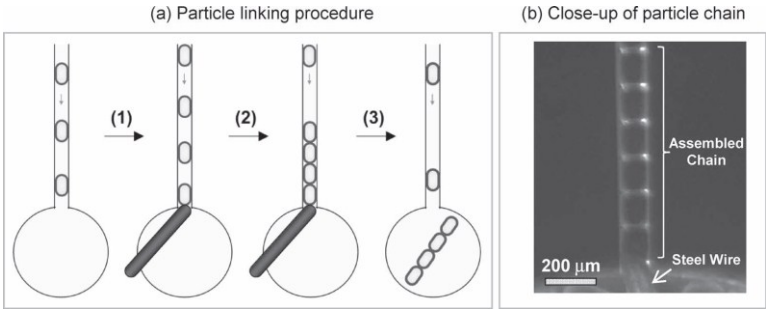

Fig. 2.17 *(a) Schematic depiction of the on-chip process for linking individual particles into chains. 1) A stainless steel wire is used as a valve to block the channel outlet, 2) the wire is held until the desired number of subunits has been accumulated on the chain, and 3) the wire is then removed and the chain is flushed into the reservoir. (b) Optical image showing a close-up of the assembled chain inside the microchannel. [Reproduced from ref. 73].*

Bottom up approach

As an alternative to the formation of compartmentalized particles from double and multiple emulsion droplets, compartmentalized structures can also be obtained by the assembly of single particles into larger structures. Jiang *et al.*[73] presented the "microfacturing" method of microfluidic fabrication of magnetic and fluorescent chains using chitosan microparticles (Fig. 2.17). They created chitosan particles on chip and then interfacially cross-linked them into stable microparticles by using a downstream flow of glutaraldehyde (GA) as a chemical "glue" and microchannel confinement as spatial template. The functional properties of these microparticles can be easily changed by introducing for example magnetic nanoparticles and/or fluorescent dyes, into the chitosan solution. This method shows big potential, because the arrangement of particles within a chain can also be controlled.

2.3 Aqueous Two Phase Systems

In the previous section we described microfluidic methods to produce CMPs from droplets produced with oil and water. One of the major drawbacks of this approach is the use of organic solvents, as they compromise the biocompatibility. In this section, we discuss the production of CMPs in all-aqueous systems.[74]

We first provide general background information on all-aqueous systems build up from two or more immiscible aqueous polymer solutions in section 2.3.1 and then discuss the use of these systems in co-flowing microfluidic (section 2.3.2) and droplet microfluidics (section 2.3.3).

2.3.1 Introduction

Aqueous two-phase systems (ATPS) are water-based solutions of polymers or of one polymer and an inorganic salt, which can form two immiscible phases. Whether phase separation occurs due to differences in hydrophobicity of the polymers and incompatibility

of the polymers in the solution depends on the concentrations and on the temperature.[75]

Mixture generally form a single phase at low concentrations, while two phases are obtained at higher concentrations as shown in the phase diagram in Fig. 2.18, where the black phase line divides the single phase form the two phase region. For a two-phase system, both phases are in equilibrium with each phase enriched in one or the other of the respective phase forming components. Both phases largely consist of water and are separated by an interface, which is characterized by a very low value of the interfacial tension. Both these features ensure a biocompatible environment in contrast to two phase systems comprised of water and an organic solvent. ATPSs are traditionally used for the extraction and purification of biomolecules,[76-82] because these biomolecules do not destabilize or denature at the interface between the two water-rich phases. ATPS have a high potential application in industry as a low cost tool, where ATPS containing polymers that are easily recycled are the most interesting for environmental reasons. ATPS were discovered in 1896 by Beijerinck,[83] although their practical use was shown much later in the mid 1940's by Albertsson[84] who used them to separate and concentrate biomaterials. This was possible due to the different physico-chemical affinities of molecules or cells to the two phases. There is no general role to predict which factors predominantly determine partitioning of specific samples between the phases.[85]

The hydrophobic interactions between the sample and the polymer molecules is the most important, but other factors like the size or conformational changes of the sample entities have also large influence.[76] Additionally the polymer or salt concentration as well as the molecular weight of the polymers can play a big role in the partitioning behavior of samples.[86] The most well-known ATPS is formed from aqueous solutions of dextran and polyethylene glycol (PEG). The system is prepared by mixing a water solution of PEG and a water solution of dextran. After a few hours separated phase are formed. In this system the bottom phase is rich in dextran (called dextran phase) and top phase is rich in PEG (called PEG phase).

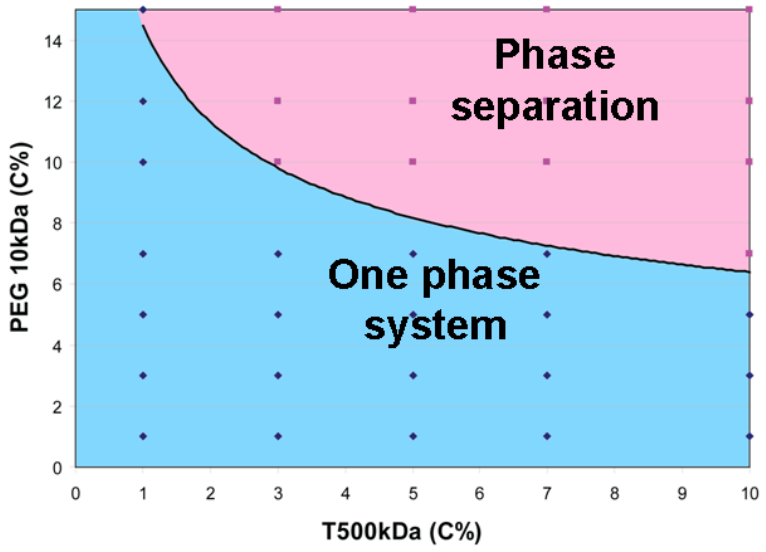

Fig. 2.18 *Phase diagram for system PEG 10 kDa/dextran 500 kDa/water.*

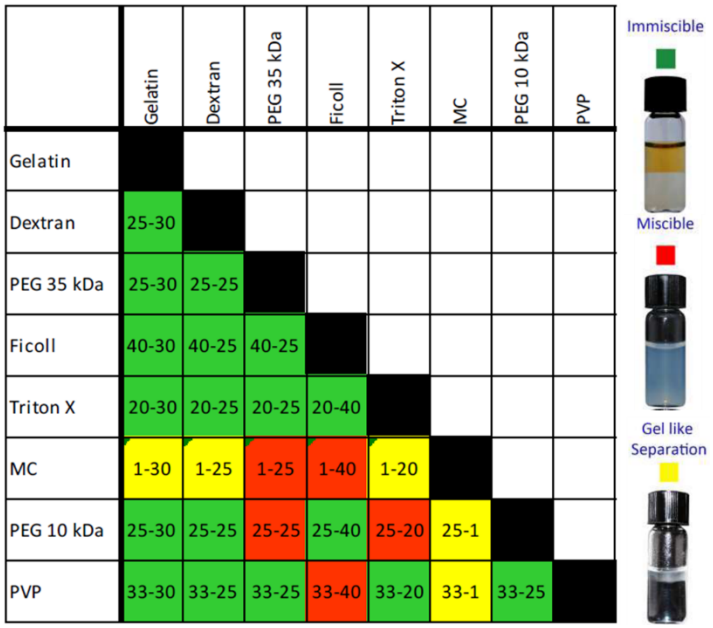

Fig. 2.19 *Aqueous two phase systems consist of two immiscible polymer solutions that are separated by a clear interface as shown in the top right figure. Whether an ATPS is obtained by mixing two aqueous polymer solutions depends on the concentration of the polymer solutions (indicated by the numbers in the table) and on the types of polymers. Apart from ATPS (indicated in green), either miscible solutions red) or gel like separations (yellow) are observed.*

Some other systems, which show phase separation, are listed in Fig. 2.19. The numbers in the squares represents the w/w concentrations of the solutions before mixing them. The left number correlates with the left column and the right number correlates with the top row. The color of the squares indicates the obtained morphology of the system: green represents phase separation (immiscible), red represents miscible, and yellow represents gel like separation.

Theoretical work on phase separation aims at predicting whether phase separation occurs. One of the most well-known models is the model by Flory and Huggins, who described phase separation from a thermodynamic perspective of the process of mixing. In the equation the free Gibbs energy of mixing ΔG_{mix} is expressed by the enthalpy of mixing ΔH_{mix}, entropy of mixing ΔS_{mix} and temperature T:

$$\Delta G_{mix} = \Delta H_{mix} - T\Delta S_{mix} \qquad (2.1)$$

When $\Delta G_{\text{mix}} < 0$ mixing occurs, when $\Delta G_{\text{mix}} \geq 0$ phase separation occurs. This equation is very general and can predict the phase separation, but it has to be adapted to the system under consideration. Eqn. (2.1) has to be modified because of the entropy effect for high molecular mass polymers. Due to high molecular mass, the polymer molecule has limited amount of conformations it can have in the space. This causes that entropy component contributes to negative ΔG_{mix} less than what would have happened for small

molecular weight molecules. It has to be noticed also that Flory and Huggins derived an expression for the enthalpy component ΔH_{mix} such that it takes three interaction parameters into account, i.e. polymer 1 - polymer 1 (w_{11}), polymer 2 – polymer 2 (w_{22}), polymer 1 – polymer 2 (w_{12}).

In the system we are using, PEG and dextran solution in water, the phase separation occurs as coacervation[87-89] which is the phenomenon of forming a liquid rich in polymer phase in equilibrium with another liquid phase. Coacervation is based on repulsion, i.e. London dispersion forces (for apolar fragments of chains) and electric charge differences (for polar part of chains). To actually get phase separation in a coacervate system, the concentrations of polymers have to be sufficient. For low concentrations the molecules cannot exert enough repulsion forces to drive the components to separate phases. Importantly the Flory-Huggins equation describes the Gibbs free energy for a mixture of two polymers. In this work we consider two polymers in one solvent. For such a system the Flory –Huggins equation has to be extended to take into account interaction between polymer 1 – solvent, polymer 2 - solvent, it is to say the hydration shell. The Flory-Huggins model has to be modified in order to account for the solvation of polymer molecules in aqueous solutions, *i. e.*, to account for the fact that water molecules may bond to some sites on the polymer molecule, leading to the formation of a hydration shell around each one. This is only to the information of for the reader and we will not go further in the explanations here since it has already been made elsewhere.[90]

2.3.2 ATPS in co-flowing microfluidics

Recently interest in all-aqueous system in microfluidics has been explored. Several groups used ATPS. ATPS were primary used in microfluidics for extraction or separation purposes. The water solutions were introduced into the channels as coflowing streams. For the extraction processes it is essential that the coflowing streams are stable and do not break up into droplets. The low value of the interfacial tension in ATPS prevents drop formation such as no special adjustments have to be made to stabilize multilaminated ATPS flows in microchannels. The stability of such flows was studied by Lu *et al.*[91] They made experiments using PEG/salt system to generate the map of the flow regimes of two phases, identifying the regions of bi-laminated and droplet flow. Co-flowing streams of PEG-rich and salt-rich solutions were used by Meagher *et al.*[92] for protein partitioning study. They dissolved small molecular tracer (FITC) in salt-rich phase and introduced it into the microfluidic channel as a middle stream, between second solution of salt stream and PEG stream. It was shown by fluorescence that the sample almost entirely diffused into the PEG stream. In a similar experiment they also showed separation of β-galactosidase and serum albumin, which were introduced together in the middle stream. Due to different affinities to PEG-rich and to salt-rich phase, these proteins can be separated almost entirely. Experiments of Meagher *et al.*[92] have a great value because they show that microfluidic device can be used for separation/purification purposes of biomolecules. Enlarging the interface area by introducing the sample in the thin middle stream reduces diffusion time which is very important when diffusions constants are very small which can be due to big size molecules (large proteins, DNA) and the high viscosity of many polymer solutions.

Since the efficiency of extracting the molecule of interest depends on affinity of that molecule to one of the phases, finding the suitable ATPS is the major problem.

Meagher *et al*.[92] addressed that problem and used genetic engineering to introduce short, hydrophobic tags to a protein of interest, which causes strong affinity to the PEG-rich phase. Other groups also demonstrated protein separation/purification in ATPS in microfluidic channel. For example Hu *et al*.[93] did the purification of membrane protein using PEG/detergent two-phase system. Huh *et al*.[94] purify bacteriorhodopsin with PEG/salt ATPS solution. Due to complexity of the purification process that light sensitive protein is only available in small amount. Successes of purification of molecules in ATPS in microfluidic channel are outstanding but very low flow rate used in microfluidics is the factor limiting throughput.

ATPS in microfluidics is also used for separation/purification of cells. Yamada *et al*.[95] used PEG/dextran system to study partitioning of plant cells. Nam *et al*.[96] studied separation of life and dead animal cells in PEG/dextran ATPS. Soo Hoo and Walker[97] also used PEG/dextran system but for separation of blood cells. In their experiment they study two configurations of PEG/dextran streams. Sample of blood cells i.e. erythrocytes and leukocytes in PEG solution is always introduced to the inlet in the middle. In one configuration the middle stream is between a second PEG solution stream and a dextran stream. In other configuration the middle stream is focused between two dextran streams. In both experiments, it is visible that leukocytes attach to the liquid/liquid interface, whereas the erythrocytes diffuse into the two bulk phases, which might be due to the larger size of the leukocytes. Low interfacial tension of ATPS is the major factor for the success of that experiment (Fig. 2.20).

Depending on the size of the cell, it can or cannot be detached from the interface. Also Tsukamoto *et al*.[98] studied separation of different types of human cells in PEG/dextran system. Another way to use ATPS in microfluidics for protein or DNA separation is electroextraction.[99-101] Specially developed microfluidic devices allow to apply electric field normal to the liquid-liquid interface. Presence of electric field causes different partitioning of the sample between phases compared to the thermodynamic equilibrium state.

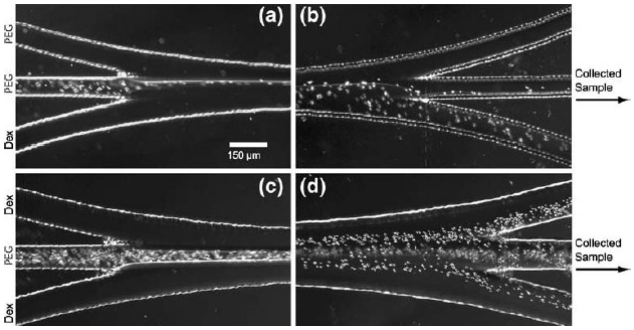

Fig. 2.20 *The one interface setup consisted of a PEG-PEG-Dex pattern. (a) Blood was introduced in the middle stream and (b) erythrocytes migrated to the Dex by the end of the channel. (c) Blood was introduced into the two interface device (Dex-PEG-Dex) which provided twice the surface area for erythrocyte migration, as shown in (d). [Reproduced from ref. 97].*

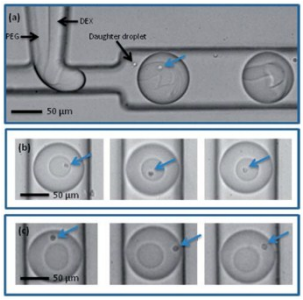

Fig. 2.21 *Cells with Ab-NIPAM conjugate in DEX at a microfluidic T-junction (a) and in a DEX droplet prior to mixing (b). Note that although small daughter droplets are formed, they do not merge with the larger ATPS droplets. After mixing, cells partition to the outer PEG phase (c). (Cells are indicated by arrows). [Reproduced from ref. 104].*

2.3.3 ATPS in droplet microfluidics

Under the conditions typical to microfluidic channels, droplets do not form spontaneously when two aqueous polymer solutions merge as evidenced from the examples presented in the previous section. The main reason is the fact that the driving force for droplet formation, i.e. interfacial tension, is very small for ATPSs. Two main approaches have been developed to facilitate the formation of ATPS droplets.

One approach relies on the use of a chaperoning oil stream to form the droplets. More specifically, water-in-oil droplets are formed that contain two aqueous polymer solutions. These solutions phase separate while the droplets form through the microchannel as for instance shown by Yasukawa *et al.*[102]. Khan *et al.*[103] showed that the internal structure of the droplets depends on the flow rate and fluid properties of the droplets such that ATPS droplets with different morphologies can be obtained. Vijayakumaer *et al.*[104] used a similar approach and demonstrated the potential of this system for bio separation by encapsulating cells in ATPS droplets. Cells that were initially in the dextran phase extracted into the PEG phase as shown in (Fig. 2.21).

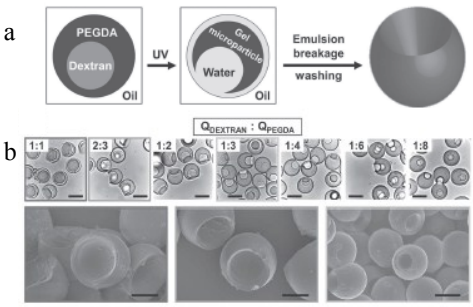

Fig. 2.22 *(a) Schematic of UV-induced droplet polymerization accompanied by shrinkage of the PEGDA shell. (b) Brightfield microscopy images of gel microparticles with a socket. The socket size is determined by the flow rate ratio of dextran and PEGDA (upper row). Scanning electron micrographs of selected samples (lower row). The scale bars denote 80 µm in the upper row and 30 µm in the lower row. [Reproduced from ref. 105].*

Huck *et al.*[105] developed an ATPS system based on dextran (for the core) and a photopolymerizable poly(ethylene glycol) diacrylate, PEGDA (for the shell). Upon UV exposure, the droplets undergo an irreversible shape transformation in which the dextran core migrates to the polymerizing PEGDA phase yielding concave dextran-PEGDA microgel particles (Fig. 22a). Precise control over the shape of the particles and the size of the socket in particular, can be exerted by the volume ratio of dextran and PEGDA in the ATPS droplet templates. Another approach that completely omits the use of organic solvents is based on external forcing. Song and coworkers[106,107] were the first to produce ATPS droplets in a microfluidic device using electrohydrodynamic actuation. In this way, they were able to form droplets for the aqueous two phase system consisting of tetrabutylammonium bromide/ammonium sulfate.

In contrast to most ATPSs, the interfacial tension in their ATPS is comparable to that of an oil-water system. To form ATPS droplets for much lower values of the interfacial tension, we developed a method based on a different type of forcing, i.e. mechanical forcing, and used it to form all-aqueous single emulsions[108,109] as well as all-aqueous double emulsions.[110] This work is described in detail in chapters 3 to 6 of this thesis. After our publication in Lab on a Chip more groups presented their work on the formation of all-aqueous single[111,112] and double[113] emulsions. Shum *et al.*[112] used a similar approach and

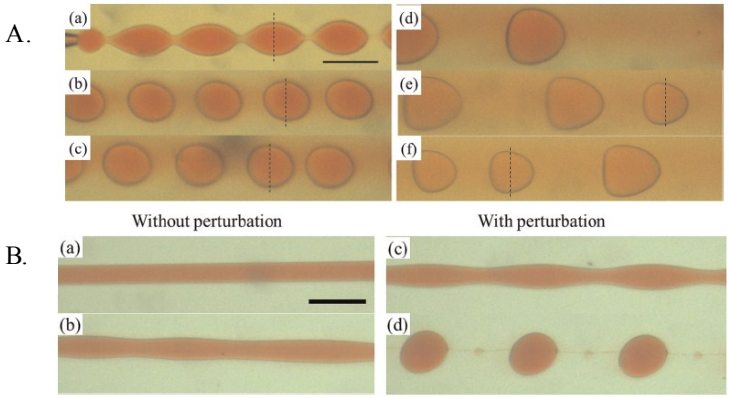

Fig. 2.23 *A. Optical microscope images of droplets of water with 17 wt. % PEG solution and 1 wt. % allura red in a continuous phase of 16 wt. % dextran solution observed at (a) 0 cm, (b) 1 cm, (c) 2 cm, (d) 3 cm, (e) 6 cm, and (f) 7 cm from the tip of the injection tip. The reddening of the continuous phase suggests that allura red in the droplets gradually diffuses into the continuous phase. Scale bar is 200 μm. B. Interfacial precipitation for enhancing encapsulation efficiency of allura red. Optical microscope images of (a)-(c) jets and (d) droplets of water with 17 wt. % PEG and 1 wt. % calcium chloride in a continuous phase of water with 16 wt. % dextran and 1 wt. % sodium carbonate. Images (a) and (c) are taken at 0.5 cm from the tip of the injection capillary while images (b) and (d) show the same jets as in (a) and (c), respectively, at 2 cm from the tip of the injection capillary. Shaking is only applied to the jet shown in (c) and (d). The calcium ions and the carbonate ions in the dispersed and continuous phases, respectively, react to form a precipitate of calcium carbonate. In (d), the satellite drops form between two larger parent drops since the addition of components for interfacial precipitation modifies the rheological properties of the fluids. Scale bar is 1 mm. [Reproduced from ref. 112].*

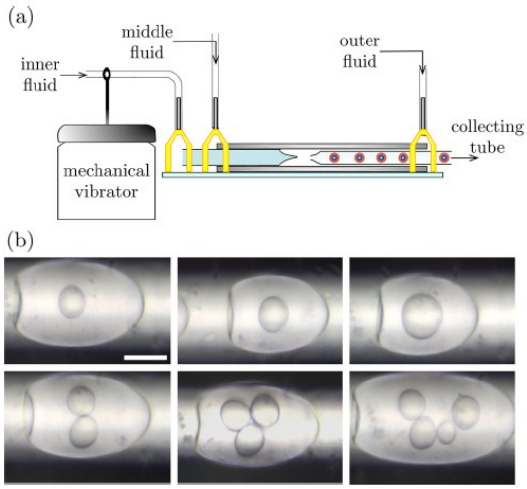

Fig. 2.24 *(a) Schematic of the setup for the generation of double emulsion. (b) w/w/w double emulsion, the size of the inner droplets as well as their numbers can be controlled by varying the frequency of excitation and the flow rates. Scale bar is 100 µm. [Reproduced from ref. 113].*

produced w/w droplets using a mechanical actuator in a glass capillary device.

They showed that dye molecules could easily diffuse from the droplet into the continuous phase (Fig. 2.23a) and developed a method based on precipitates and gels at the w/w interfaces of these droplets to prevent rapid diffusion (Fig. 2.23B). This is an important step towards high efficiency encapsulation in w/w emulsions. Sauret and Shum[113] extended their work by embedding an additional capillary in the configuration shown in Fig. 2.24, that allowed them to encapsulating multiple droplets inside single emulsion droplets with a good control over the number and size of encapsulated droplets.

2.4 Summary

Through this literature survey, the reader has been invited to explore the different technics, methods and processes, from lithography to microfluidics, used to produce microparticles. Research and development on these technics did not only lead to the achievement of particles of various shapes (some are very complex) but also allowed the use of these particles into various applications. Moreover, these particles can be used as building blocks to achieve larger structured particles. As shown in this chapter, ATPS in droplet-based microfluidics is a powerful tool to access these type of particles. Rheology and theoretical knowledge and recent research on ATPS and microfluidic, allow us today to present this thesis, inspired from the examples presented here.

Appendix

Rayleigh-Plateau theory of liquid jet breakup

In this section, we briefly review basic theory on the Rayleigh-Plateau instability. This theory explains whether and how fast a thread breaks up into droplets and hence is important to better understand the work described in this thesis. For a detailed description, we refer the reader to textbooks and reviews.[114,115]

Let us first address the question whether a fluid thread breaks up into droplets. Like Rayleigh, we consider a cylindrical fluid thread and introduce sinusoidal perturbations to its surface as shown in Fig. 2.25.These perturbations are characterized by a wavelength λ and a small amplitude ε. This tread is stabilized to its original cylindrical shape in case the pressure in the buldged area P_{buldged} is larger than the pressure in the pinched area P_{pinched}, as fluid flows from the buldged area to the pinched area. By contrast, breakup occurs for $P_{\text{buldged}} < P_{\text{pinched}}$. We calculate these pressures based on the Young-Laplace law, which relates the pressure difference between the inside and the outside of the thread to the curvature of the interface and the interfacial tension. The curvature can be calculated from the two radii of curvature. For the pinched area, the radius of curvature in the radial direction is R_0-ε, while the radius of curvature in the axial direction of the thread equals -$1/\varepsilon k^2$, with k the wavenumber ($k = 2\pi/\lambda$). Under the assumption that the pressure around thread is uniform and setting it to zero for simplicity, the pressure in the buldged and pinched areas can be written as

$$P_{bulged} = \gamma\left(\frac{1}{R_0+\varepsilon} + \varepsilon k^2\right) \tag{2.2}$$

$$P_{pinched} = \gamma\left(\frac{1}{R_0-\varepsilon} - \varepsilon k^2\right) \tag{2.3}$$

Comparing these pressures, we find that breakup occurs for wavenumbers corresponding to

$$kR_0 \leq 1 \tag{2.4}$$

This simple analysis predicts whether the thread breaks, but it does not predict how fast the perturbations grow. To study the dynamics of breakup, Rayleigh introduced small sinusoidal perturbations to the thread of the form

$$(x,t) = R_0 + \varepsilon e^{\omega t + ikx} \tag{2.5}$$

with ω the growth rate of the perturbation. Applying linear stability theory, Rayleigh was the first to calculate so called dispersion relations $\omega(k)$. For a viscous thread with a viscosity η in vacuo, the dispersion relation equals[116]:

$$-i\omega = \frac{\gamma}{2R_0\eta}\frac{1-(kR_0)^2}{1+(kR_0)^2\left[1-\frac{I_0R_0}{I_1(kR_0)^2}\right]} \tag{2..6}$$

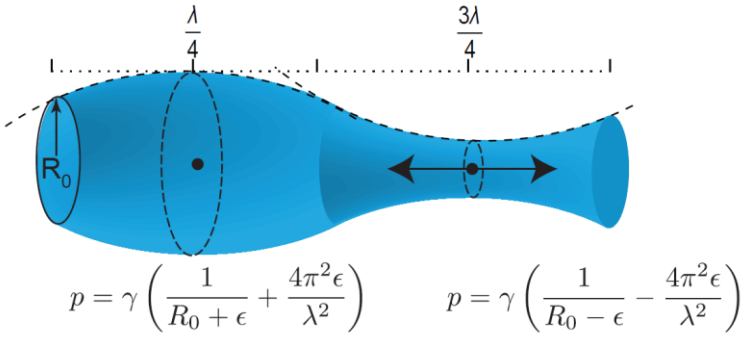

Fig. 2.25 *A cylindrical fluid thread with initial radius R_0 is perturbed with sinusoidal perturbations characterized by a wavelength λ and amplitude ε.*

with I_0 and I_1 the modified Bessel functions of the first kind. This dispersion relation can be used to calculate the wavenumber for which perturbations grow ($-i\omega > 0$) such that the thread breaks or die out ($-i\omega < 0$) such that the thread stabilizes. Additionally, it allows one to calculate the growth rate of the perturbations that grow fastest. The dimensionless dispersion relation is plotted in Fig. 2.26, where we used the viscous time scale $\tau = \eta R_0/\gamma$ to non-dimensionalize the growth rate. This curve confirms the previously derived finding that perturbations with $kR_0 > 1$ are stable. Additionally, it shows that perturbations with a wavenumber $kR_0 = 0.679$ are fastest and outgrow the other wavenumbers.

After Rayleigh's pioneering work on viscous threads in vacuum, dispersion relations for all kinds of other situations have been derived. Important extensions are those derived for viscous threads surrounded by another viscous fluid in unconfined,[117] and confined systems.[118,119] For a fluid thread with of radius r_0 and viscosity η_i flowing through a cylindrical channel of radius R and focused by a stream of viscosity η_e, Guillot *et al.*[119] found the dispersion relation to be equal to

$$\omega = \frac{\gamma}{16\,\eta_e R}\,\frac{F(x,\lambda)(k^2-k^4)}{x^9(1-\lambda^{-1})-x^5} \qquad (2.7)$$

with k the wavenumber of the perturbation made dimensionless with the initial radius of the tread, and x the dimensionless thread radius defined as $x = r_0/R$. Following their terminology, we now use λ for the viscosity ratio, which is defined as $\lambda = \eta_i/\eta_e$. The function $F(x, \lambda)$ equal to $F(x, \lambda) = x^4(4 - \lambda^{-1}+4\ln x) + x^6(-8+4\,\lambda^{-1}) + x^8\,(4\text{-}3\,\lambda^{-1} - (4 - 4\,\lambda^{-1})\ln x)$. This expression can be used to show that confinement not only slows down the growth of perturbations, but also shifts the wavenumber of the fastest growing perturbations. Guillot *et al.*[119] used it successfully to predict whether droplets breakup from a confined fluid thread.

The dispersion relation by Guillot *et al.*[119] was derived for two immiscible Newtonian fluids with a sharp interface. In this thesis, we use their theoretical model to understand the breakup of fluid threads composed of immiscible aqueous polymer solutions flowing through a microchannel.

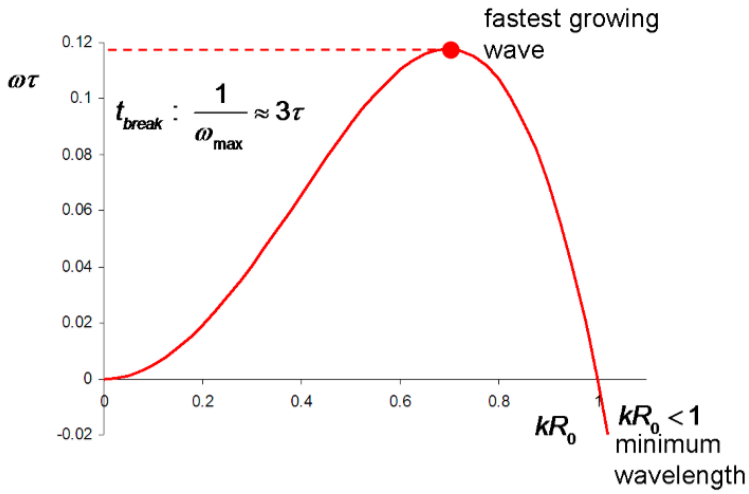

Fig. 2.26 *Dispersion relation $-i\omega(k)\tau$ as derived by Rayleigh for a viscous thread in vacuum. The maximum of the curve shows that perturbations grow fastest for kR_0=0.697, while perturbations characterized by wavenumbers kR_0>1 yield a stable*

References

1 S. C. Glotzer and M. J. Solomon, *Nature Mater.*, 2007, **6**, 557-562.

2 S. H. Kim, J. M. Lim, S. K. Lee, C. J. Heo and S. M. Yang, *Soft Matter*, 2010, **6**, 1092-1110.

3 X. Xu, T. H. Gibbons and M. B. Cortie, *Gold Bull.*, 2006, **39**, 156-165.

4 J. Q. Liu, B. Cankurtaran, L. Wieczorek, M. J. Ford and M. Cortie, *Adv. Funct. Mater.*, 2006, **16**, 1457-1461.

5 M. Es-Souni, H. Fischer-Brandies and M. Es-Souni, *Adv. Funct. Mater.*, 2008, **18**, 3179-3188.

6 M. Brust, D. Bethell, C. J. Kiely and D. J. Schiffrin, *Langmuir*, 1998, **14**, 5425-5429.

7 M. Brust, D. Bethell, D. J. Schiffrin and C. J. Kiely, *Adv. Mater.*, 1995, **7**, 795..

8 H. Nakanishi, K. J. M. Bishop, B. Kowalczyk, A. Nitzan, E. A. Weiss, K. V. Tretiakov, M. M. Apodaca, R. Klajn, J. F. Stoddart and B. A. Grzybowski, *Nature*, 2009, **460**, 371-375.

9 C. Mavrakis and V. Kiosseoglou, *Food Hydrocolloid*, 2008, **22**, 854-861.

10 A. Lamprecht, U. Schafer and C. M. Lehr, *J. Microencapsul.*, 2001, **18**, 347-357.

11 B. Cara, F. J. Moyano, B. Gander and M. Yufera, *J. Microencapsul.*, 2007, **24**, 505-514.

12 Y. H. Wen, M. R. Gallego, L. F. Nielsen, L. Jorgensen, H. Everland, E. H. Moller and H. M. Nielsen, *J. Control Release*, 2011, **156**, 11-20.

13 K. Park, *J. Control Release*, 2011, **156**, 1-1.

14 V. T. Tran, J. P. Benoit and M. C. Venier-Julienne, *Int. J. Pharmaceut.*, 2011, **407**, 1-11.

15 L. Han, D. R. Daniel, M. M. Maye and C. J. Zhong, *Anal. Chem.*, 2001, **73**, 4441-4449.

16 F. P. Zamborini, M. C. Leopold, J. F. Hicks, P. J. Kulesza, M. A. Malik and R. W. Murray, *J. Am. Chem. Soc.*, 2002, **124**, 8958-8964.

17 Y. Joseph, I. Besnard, M. Rosenberger, B. Guse, H. G. Nothofer, J. M. Wessels, U. Wild, A. Knop-Gericke, D. S. Su, R. Schlogl, A. Yasuda and T. Vossmeyer, *J. Phys. Chem. B*, 2003, **107**, 7406-7413.

18 J. Luo, V. W. Jones, M. M. Maye, L. Han, N. N. Kariuki and C. J. Zhong, *J. Am. Chem. Soc.*, 2002, **124**, 13988-13989.

19 E. P. K. Currie and M. Tilley, *J. Soc. Info. Display*, 2005, **13**, 773-780.

20 K.-C. Chang, H.-F. Lin, C.-Y. Lin, T.-H. Kuo, H.-H. Huang, S.-C. Hsu, J.-M. Yeh, J.-C. Yang and Y.-H. Yu, *J. Nanosci. Nanotechnol.*, 2008, **8**, 3040-3049.

21 G. X. Shen, Y. C. Chen and C. J. Lin, *Thin Solid Films*, 2005, **489**, 130-136.

22 X. T. Zhang, O. Sato, M. Taguchi, Y. Einaga, T. Murakami and A. Fujishima, *Chem. Mater.*, 2005, **17**, 696-700.

23 H. Hattori, *Adv. Mater.*, 2001, **13**, 51-54.

24 B. G. Prevo, Y. Hwang and O. D. Velev, *Chem. Mater.*, 2005, **17**, 3642-3651.

25 S. K. Smoukov, K. J. M. Bishop, B. Kowalczyk, A. M. Kalsin and B. A. Grzybowski, *J. Am. Chem. Soc.*, 2007, **129**, 15623-15630.

26 G. F. Fu, P. S. Vary and C. T. Lin, *J. Phys. Chem. B*, 2005, **109**, 8889-8898.

27 B. Kowalczyk, M. Byrska, G. Mahmud, S. Huda, K. Kandere-Grzybowska and B. A. Grzybowski, *Langmuir*, 2009, **25**, 1905-1907.

28 B. Kowalczyk, I. Lagzi and B. A. Grzybowski, *Nanoscale*, 2010, **2**, 2366-2369.

29 N. R. Jana, L. Gearheart and C. J. Murphy, *J. Phys. Chem. B*, 2001, **105**, 4065-4067.

30 Z.-C. Xu, C.-M. Shen, C.-W. Xiao, T.-Z. Yang, H.-R. Zhang, J.-Q. Li, H.-L. Li and H.-J. Gao, *Nanotechnol.*, 2007, **18**, 115608–115612.

31 L. Manna, E. C. Scher and A. P. Alivisatos, *J. Am. Chem. Soc.*, 2000, **122**, 12700-12706.

32 R. C. Jin, Y. W. Cao, C. A. Mirkin, K. L. Kelly, G. C. Schatz and J. G. Zheng, *Science*, 2001, **294**, 1901-1903.

33 K. M. Keville, E. I. Franses and J. M. Caruthers, *J. Coll. Interf. Sci.*, 1991, **144**, 103-126.

34 D. Dendukuri, D. C. Pregibon, J. Collins, T. A. Hatton and P. S. Doyle, *Nature Mater.*, 2006, **5**, 365-369

35 O. Cayre, V. N. Paunov and O. D. Velev, *J. Mater. Chem.*, 2003, **13**, 2445-2450.

36 K. H. Roh, D. C. Martin and J. Lahann, *Nature Mater.*, 2005, **4**, 759-763.

37 K. Braeckmans, S. C. De Smedt, M. Leblans, R. Pauwels and J. Demeester, *Nature Rev. Drug Discov.*, 2002, **1**, 447-456.

38 V. N. Manoharan, M. T. Elsesser and D. J. Pine, *Science*, 2003, **301**, 483-487.

39 Y. D. Yin, Y. Lu, B. Gates and Y. N. Xia, *J. Am. Chem. Soc.*, 2001, **123**, 8718-8729.

40 J. P. Rolland, B. W. Maynor, L. E. Euliss, A. E. Exner, G. M. Denison and J. M. DeSimone, *J. Am. Chem. Soc.*, 2005, **127**, 10096-10100.

41 C. J. Hernandez and T. G. Mason, *J. Phys. Chem. C*, 2007, **111**, 4477-4480.

42 S. S. Shankar, A. Rai, B. Ankamwar, A. Singh, A. Ahmad and M. Sastry, *Nature Mater.*, 2004, **3**, 482-488.

43 S. Brown, M. Sarikaya and E. Johnson, *J. Mol. Bio.*, 2000, **299**, 725-735.

44 V. Bansal, A. Sanyal, D. Rautaray, A. Ahmad and M. Sastry, *Adv. Mater.*, 2005, **17**, 889-892.

45 S. Sacanna, W. T. M. Irvine, P. M. Chaikin and D. J. Pine, *Nature*, 2010, **464**, 575-578.

46 Y. Wang, B. H. Guo, X. Wan, J. Xu, X. Wang and Y. P. Zhang, *Polymer*, 2009, **50**, 3361-3369.

47 S. A. Walker, M. T. Kennedy and J. A. Zasadzinski, *Nature*, 1997, **387**, 61-64.

48 M. S. Long, C. D. Jones, M. R. Helfrich, L. K. Mangeney-Slavin and C. D. Keating, *P. Natl. Acad. Sci. USA*, 2005, **102**, 5920-5925.

49 F. Szoka and D. Papahadjopoulos, *Annu. Rev. Biophys. Bio.*, 1980, **9**, 467-508.

50 B. G. De Geest, S. De Koker, K. Immesoete, J. Demeester, S. C. De Smedt and W. E. Hennink, *Adv. Mater.*, 2008, **20**, 3687-3691.

51 S. Lone, S. H. Kim, S. W. Nam, S. Park, J. Joo and I. W. Cheong, *Chem. Comm.*, **47**, 2634-2636

52 Z. Nie, W. Li, M. Seo, S. Xu and E. Kumacheva, *J. Am. Chem. Soc.*, 2006, **128**, 9408-9412

53 R. Chandrawati, L. Hosta-Rigau, D. Vanderstraaten, S. A. Lokuliyana, B. Stadler, F. Albericio and F. Caruso, *Acs Nano*, 2010, **4**, 1351-1361.

54 Z. Fu, M. A. Ochsner, H.-P. M. de Hoog, N. Tomczak and M. Nallani, *Chem. Comm.*, 2011, **47**, 2862-2864.

55 D. Dendukuri, S. S. Gu, D. C. Pregibon, T. A. Hatton and P. S. Doyle, *Lab Chip*, 2007, **7**, 818-828.

56 J.-H. Jang, D. Dendukuri, T. A. Hatton, E. L. Thomas and P. S. Doyle, *Angew. Chem. Int. Ed.*, 2007, **46**, 9027-9031.

57 D. Dendukuri, and P. S. Doyle, *Adv. Mater*, 2009, **21**, 1-16.

58 R. Seemann, M. Brinkmann, T. Pfohl and S. Herminghaus, *Rep. Prog. Phys.*, 2012, **75**, 016601.

59 S. Neethirajan, I. Kobayashi, M. Nakajima, D. Wu, S. Nandagopal and F. Lin, *Lab Chip*, 2011, **11**, 1574-1586.

60 Y. Lu, Y. D. Yin and Y. N. Xia, *Adv. Mater.*, 2001, **13**, 271-274.

61 S. C. Glotzer, *Science*, 2004, **306**, 419-420.

62 J. A. Champion, Y. K. Katare and S. Mitragotri, *J. Control Release*, 2007, **121**, 3-9.

63 S. Yang, F. Guo, B. Kiraly, X. Mao, M. Lu, K. W. Leong and T. J. Huang, *Lab Chip*, 2012, **12**, 2097-2102.

64 S. Dubinsky, H. Zhang, Z. Nie, I. Gourevich, D. Voicu, M. Deetz and E. Kumacheva, *Macromol.*, 2008, **41**, 3555-3561.

65 J. Wan and H. A. Stone, *Soft Matter*, 2010, **6**, 4677-4680.

66 C.-X. Zhao and A. P. J. Middelberg, *Angew. Chem. Int. Ed.*, 2009, **48**, 7208-7211.

67 A. S. Utada, E. Lorenceau, D. R. Link, P. D. Kaplan, H. A. Stone and D. A. Weitz, *Science*, 2005, **308**, 537-541

68 S. Okushima, T. Nisisako, T. Torii and T. Higuchi, *Langmuir*, 2004, **20**, 9905-9908

69 T. Teranishi, *Small*, 2006, **2**, 596-598.

70 L. L. A. Adams, T. E. Kodger, S.-H. Kim, H. C. Shum, T. Franke and D. A. Weitz, *Soft Matter*, 2012, **8**, 10719-10724.

71 A. R. Abate and D. A. Weitz, *Small*, 2009, **5**, 2030-2032

72 D. Lee and D. A. Weitz, *Small*, 2009, **5**, 1932-1935.

73 K. Jiang, C. Xue, C. Arya, C. Shao, E. O. George, D. L. DeVoe and S. R. Raghavan, *Small*, **7**, 2470-2476.

74 O. Franssen and W. E. Hennink, *Int. J. Pharmaceut.*, 1998, **168**, 1-7.

75 D. Forciniti, C. K. Hall and M. R. Kula, *J. Biotechnol.*, 1990, **16**, 279-296.

76 P.-A. Albertson, ed., *Partition of Cell Particles and Macromolecules, 3rd ed.; Wiley: New York, NY, USA*, 1986.

77 H. B. Walter, D, ed. F. Academic Press: Orlando, USA, 1985.

78 R. Hatti-Kaul, *Aqueous two-phase systems - A general overview*, 2000.

79 B. Y. Zaslavsky, ed. N. Marcel Dekker: New York, USA, 1995.

80 H.-O. Johansson, F. M. Magaldi, E. Feitosa and A. Pessoa, Jr., *J. Chromatogr. A*, 2008, **1178**, 145-153.

81 H.-O. Johansson, M. Ishii, M. Minaguti, E. Feitosa, T. C. Vessoni Penna and A. Pessoa, Jr., *Sep. Purif. Technol.*, 2008, **62**, 166-174.

82 S. Saravanan, J. R. Rao, B. U. Nair and T. Ramasami, *Process. Biochem.*, 2008, **43**, 905-911.

83 M. W. Beijerinck, *Col. Polym. Sci.*, 1910, **7**, 16-20.

84 P. A. Albertsson, *Nature*, 1958, **182**, 709-711.

85 S. Hardt and T. Hahn, *Lab Chip*, 2012, **12**, 434-442.

86 A. D. Diamond and J. T. Hsu, *Adv. biochem. engineer./biotechnol.*, 1992, **47**, 89-135.

87 H. G. B. de Jong and H. R. Kruyt, *Kolloid Z*, 1930, **50**, 41-52.

88 C. J. Vanoss and R. J. Good, *J. Disper. Sci. Technol.*, 1988, **9**, 355-362.

89 C. H. Bamford and H. Tompa, *Trans. Faraday. Soc.*, 1950, **46**, 310-316.
90 P. A. Pessoa and R. S. Mohamed, *Braz. J. Chem. Eng.*, 2001, **18**, 449-458.
91 N. Zhang, T. Pompe, I. Amin, R. Luxenhofer, C. Werner and R. Jordan, *Macromol. Biosci.*, 2012, **12**, 926-936.
92 R. J. Meagher, Y. K. Light and A. K. Singh, *Lab Chip*, 2008, **8**, 527-532.
93 R. Hu, X. Feng, P. Chen, M. Fu, H. Chen, L. Guo and B.-F. Liu, *J. Chromato. A*, 2012, **1218**, 171-177.
94 Y. S. Huh, C.-M. Jeong, H. N. Chang, S. Y. Lee, W. H. Hong and T. J. Park, *Biomicrofluidics*, 2010, **4,** 14103.
95 M. Yamada, V. Kasim, M. Nakashima, J. Edahiro and M. Seki, *Biotechnology and Bioengineer.*, 2004, **88**, 489-494.
96 K. H. Nam, W. J. Chang, H. Hong, S. M. Lim, D. I. Kim and Y. M. Koo, *Biomed. Microdev.*, 2005, **7**, 189-195.
97 J. R. SooHoo and G. M. Walker, *Biomed. Microdev.*, 2009, **11**, 323-329.
98 M. Tsukamoto, S. Taira, S. Yamamura, Y. Morita, N. Nagatani, Y. Takamura and E. Tamiya, *Analyst.*, 2009, **134**, 1994-1998.
99 T. Hahn, G. Muenchow and S. Hardt, *J. Phys. Condens. Matter*, 2011, **23**, 184107+08.
100 T. Hahn and S. Hardt, *Soft Matter*, 2011, **7**, 6320-6326.
101 G. Muenchow, S. Hardt, J. P. Kutter and K. S. Drese, *Lab Chip*, 2007, **7**, 98-102.
102 M. Yasukawa, E. Kamio and T. Ono, *Chem. Phys. Chem.*, 2011, **12**, 263-266.
103 S. H. S. Lee, P. Z. Wang, S. K. Yap, T. A. Hatton and S. A. Khan, *Biomicrofluidics*, 2012, **6**, 022007.
104 K. Vijayakumar, S. Gulati, A. J. deMello and J. B. Edel, *Chem. Sci.*, 2010, **1**, 447-452.
105 J. Thiele, A. R. Abate, H. C. Shum, S. Bachtler, S. Forster and D. A. Weitz, *Small*, 2010, **6**, 1723-1727.
106 Y. S. Song, Y. H. Choi and D. H. Kim, *J Chromato. A*, 2007, **1162**, 180-186.
107 Y. H. Choi, Y. S. Song and D. H. Kim, *J. Chromato. A*, 2010,**1217**, 3723-3728.
108 I. Ziemecka, V. van Steijn, G. J. M. Koper, M. Rosso, A. M. Brizard, J. H. van Esch and M. T. Kreutzer, *Lab Chip*, 2011, **11**, 620-624.
109 S. D. Geschiere, I. Ziemecka, V. van Steijn, G. J. M. Koper, J. H. v. Esch and M. T. Kreutzer, *Biomicrofluidics*, 2012, **6**, 22007-2200711.
110 I. Ziemecka, V. van Steijn, G. J. M. Koper, M. T. Kreutzer and J. H. van Esch, *Soft Matter*, 2011, **7**, 9878-9880.
111 D. Lai, J. P. Frampton, S. A. Hari and S. Takayama, *Lab Chip*, 2011, **11**, 3551-3554.
112 H. C. Shum, J. Varnell and D. A. Weitz, *Biomicrofluidics*, 2012, **6,** 012808.
113 A. Sauret and H. C. Shum, *Appl. Phys. Lett.*, 2012, **100,** 154106.
114 J. Eggers, *Rev. Mod. Phys.*, 1997, **69**, 865-929.
115 P. Garstecki, A. M. Ganan-Calvo and G. M. Whitesides, *Bull. Pol. Acad. Sci.*, 2005, **53**, 361-372.
116 J. Eggers and E. Villermaux, *Rep. Prog. Phys.*, 2008, **71**, 036601.
117 S. Tomotika, *Proc. R. Soc. Lon. Ser.-A*, 1936, **153**, 0302-0318.
118 P. Guillot, A. Colin and A. Ajdari, *Phys. Rev. E*, 2008, **78,** 016307.
119 P. Guillot, A. Colin, A. S. Utada and A. Ajdari, *Phys. Rev. Lett.*, 2007, **99**, 104502.

Monodisperse hydrogel microspheres by forced droplet formation in aqueous two-phase systems*

3

Abstract

This chapter presents a method to form micron-sized droplets in an aqueous two-phase system (ATPS) and to subsequently polymerize the droplets to produce hydrogel beads. Owing to the low interfacial tension in ATPS, droplets do not easily form spontaneously. We enforce the formation of drops by perturbing an otherwise stable jet that forms at the junction where the two aqueous streams meet. This is done by actuating a piezo-electric bending disc integrated in our device. The influence of forcing amplitude and frequency on jet breakup is described and related to the size of monodisperse droplets with a diameter in the range between 30 and 60 μm. Rapid on-chip polymerization of derivatized dextran inside the droplets created monodisperse hydrogel particles. This work shows how droplet based microfluidics can be used in all-aqueous, surfactant-free, organic-solvent-free biocompatible two-phase environment.

* Published as: I. Ziemecka, V. van Steijn, G. J. M. Koper, M. Rosso, A. M. Brizard, J. H. van Esch and M. T. Kreutzer; Monodisperse hydrogel microspheres by forced droplet formation in aqueous two-phase systems, *Lab on a Chip*, 2011, 11, 620-624

3.1 Introduction

Aqueous two-phase systems (ATPS) consist of two immiscible aqueous solutions, which display a relatively low interfacial tension, typically of the order of 0.1mN/m. The combination of an all-aqueous environment and the low interfacial tension makes these systems ideal for purification and extraction of biomolecules, such as proteins and enzymes as well as living cells, since they provide the mild conditions that do not denature or destabilize these biomaterials.[1,2] Examples of miniaturized extraction and purification using ATPS solvent combinations include fast and efficient separation of cells,[3] and partitioning and purification of proteins.[4] In all of these applications, the two phases flow in parallel, separated by a stable interface that does not collapse into droplets. In fact, as we will describe below, it is rather hard to produce droplets in these water-in-water systems in comparison to organic-water systems.

Our work is motivated by the desire to exploit, in an all-aqueous environment, all the advantages of droplet microfluidics, such as the use of droplets as vessels for synthesis or microcrystal formation and reactions at the interface to produce capsules. An important motivation to develop a droplet-based system is subsequent polymerization of the droplets to create hydrogel particles for delivery of drugs or cells, such as shown by Jain *et al*.,[5] who used conventional methods to create an ATPS emulsion of extracted biomaterials. For many aspects of pharmaceutical use of microgels, such as bio-distribution, uptake and release rate, the control of the droplet size and size distribution is crucial,[6] and microfluidic miniaturization can be an attractive route to generate monodisperse droplets and microgels.[7]

While the creation of droplets of high monodispersity is well developed in microfluidic devices,[8] the low interfacial tension of ATPS limits the range of flow rates that allow spontaneous formation of droplets.[9,10] In short, for a given channel shape, viscosity ratio and flow ratio, the transition from a 'droplets' regime with monodisperse droplets to a less monodisperse 'jetting' regime, depends only on $Ca = \mu U/\gamma$, the ratio of viscous stresses ($\mu U/r$) to surface stresses (γ/r), with U the thread velocity, μ the thread viscosity, γ the interfacial tension and r the thread radius. In this context, the capillary number can be viewed as the ratio of a characteristic break-up time $t_{break} \sim \mu r/\gamma$ and a flow time $t_{flow} \sim r/U$. Now, a hundred-fold reduction in interfacial tension, not uncommon for aqueous two-phase systems in comparison with water-organics systems, requires a hundred-fold reduction in flow speed to still be able to form drops spontaneously. To maintain a wide range of practical flow rates, external forcing is needed to break up the otherwise stable thread. An example of such forcing was developed by Song and coworkers,[11,12] who generated droplets using electrohydrodynamic forcing in a ionic ATPS with a interfacial tension of 5 mN/m. In their method, unidentified electrostatic forces, due to surface charges or bulk charges, are important during the formation of droplets.

In this work, we demonstrate an all-mechanical piezoelectric forcing (similar to piezoelectric on-demand droplet generation)[13] to create water-in-water droplets, where we control the size of the droplets independent of flow rates, and we polymerize these droplets on-chip. Interestingly, these droplets can be created for a wide range of flow conditions, well outside the 'droplet' regime for the situation without forcing. Using only mechanical actuation ensures that we are not constrained in our choice of ATPS phases by surface charge requirements, enabling us, instead, to optimize our phase composition for gelation and/or polymerization. Of course, apart from the polymerization, the use of droplet microfluidics has all the well-known advantages such as selection, traffic control, sorting,

rapid mixing and fast extractionand mass transfer.[14] The ability to do so in a surfactant-free, organic-solvent-free all-aqueous system that is fully biocompatible is very attractive.

3.2 Experimental

Dextran solution 20 % w/w (av. molar mass 110 kg/mol from Leuconostoc ssp., Fluka) and polyethylene glycol solution 10 % w/w (av. molar mass 35 kg/mol, Fluka) were prepared by dissolving the powders in water using ultrasonication. Phase separation of the two solutions occurred 5 minutes after mixing them in a test tube. The interfacial tension between the phase-separated liquids was 0.10 ± 0.05 mN/m, as measured by the pendant drop method (Kruss, EasyDrop). The values represent the statistical average and standard deviation of the interfacial tension of sixteen independently measured droplets. The contrast of the pendant droplet in the liquid environment was enhanced manually to allow for automatic detection and fitting.

The viscosity of the solutions was measured using a rheometer with couette geometry (TA Instruments AR-G2) at a temperature of 25ºC. The average viscosity for the shear rate in the range 1 - 100 s^{-1} was 58.1 ± 0.2 mPas and 22 ± 0.1 mPas for dextran and PEG solution respectively.

To create hydrogel particles, we synthesized a glycidyl methacrylate derivatized dextran (dex-GMA) using the recipe of Van Dijk-Wolthuis *et al.*[16] The derivatized dextran was synthesized as follows. Dextran T500 (MW = 500000 g/mol, Fluka) (5 g) was dissolved in dimethyl sulfoxide (DMSO, 45 mL) in a stoppered 250 mL round-bottom flask under nitrogen atmosphere. After dissolution of 1.0 g 4-(N,N-Dimethylamino)pyridine (DMAP, MW = 122.17 g/mol, 81.85 mmol), 0.876 g of hydroxyethyl methacrylate (HEMA, MW=130 g=mol, 67.4 mmol) was added. The solution was stirred at room temperature for 48 h. Reaction was stopped by adding (an equimolar amount) of 4 M HCL (2.046 mL, 8.185 mmol) to neutralize the DMAP. The reaction mixture was transferred to a dialysis tube and extensively dialyzed for 10 days against demineralized water at RT. Water was removed by evaporation and by freeze-drying. White product (3.4359 g) was obtained. From NMR (and eq. provided in ref. 16) we calculated degree of substitution DS=15.

For the polymerization experiments, one solution contained 10 w/w % PEG (MW = 35000) and 185 mg/ ml ammonium peroxydisulfate (APS), and the other solution contained a saturated (≈ 10 w/w %) dex-GMA in 0.22 M KCl and 2 v/v % of N,N,N',N'-tetramethylethylenediamine (TEMED).

In our droplet experiments, we used the device as shown in Fig. 3.1. It consists of a flow focusing junction where one of the two immiscible liquids was injected as a thin jet inside the other liquid. The inner liquid was the dextran solution, fed at a flow rate of 6 µl/h, and the outer liquid was the PEG solution fed at a rate between 60 and 84 µl/h. Syringe pumps (Harvard Apparatus PicoPlus) were used to drive our solutions into the microfluidic device. The coflowing liquids subsequently entered the main channel (width 100 ± 5 µm, height 85 ± 5 µm) and, further downstream, a meandering 300 µm wide channel, which was connected to outflow. The remaining channels shown in Fig. 3.1 were filled with water and closed. They have no function in our experiment.

Fabrication of our microfluidic device was done using soft lithography. In brief, a 4-inch silicon wafer was patterned by exposing a layer of photo-resist (SU8-2050, Micro Resist Technology GmbH, Germany) to UV light (EVG-620, total energy: 250 mJ/cm^2) through an optical transparency containing the design of the microchannel network. After

development of the resist, the patterned wafer was used as a master to replicate the structure in poly(dimethylsiloxane) (PDMS). Our devices were constructed from two layers of PDMS. After curing the first 1 mm thin layer, a piezoelectric bending disc (0.5 in. diameter, Piezo Systems, Cambridge, MA, max. displacement 19.1 μm at 180 V) was placed on top of the center the fluid reservoir, and covered with a second thicker layer of PDMS. In this way, the piezo disc was embedded in the PDMS chip and separated from the fluid reservoir by a 1 mm thin PDMS membrane. Both the first and second layer of PDMS were prepared using a 10:1 prepolymer/curing agent mixture (Sylgard 184, Dow Corning). After curing the second layer at 68 °C for 2 hours, the PDMS structure was removed from the patterned wafer, cut to size, and provided with holes for the fluid connections. The channels were closed by irreversibly bonding a glass slide to the PDMS structure using an oxygen plasma treatment (Harrick PDC-002).

Visualization of the measurements was performed using an inverted microscope (Zeiss, Axiovert 100M) equipped with a black and white camera (AxioCam). In our experiments, the jet was destabilized by applying a sinusoidal voltage, generated by a function generator (33120A, Hewlett Packard) and amplified using a linear amplifier (Trek 50/750).

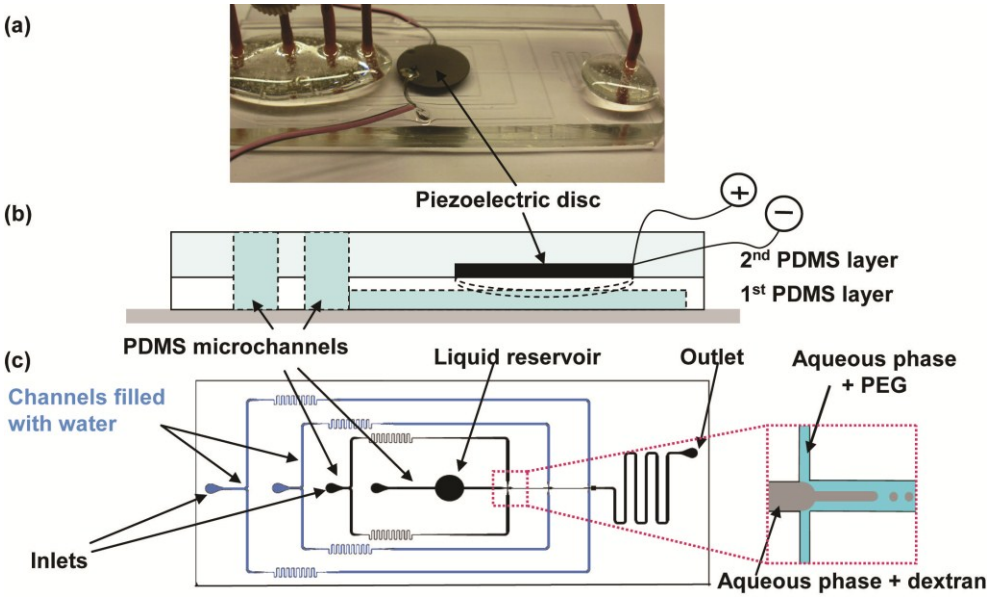

Fig. 3.1 *(a) Microfluidic device including a flow-focusing junction and a piezoelectric bending disc actuator (b) lateral view of the piezo-electric actuation device, (c) scheme of the microfluidic network.*

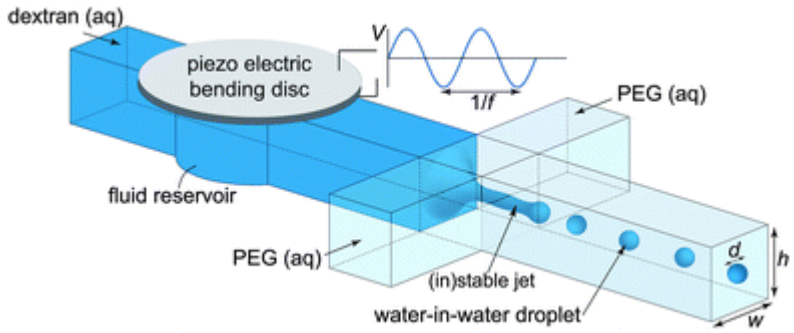

Fig. 3.2 *Microfluidic device used for the controllable formation of microscopic-sized water-in-water droplets. Droplets are periodically released by perturbing the jet that forms at the junction where the stream of dextran solution and PEG solution meet. This is done by applying a sinusoidal AC voltage with amplitude V and frequency f to the piezoelectric bending disc embedded in our device on top of the central channel. The bending disc squeezes the channel below it, accellerating the liquid inside it.*

3.3 Results and discussion

Our method for controlled droplet formation is illustrated in Fig. 3.2. We injected the dextran solution into the central channel of our device, and the PEG solution into the two side feeds. We first describe the flows that were found without actuating the piezoelectric disc. We found that dripping occurred for flow rates (q_{PEG}, q_{dex}) = (20, 2) mL h^{-1} and lower. For higher q_{PEG} and/or higher q_{dex}, jetting occurred. The flow rates that mark this transition between regimes in our 100 ± 5 x 85 ±5 mm^2 channel agree within acceptable limits with those predicted by Guillot *et al.*[10] for a rectangular channel of 100 x100 μm^2. The jet radius ranged from r_0 =13 ± 1 µm for q_{PEG} = 60 µl h^{-1} to r_0 = 10 ± 1 µm for q_{PEG} = 84 µl h^{-1}. Note that these radii are small compared to the width and height of the central channel. Stabilizing effects of confinement[10,18,19] are small for such thin jets.

Experimentally, we found that our threads were very stable, as shown in Fig. 3.3(a-c). Occasionally, we did observe spontaneous breakup of the jet, relatively far (»1 cm) from the junction. The stability of our jet is remarkable, because theory predicts growth rates Re(ω) for initial disturbances of the thread interface $\tilde{}$ $^{ikz+\omega t}$ of the order of 20 s^{-1}, suggesting that these threads should break up in less than 0.5 s, or, for the centerline flow speed U of 4 mm s^{-1}, within 2 mm for our experimental conditions. In agreement with this theoretical analysis, Guillot *et al.*[9] predicted fast break-up of threads with $2r_0/h < 0.5$ and stable threads for $2r_0/h > 0.5$, and confirmed this using glycerin / water in silicon oil. At present, we can only speculate about why our jets are so stable. We anticipate that particular properties of ATPS play a role. The present experiment involves more complex polymer solutions that exhibit more complex interfacial properties than pure liquids and hence the damping of fluctuations may be stronger than calculated for simple liquids. Finally, when the jet breaks far from the junction, that break up is always irregular, in agreement with the notion that it is caused by very slow amplification of noise in the system.

3.3.1 Forced droplet formation

We now describe the flow regimes that were obtained by actuating the piezoelectric disc. When applying a sinusoidal AC voltage with frequency f and amplitude V to the piezo disc, the disc periodically bends up and down causing a disturbance in the flow. This disturbance, of much greater amplitude than the white-noise disturbances that cause unforced break-up, reproducibly breaks up the jet into droplets. Various break-up schemes were observed, depending mostly on the applied frequency. An example of breakup is shown in Fig. 3.3d-f: a corrugated jet (Fig. 3.3d) breaks up into elongated and corrugated droplets (Fig. 3.3e) and finally forms pairs of droplets further downstream (Fig. 3.3f).

Droplets were obtained for a much wider range of flow conditions using piezo-electric actuation than without. Fig. 3.4 shows a phase map of outer flow rate q_{PEG}, to inner flow rate q_{dex}. The dotted line indicates the theoretical transition from jetting to dripping that we confirmed for non-forcing flows. In comparison to unforced droplet formation, we could increase the flow rate of the inner stream with at least an order of magnitude, and the flow rate of the outer stream with almost two orders of magnitude, and still create monodisperse droplets.

3.3.2 Droplet size and monodispersity

In order to further characterize the effect of forcing, we studied droplet formation for voltages between $V = 3$ and 25 V and frequencies between $f = 2$ and 50 Hz for the flow conditions of Fig. 3.3, i.e. $q_{PEG} = 60$ µl h^{-1}, $q_{dex} = 6$ µl h^{-1}.

A summary in the form of a map of voltages and frequencies presented in Fig. 3.5a shows under which conditions we obtained monodisperse and polydisperse droplets. Note that whether drop populations are monodisperse or polydisperse strongly depends on the actuation frequency, with a value of $f \approx 15$ Hz that marks the transition, and only slightly on the amplitude of the voltage applied to the piezo disc.

Perhaps the most useful regime was obtained for frequencies between 20 and 50 Hz, because monodisperse droplets were reproducibly formed with diameters below 60 µm, and coefficients of variation below 10% (Fig. 3.5c and 3.5d). The upper bound of 50 Hz can be understood in terms of standard Rayleigh-Plateau theory.[20] This linear stability

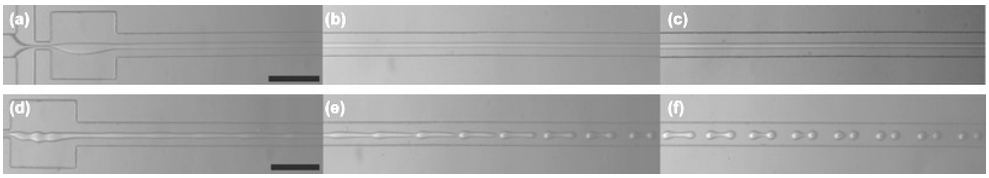

Fig. 3.3 *(a-c): Jetting of the aqueous two-phase flow under steady feed conditions, i.e. without piezo-electrical actuation to induce oscillations. The jet is stable and does not break up at the location of focussing (a), not at 2 mm downstream (b), not at 5 mm downstream (c). (d-f): Formation of droplets from the jet in (a) by perturbing the jet through actuation of the piezo disc using a sinusoidal voltage with frequency f = 20 Hz and amplitude V= 3 V. At 2 mm downstream of the focussing (e), the jet breaks up, and the resulting long droplets break into two droplets at 5 mm downstream (f). qPEG = 60 µl h-1, qdex = 6 µl h-1. Scale bars: 250 mm.*

analysis of small disturbances predicts that dimensionless wavenumbers $kr_0 > 1$ are always stable and wavenumbers $kr_0 < 1$ are unstable. This result holds when extended to viscous two-fluid systems.[21] The wavenumber is related to the forcing frequency by $k = 2\pi f/U$. The frequency that corresponds to the cut-off wavenumber $kr_0 = 1$ reads $f = 50$ Hz for the values of $U = 4$ mm/s and $r_0 = 11$ µm. This theoretical value agrees with the observed maximum frequency at which break up is still observed.

Below $f = 10$ Hz, relatively large droplets formed directly at the junction. Depending on the frequency, the diameter of the droplets ranged between 70 and 150 µm. Although the size of the droplets was regular for fixed frequency and voltage, the droplets were accompanied by many small satellites with sizes between 10 and 40 µm as shown in Fig. 3.5b. The satellites form by the breakup of a very thin jet that forms just before the large drop pinches off, as the large droplet advances when the feed flow rate is at its minimum over the oscillation period. The number of satellites hereby reduced with increasing frequency.

For frequencies between 10 and 20 Hz, we observed both the formation of polydisperse droplets (Fig. 3.5c) as well as monodisperse droplets (Fig. 3.5d). It is interesting to observe the case of $f = 20$ Hz, which corresponds to an imposed wavelength that is exactly twice as long as the fastest growing wavelength, given by $kr_0 \approx 0.7$. Exciting the feed oscillations at twice this wavelength causes the jet to break up into droplets-pairs forming blobs, such as shown in Fig. 3.3(e-f). In this respect, the interaction of forcing frequency and natural frequency of the jet resembles the dynamics reported for the shearing of droplets from a side injection into a microchannel.[22] For the simpler case of an in viscid jet in vacuo, the effect of forcing has been extensively studied in relation to ink-jet printing.[23] Although these results cannot be directly translated to our viscous two-fluid system, they do show that the formation of satellite droplets may be suppressed or

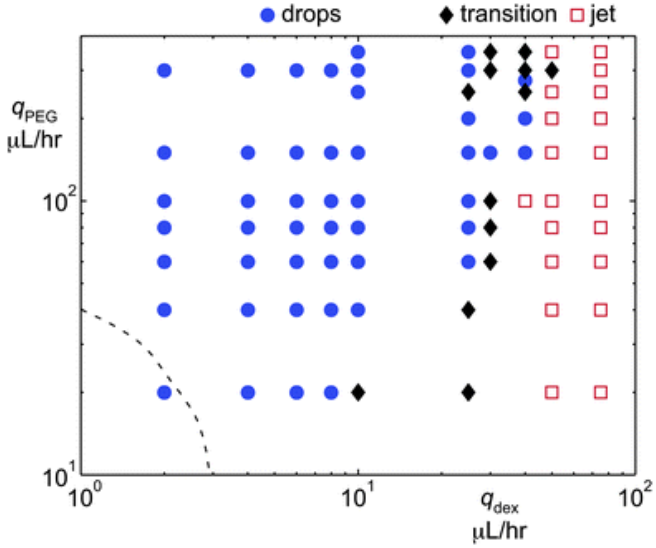

Fig. 3.4 *Experimental phase map of inner flow rate versus outer flow rate, under piezoelectric actuation. The dashed line indicates the calculated drops-jet transition for unforced flow, based on ref. 10, which we confirmed in our experiments without forced oscillations.*

enhanced, depending on the relation between forcing wavenumber and fastest-growing wavenumber, which is qualitatively in agreement with our observations.

It is interesting to note that the location where the jet breaks up into droplets depends on the actuation frequency. For low frequencies, drops form directly at the junction. For frequencies around 10 Hz, drops are released from the jet a distance of a few mm downstream the junction. We observed that this distance increases with frequency. While it is tempting to relate this purely to hydrodynamic stability, another effect is also at play. We observe that as the frequency increases, the amplitude of the initial disturbances decreases. The cause of this damping may be in the piezoelectrics itself, or in the slow elastic response of the PDMS.[24]

To close the discussion on forced droplet formation, we show how drop size depends on the flow rates and the frequency of the sinusoidal voltage applied to the piezo disc. For the monodisperse regime shown in Fig. 3.5e, we plotted the drop diameter as a function of the frequency in Fig. 3.6 for five different flow rates of PEG solution in the range q_{PEG} = 60–84 µl h^{-1}. The flow rate of the dextran solution was fixed at q_{dex} = 6 µl h^{-1}. For fixed values of the flow rates, the graph shows that drop size can be effectively controlled by the frequency.

The frequency and flow-rate dependence on drop size can be understood from the simplest theoretical analysis based on conservation of mass. This analysis teaches that the rate at which the dextran solution flows into the jet, q_{dex}, equals the rate vf_d, at which it leaves the jet as drops, with v the drop volume and f_d the frequency at which drops are generated. We found experimentally that the frequency of drop formation is comparable to the actuation frequency of the piezo disc, $f = f_d$. In some cases (for instance that displayed in Fig. 3.3e) the drop initially released from the jet subsequently split up into two drops. For these cases, the volume v is divided over two equal-sized spherical drops with diameter d.

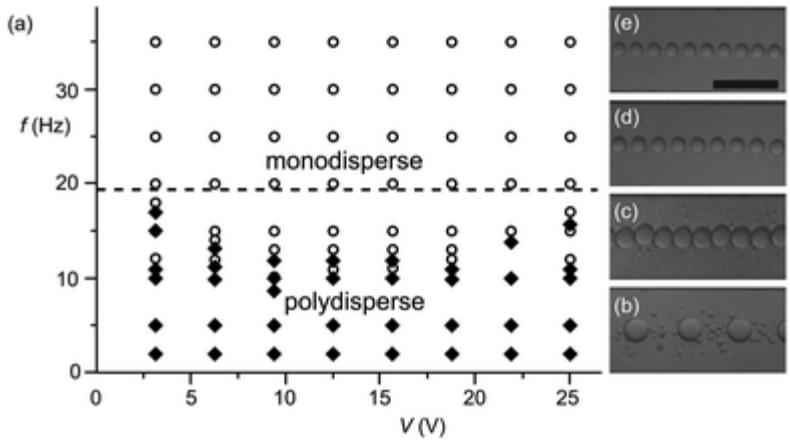

Fig. 3.5 *(a) Influence of amplitude and frequency on the polydispersity of droplets. Solid diamonds: droplets with satellites and polydisperse droplets. Open circles: monodisperse droplets. (b-e) Droplets of dextran solution created in PEG solution by jet break-up with actuation frequencies of (b) 5 Hz (c) 10 Hz (d) 15 Hz (e) 20 Hz. For all experiments, qPEG = 60 µl h-1, qdex = 6 µl h-1, V = 12.5 V. Scale bar: 250 mm.*

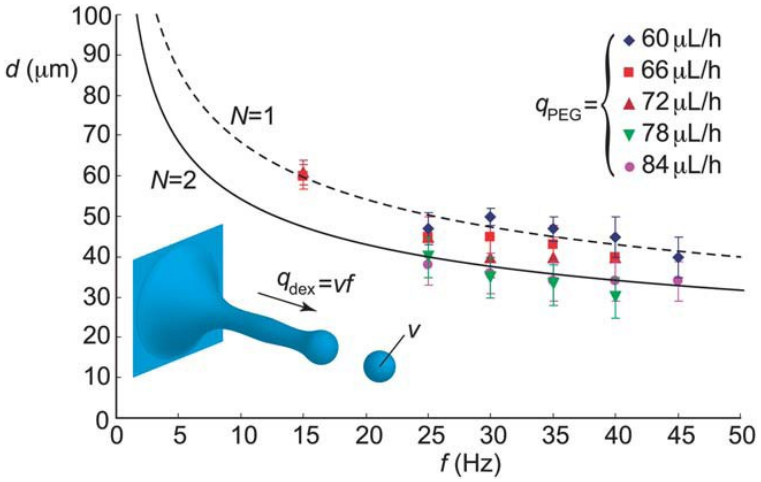

Fig. 3.6 *Diameter of the droplets measured in the monodisperse regime indicated in Fig. 4e as a function of the actuation frequency of the piezo disc for five different flow rates of PEG solution and a fixed rate of flow of dextran solution of qdex = 6 μl h-1. The dashed line is computed for the case that drops initially released from the jet do not subsequently split up into two equal-sized drops (N = 1), whereas the solid line shows the prediction in case split up occurs (N = 2).*

In general, the volume v relates to the final drop diameter as $v = N\pi d^3/6$, where N is either one or two depending on whether this splitting up occurs. The drop diameter hence relates to the flow rate of dextran and the frequency applied to the piezo as $d = (6q_{dex}/N\pi f)^{1/3}$. The prediction of the drop diameter using this simplest model is shown in Fig. 3.6. The dashed line shows the prediction in case the drops initially released from the jet do not subsequently split up ($N = 1$), whereas the solid line shows the prediction in case split up does take place ($N = 2$). Despite its simplicity, this model adequately describes the experimental data.

3.3.3 Microgel formation

With the conditions to generate monodisperse droplets firmly established, we proceed to make hydrogel particles at those conditions. We synthesized a methacrylate derivatized dextran (dex-GMA), of which polymerization of the methacrylate groups leads to the formation of a cross-linked hydrogel in water.[16]

The polymerization occurs via a radical mechanism, which was started by the introduction of the radical initiator ammonium peroxydisulfate via the PEG-rich stream. To accelerate the crosslinking, TEMED was added to the dex-GMA-rich phase. Upon contact of the two phases, APS diffuses to the dex-GMA-rich phase, where it reacts with TEMED to form the radicals that start the crosslinking and hence the gel formation (Fig. 3.7).

We could control the rate of polymerization through the concentration of TEMED. The polymerization, at high concentrations of TEMED, is fast enough to run to completion during the short residence time of the droplets in the PDMS microchip. We ran the reaction while actuating the piezoelectric disc ($V = 15$ V, $f = 35$ Hz), and found no difference in flow behavior with respect to the non-reactive solutions. We collected the microgel beads and

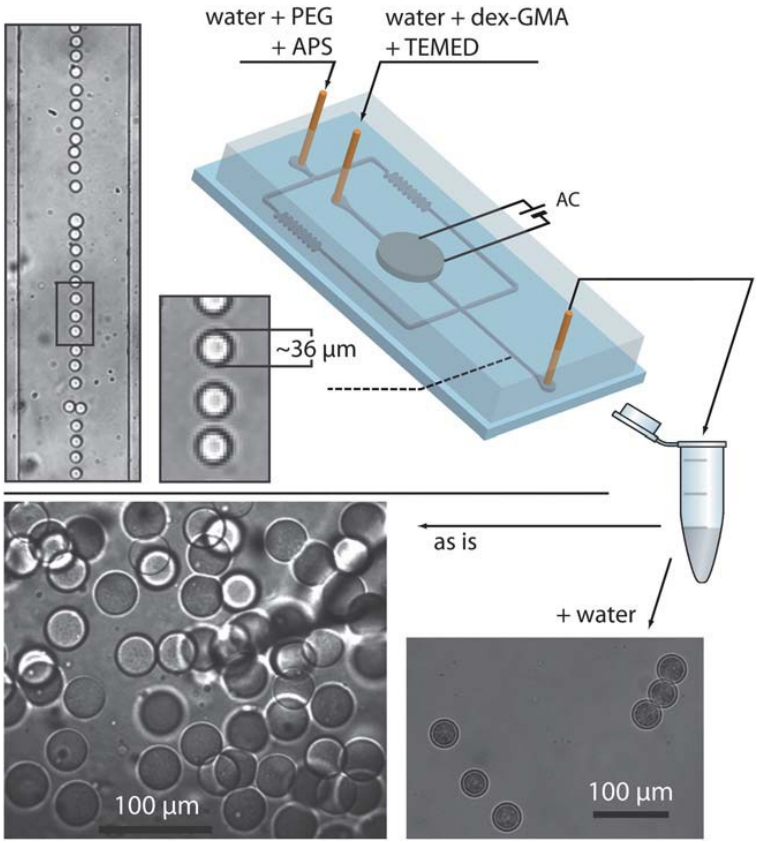

Fig. 3.7 *Hydrogel microsphere formation for aqueous two-phase droplets. We introduce the functionalized dextran-rich phase and the initiator containing PEG-rich phase and create monodisperse droplets on chip. Upon contact, the polymerization immediately starts. The eluent is collected and diluted, such that the two-phase system collapses. That single phase contains microgel bead of the same size as the generated droplets.*

subsequently dissolved them in water. This dilution destroys the two-phase system and causes unpolymerized dextran droplets to dissolve. After polymerization, however, stable beads remained, indicating that the cross-linking of the dextran-rich phase has occurred.

The size of these beads corresponded to the size of the monodisperse droplets produced in the microchannel ($d = 36 \pm 2$ µm).

The hydrogel beads were stable. We manipulated them with micropipettes and subjected them to vortex stirring, dried them on a glass slides and rehydrated them, recovering the round beads that we started with.

3.4 Conclusion and outlook

We presented a method to controllably and reproducibly form monodisperse water-in-water droplets with a diameter in the range between 30 to 60 μm, created by forcing oscillations in the feed with frequencies up to 50 Hz. Droplet sizes can be controlled by the actuation frequency of the piezo disc embedded in our device and the flow rates at which the aqueous solutions are supplied. We also demonstrated the possibility to produce monodisperse hydrogel beads from the same monodisperse droplets.

After demonstrating the potential of microfluidic ATPS in droplet microfluidics, it seems worthwhile to extend the applications to reactions, extractions and encapsulation in this all aqueous environment. We believe the ability to use an aqueous phase to supply drops with chemicals, biomaterials and larger objects like cells and vesicles, or remove those from drops extends the potential of droplet microfluidics enormously.

References

1 P. A. Albertsson, *Nature*, 1956, **177**, 771–774; P. A. Albertsson, Partitioning of Cell Particles and Macromolecules, Wiley, New York, 1986.

2 H. Walter, G. Johansson and D. E. Brooks, *Anal. Biochem*., 1991, **197**, 1–18.

3 M. Yamada, V. Kasim, M. Nakashima, E.J. and M. Seki, *Biotechnol. Bioeng*., 2004, **88**, 489–494; K. H. Nam, W. J. Chang, H. Hong, S. M. Lim, K.D.I. and Y. M. Koo, *Biomed. Microdevices*, 2005, **7**, 189–195; J. R. SooHoo and G. M. Walker, *Biomed. Microdevices*, 2009, **11**, 323–329; M. Tsukamoto, S. Taira, S. YamamuraY. Morita, N. Nagatani, Y. Takamura and E. Tamiya, *Analyst*, 2009, **134**, 1994–1998.

4 G.Münchow, S. Hardt, J. P. Kutter and K. S. Drese*, Lab Chip*, 2007, **7**, 98–102; R. J. Meagher, Y. K. Light and A. K. Singh, *Lab Chip*, 2008, **8**, 527–532.

5 S. Jain, W. T. Yap and D. J. Irvine, *Biomacromolecules*, 2005, **6**, 2590– 2600.

6 R. J. H. Stenekes, O. Franssen, E. M. G. van Bommel, D. J. A. Crommelin and W. E. Hennink, *Pharm. Res*., 1998, **15**, 557–561.

7 E. Tumarkin and E. Kumacheva, *Chem. Soc. Rev*., 2009, **38**, 2161– 2168.

8 G. F. Christopher and S. L. Anna, *J. Phys. D: Appl. Phys*., 2007, **40**, R319–R336; C. N. Baroud, F. Gallaire and R. Dangla, *Lab Chip*, 2010, **10**, 2032–2045.

9 P. Guillot, A. Colin, A. S. Utada and A. Ajdari, *Phys. Rev. Lett*., 2007, **99**, 104502.

10 P. Guillot, A. Colin and A. Ajdari, *Phys. Rev. E*, 2008, **78**, 016307.

11 Y. S. Song, Y. H. Choi and D. H. Kim, *J. Chromatogr. A*, 2007, **1162**, 180–186.

12 Y. H. Choi, Y. S. Song and D. H. Kim, *J. Chromatogr. A*, 2010, **1217**, 3723–3728.

13 J. Xu and D. Attinger*, J. Micromech. Microeng*., 2008, **18**, 065020; A. Bransky, N. Korin, M. Khoury and S. Levenberg, *Lab Chip*, 2009, **9**, 516–520.

14 B. G. De Geest, J. P. Urbanski, T. Thorsen, J. Demeester and S. C. De Smedt, *Langmuir,* 2005, **21**, 10275–10279; A. B. Theberge, F. Courtois, Y. Schaerli, M. Fischlechner, C. Abell, F. Hollfelder and W. T. S. Huck, *Ang. Chem. Int. Ed*, 2010, **49**, 2–25; A. Huebner, S. Sharma, M. Srisa–Art, F. Hollfelder, J. B. Edel and A. J. Demello, *Lab Chip*, 2008, **8**, 1244–1254; B. T. Kelly, J. C. Baret, V. Talyab and A. D. Griffiths, *Chem. Comm*., 2007, 1773–1788; S.-Y. Tech, R. Lin, L.-H. Hung and A. P. Lee, *Lab Chip*, 2008, **8**, 198–220.

15 P. G. Mazzola, A. M. Lopes, F. A. Hasmann, A. F. Jozala, T. C. V. Penna, P. O. Magalhaes, C. O. Rangel-Yagui and A. Pessoa, *J. Chem. Technol. Biotechnol*., 2008, **83**, 143–157.

16 W. N. E. van Dijk-Wolthuis, O. Franssen, H. Talsma, M. J. van Steenbergen, J. J. K. van den Bosch and W. E. Hennink, *Macromolecules*, 1995, **28**, 6317–6322. **17** M. T. Kreutzer, A. Gunther and K. F. Jensen, *Anal. Chem*., 2008, **80**, 1558–1567.

18 B. Dollet, W. van Hoeve, J. P. Raven, P. Marmottant and M. Versluis, *Phys. Rev. Lett*., 2008, **100**, 034504.

19 K. J. Humphry, A. Ajdari, A. Fern_andez-Nieves, H. A. Stone and D. A. Weitz, *Phys. Rev. E*, 2009, **79**, 056310.

20 J. Eggers and E. Villermaux, *Rep. Prog. Phys*., 2008, **71**, 036601.

21 H. A. Stone and M. P. Brenner, *J. Fluid Mech*., 1996, **318**, 373–374.

22 H. Willaime, V. Barbier, L. Kloul, S. Maine and P. Tabeling, *Phys. Rev. Lett*., 2006, **96**, 054501.

23 K. C. Chaudhary and L. Redekopp, *J. Fluid Mech*., 1980, **96**, 257– 274; K. C. Chaudhary and T. Maxworthy, *J. Fluid Mech*., 1980, **96**, 275–286; K. C. Chaudhary and T. Maxworthy, *J. Fluid Mech*., 1980, **96**, 287–297.

24 D. C. Leslie, C. J. Easley, E. Seker, J. M. Karlinsey, M. Utz, M. R. Begley and J. Landers, *Nat. Phys*., 2009, **5**, 231–235.

Slow growth of the Rayleigh-Plateau instability in aqueous two phase systems*

4

Abstract

This chapter studies the Rayleigh-Plateau instability for co-flowing immiscible aqueous polymer solutions in a microfluidic channel. Careful vibration-free experiments with controlled actuation of the flow allowed direct measurement of the growth rate of this instability. Experiments for the well-known aqueous two phase system (ATPS, or aqueous biphasic systems) of dextran and polyethylene glycol solutions exhibited a growth rate of 1 s^{-1}, which was more than an order of magnitude slower than an analogous experiment with two immiscible Newtonian fluids with viscosities and interfacial tension that closely matched the ATPS experiment. Viscoelastic effects and adhesion to the walls were ruled out as explanations for the observed behavior. The results are remarkable because all current theory suggests that such dilute polymer solutions should break up faster, not slower, than the analogous Newtonian case. Microfluidic uses of aqueous two phase systems include separation of labile biomolecules but have hitherto be limited because of the difficulty in making droplets. The results of this work teach how to design devices for biological microfluidic ATPS platforms.

* Published as: I. Ziemecka, S. D. Geschiere (co-first author), V. van Steijn, G. J. M. Koper, J. H. van Esch and M. T.Kreutzer; Slow Growth of the Rayleigh-Plateau Instability in Aqueous Two Phase Systems, *Biomicrofluidics*, 2012, 6, 022007

4.1 Introduction

This paper describes the remarkable features of breakup into droplets, and lack of this breakup, of phase-separating polymer solutions. Cylindrical jets of one fluid inside another fluid are unstable and break up into droplets, as one can easily verify at the kitchen sink by running a thin liquid jet from the faucet. This fluid instability was first described by Plateau and Rayleigh,[1-3] and there is a rich body of literature on the subject.[4] Particularly relevant for this work is the breakup at low Reynolds number[5] and the breakup of a jet that is confined by nearby walls.[6-10] The understanding that emerges from the detailed analysis of these different cases is the following: perturbations of wavelength longer than the circumference of the jet grow with time (or distance traveled by the jet). The growth rate typically has a maximum for a certain wavelength, and except for the purely viscous case, decays to zero as the wavelength goes to infinity. Linear stability analysis of a thread of radius $r = r_0 + \varepsilon e^{\omega t + ikz}/r_0$ yields, for all these situations of varying complexity, dispersion relations $\omega\tau = f(k)$ that give the growth rate ω as a function of the perturbation wavenumber k, normalized on a characteristic time $\tau = \mu r_0/\gamma$ for small Reynolds-number flows.

Many biologically relevant fluids are non-Newtonian. By and large, complex rheology does not markedly change the linear instability on the thread, but it becomes important as the time scale of the flow approaches the relaxation time in the fluid just before pinch-off of droplets. In other words, viscoelasticity of a thread increases the growth rate slightly[11] in the linear (small perturbation) regime, while non-linear terms that dominate when the perturbation has become large, slow down the growth, even suppressing satellite droplet formation and, characteristically, resulting in the longtime survival of thin threads that connect large droplets, much like water droplets on the thread of a spider web.[4] More important is the fact that the threads under axial tension are stable.[12] Unrelaxed axial tension (hereafter: tension) strongly stabilizes a jet for as long as the tension is larger than the capillary pressure in the thread, but after the tension has relaxed the instability kicks in, such that the overall effect is a delay in the onset of instability, not a slowdown of the growth.

Aqueous two-phase systems (ATPS) constitute an especially relevant class of fluids for biological microfluidic applications.[13,14] Beijerinck[15] showed over a century ago that solutions of starch and agar in water form two phases, and many other combinations of incompatible salt or polymer solutions have been found since. The discovery that many labile biomolecules prefer one aqueous phase over the other allows separation of such molecules without denaturation.[16,17] Use of these fluids in droplet microfluidics, in spite of their promise in biochemically relevant separations, has lagged significantly behind the use of aqueous droplets of biological materials surrounded by simpler oils and organic solvents.[18,19] One of the reasons is that controlled and reliable droplet formation has turned out to be difficult. Successful droplet formation in ATPS has, invariably, required external forcing, either mechanically as demonstrated recently by us[20,21] and others[22] or by electrohydrodynamical actuation.[23,24] In other words, relying on the spontaneous formation of monodisperse droplets that is observed in oil/water microfluidic applications fails for aqueous two phase systems. Rather, we and others have observed either threads that survived indefinitely inside the channel without ever breaking up or more erratic droplet formation far downstream. Both are undesired flow behavior for droplet microfluidics.

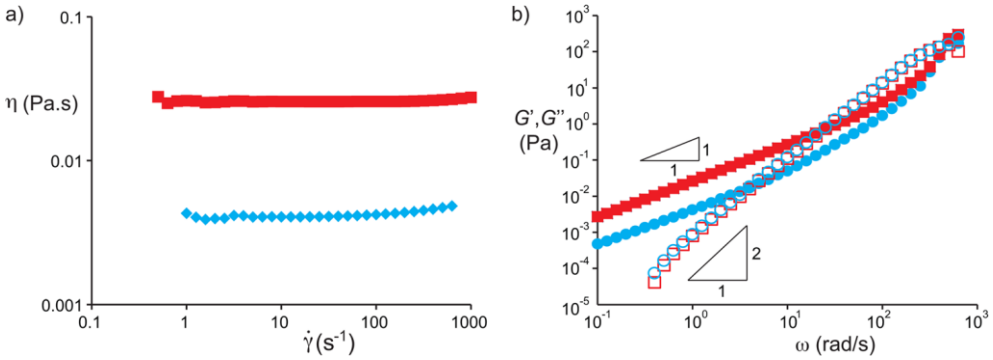

Fig. 4.1 *Rheological properties of the two aqueous polymer solutions: 10% w/w dextran in water (squares) and 7% w/w polyethylene glycol in water (diamonds). (a) Steady shear viscosity versus shear rate. (b) Storage (G') and loss (G") moduli measured in small amplitude oscillatory shear.modulus G'(ω) and loss modulus G"(ω) are plotted in Fig. 4.1(b) for both solutions. From the crossover of G'(ω) and G"(ω), we estimate relaxation times* $\tau_{r,dex} \approx 0.03$ *s and* $\tau_{r,PEG} \approx 0.3$ *s.*

The aim of this work is to quantify the growth rate of ATPS threads and to determine why they can survive without breaking up. On the one hand, we seek to characterize the instability in order to produce better droplet streams. On the other hand, the instability is markedly different from previous studies, and the experiments will guide further theoretical work. We first discuss flow of an analogous Newtonian system and then replace the Newtonian fluids, stepwise, with the aqueous polymer solutions, which by-and-large confirms existing knowledge. We then describe flow focusing of the well-known ATPS of dextran and polyethylene glycol solutions, and we quantify the break-up rate, which is much smaller than that of the equivalent Newtonian case. This is remarkable, because all current theory predicts that the growth rate should be larger. We also find that much more vigorous forcing is required to enhance break-up, compared to the Newtonian case. Finally, we show that eventually gravity becomes important. Even at the tiny density differences of ATPS, the thread sinks, touches the walls, and becomes stable indefinitely.

4.2 Experimental

4.2.1 Fluids used in the experiments

A dextran (dex) solution, 10% w/w (average molar mass 500 kg/mol, Aldrich) and a polyethylene glycol (PEG) solution, 7% w/w (average molar mass 10 kg/mol, Sigma) were prepared by dissolving the polymers in water using ultrasonication. Before injecting the solutions in the microfluidic devices, the solutions were filtered using filters having 0.45 μm pores. The interfacial tension of an ATPS is typically very low compared to the interfacial tension of an oil-water interface. For PEG and dextran, values typically range from several tens of μN/m for short polymers at low concentrations[25] to several hundreds of μN/m for long polymers at high concentrations.[26-28] For our system, the interfacial tension is γ = 0.3mN/m at 25°C, and almost independent of temperature in the range between 4 °C and 40°C[26] The densities of the fluids were ρ_{PEG} = 1018 kg/m^3 and ρ_{DEX} = 1044 kg/m^3. We characterized the rheological properties of the solutions[29] using a rheometer with Couette

geometry (TA Instruments AR-G2) at a temperature of 26 °C. The steady-state shear viscosities for the PEG and dextran solution were 4.4 mPas and 21.4 mPas, respectively, measured for shear rates in the range 1–100 s^{-1} as shown in Fig. 4.1(a).

As Newtonian analogs of the dextran and PEG solutions, we used a water/glycerol mixture with a viscosity of 22 mPas and pure hexadecane, using Tween 20 and Span 80 as surfactants to bring the interfacial tension down to closely match the value of the interfacial tension of the ATPS.[30] The interfacial tension in such systems comprising a surfactant and a co-surfactant can be much lower compared to systems without a co-surfactant. Similar fluids and surfactants have previously been used by Guillot and co-workers[6-8] to study the Rayleigh-Plateau instability of a confined thread of water in oil. High surfactant concentrations ensure that the characteristic time of diffusion near the interface, t, is small compared to the time scale of the breakup process. Estimating the diffusional distance, l, from the ratio of the interfacial concentration, Γ, and the bulk concentration, c, we find $t \sim l^2/D \sim \Gamma^2/Dc^2$. For Span 80, the diffusion coefficient,[31] $D \sim 10^{-11}$ m^2/s, the interfacial concentration,[32] $\Gamma \sim 10^{-6}$ mol/m^2, and the bulk concentration, $c \sim 10$ mol/m^3, such that the diffusion time is of the order of $t \sim 1$ ms, which is much shorter than the time to breakup. This explains why dynamic effects that occur at dilute ($c \sim \Gamma/r_0$) surfactant concentrations[33] do not play a significant role in the breakup dynamics.

4.2.2 Chip fabrication and operation

Fabrication of our microfluidic device was done using soft lithography. In brief, a 4-in. silicon wafer was patterned by exposing a layer of photo-resist (SU8-2050, Micro Resist Technology GmbH, Germany) to UV light through a high-resolution transparency mask containing the two-dimensional design of the microchannel network. This patterned wafer was subsequently used as a master to replicate the structure in poly(dimethylsiloxane) (PDMS). Our microfluidic devices were build up from two layers of PDMS that were prepared using a mixture of prepolymer and curing agent (Sylgard 184, Dow Corning) in a 10:1 ratio by weight. After curing the first 1 mm thin layer, a piezoelectric bending disc (0.5 in. diameter, Piezo Systems, Cambridge, MA) was placed on top of this layer and covered by a second thicker layer of PDMS. In this way, the piezo disc was embedded in the PDMS chip and separated from the fluid reservoir underneath it by an approximately 1mm thin PDMS membrane, see Fig. 4.2. After curing this second layer, the PDMS structure was removed from the master. In the ATPS experiments, channels were sealed by irreversibly bonding a glass slide to the PDMS structure using an oxygen plasma treatment (Harrick PDC-002). In the oil-water experiments, sealing was done against a glass slide precoated with a thin layer of PDMS. After bonding, these devices were baked overnight at 120°C to ensure hydrophobic recovery of PDMS.

To study the interfacial dynamics under forcing, we actuated the piezo-electric bending disc by applying a sinusoidal voltage to the disc. As a result, the disc contracts and relaxes such that fluid is pushed out and pulled into the reservoir underneath the disc. The frequency of the forcing hence equals the frequency of the sinusoidal voltage. To verify that we can control the amplitude of perturbations applied to the thread as well, we measured how the voltage applied to the disc translates into movement inside the main channel. To this end, we placed a bubble inside the main channel that has a height and width of 100 μm and tracked the motion of this bubble under actuation of the piezo disc. We found that the displacement of the bubble is proportional to the amplitude of the AC voltage applied to the disc. Slight differences were observed in the proportionality constant when using different

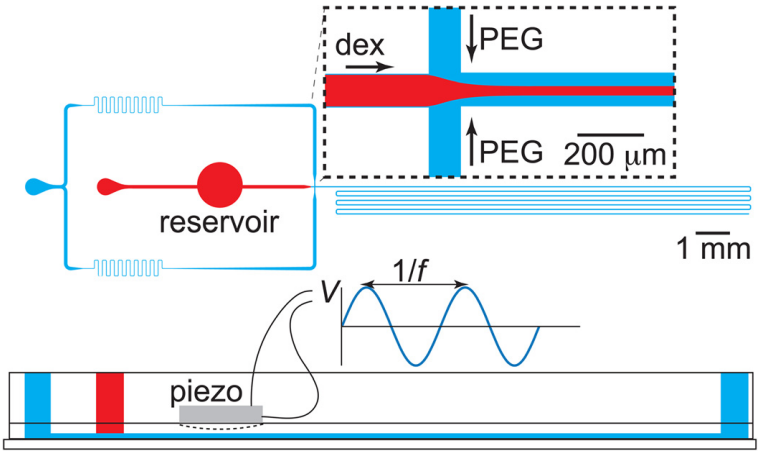

Fig. 4.2 *Top view sketch of the microfluidic device used to study the stability of fluid threads that form when coflowing the two immiscible streams. Both aqueous polymer solutions are injected through separate inlets and meet at a cross junction, after which they flow through a centimeters long channel. On top of the fluid reservoir that has been incorporated in the path between the inlet of the stream of dextran and the junction, a piezo-electric bending disc is positioned as shown in the side view in the bottom of the image. Applying a sinusoidal voltage with amplitude V and frequency f to the disc makes the disc periodically contract and relax, hereby pushing fluid in and out of the reservoir. In this way, the response of the jet to periodic perturbations was studied.*

devices, which can be attributed to differences in thickness of the membrane between disc and fluid reservoir. Modulation of the thread velocity causes the modulation of the thread radius,[34] thus allowing a precise analysis of growth rates from controlled perturbations, of known amplitude and frequency, instead of uncontrolled noisy perturbations.

To prevent any disturbances, other than the intentional ones through the piezo disc, special care was taken in the design of the setup. In particular, we were unable to dampen pulsations from syringe pumps. All experiments were performed on vibration-free optical tables, using gravity to feed the fluids from containers of adjustable height. As a result, the flow rates could not be set in an experiment and were only measured by video analysis after the experiments.

4.3 Results and discussion

4.3.1 Thread break-up of using immiscible Newtonian fluids

We first measure the growth of perturbations using two immiscible Newtonian fluids, which is well understood, before we discuss what happens in ATPS systems. In these experiments, care was taken to closely match conditions and fluid properties to the ATPS system. Fig. 4.3a shows an aqueous thread composed of a solution of glycerol and water, which is focused by a stream of hexadecane. This thread breaks up into droplets 2 mm downstream the focusing section, or, equivalently, after 0.44 s. Before comparing this

breakup time to that observed in ATPS systems in Sec 4.3.3, we first compare this value with the theoretical prediction of the growth rate in the Rayleigh-Plateau instability for confined threads in microchannels by Guillot *et al*.[6] For a thread of radius r_0 and viscosity η_i flowing through a cylindrical channel of radius R and focused by a stream of viscosity η_e, the rate ω at which disturbances grow equals

$$\omega = \frac{\gamma}{16\eta_e R}\frac{F(x,\lambda)(k^2-k^4)}{x^9(1-\lambda^{-1})-x^5} \qquad (4.1)$$

In this equation, k is the dimensionless wavenumber of the perturbation, x is the dimensionless thread radius defined as $x = r_0/R$; λ is the viscosity ratio defined as $\lambda = \eta_i/\eta_e$ and the function $F(x, \lambda)$ is equal to $F(x, \lambda) = x^4(4 - \lambda^{-1}+4\ln x) + x^6(-8+4\lambda^{-1}) + x^8(4-3\lambda^{-1} - (4 - 4\lambda^{-1})\ln x)$. Substituting the values of the fluid properties (η_i = 22 mPas; η_e = 3.3 mPas; $\lambda = \eta_i/\eta_e$ = 6.6; γ = 0.2 mN/m), together with the values for the radii of the thread (r_0 = 14 μm) and the channel (R = 40 μm, x = 0.35), the dispersion relation (Eq. (4.1)) predicts a maximum growth rate of ω ($k \approx 0.7$) $\approx 78s^{-1}$ for the tread shown in Fig. 4.3(a). Assuming that perturbations ε_0 at the entrance initially are of nanometer size and perturb the radius as $r = r_0 + \varepsilon_0 e^{ikz/r_0+\omega t}$ until $\varepsilon_0 e^{\omega t} = r_0$, we predict the break up at $t = \omega^{-1}\ln(13\mu m/1nm)$ = 0.14 s, clearly of the same order of magnitude as the experimentally observed value of t = 0.44 s.

We studied the stability of the thread for different dimensionless thread radii x by moving the feed container of the water/glycerol up and down. Thinner jets break up earlier and become even *absolutely* unstable (i.e., they immediately break up at the junction, as opposed to *convectively* unstable jets that are convected away while the perturbation grows), all in a good agreement with the analysis of confined Newtonian fluids.

The thread breakup in Fig. 4.3(a) occurred without applying external forcing. Fig. 4.3(b) shows what happened when we applied a voltage of 100 mV to the piezo-electric disc. The focusing thread moved visibly in an oscillatory manner with a small amplitude of several micrometers. Note that the voltage is much smaller than the maximum voltage of 180 V. Nevertheless, this small disturbance in the thread velocity was sufficient to reduce the breakup time to less than 0.1 s such that droplets released at the junction as shown in Fig. 4.3(b).

Strong viscoelasticity can have a marked influence on droplet formation. We measured the effect of viscoelasticity of each of the ATPS working fluids in combination with a Newtonian fluid. We both measured a thread of the dextran solution coflowing with hexadecane (γ = 4 mN/m), and with a thread of hexadecane surrounded by a PEG solution (γ = 0.2 mN/m). When PEG was the outer solution, we observed a little change with respect to the fully Newtonian case, and we observed direct droplet formation at the junction for small hexadecane flow rates. When a viscoelastic dextran thread was coflowing with hexadecane, we also observed break up directly at the junction, in agreement with recent reports that dripping at the junction is more prominent in viscoelastic flows.[35] Also, we did not observe delayed dripping or slow necking that is such a distinctive feature of tension in the forming thread.[36] The absence of these directly observable indicators of viscoelasticity leads us to conclude that for our ATPS fluids, the buildup of tension in the thread is small relative to the capillary pressure.

4.3.2 Rayleigh-Plateau instability of the dextran-PEG system

We now consider an experiment with the two aqueous solutions of dextran and PEG, as depicted in Fig. 4.4. A thread of dextran solution of radius $r_0 = 12$ µm is focused in a microchannel of cross section w x h = 100 µm x 100 µm, in the coflowing PEG solution at a velocity $U = 5$ mm/s. This is essentially the same experiment as the one we reported for water/glycerol and hexadecane in Fig. 4.3: the same (steady-shear) viscosities, similar interfacial tension, similar flow rates, and the same channel geometry. The difference is striking: ATPS threads did not break up at a distance comparable to the 2 mm observed in the analogous Newtonian case. The thread in this experiment does break up, erratically, as can be seen from the rough droplets in the channel at the bottom of the micrograph in Fig.4.4(a), after about 40 mm. It hence takes roughly 20 times as long as the Newtonian equivalent.

We first rule out that the long delay of thread break-up is caused by sticking to the wall. When threads do stick to the wall, they are much more stable.[37] To verify whether the thread touches the walls, we imaged the cross section of the channel using a confocal microscope by stacking images taken at different focal planes. We hereby used derivatives of PEG-rhodamine-B and dex-fluorescein to both label the thread and the surrounding fluid and recorded their fluorescence simultaneously. For the thread shown in Fig. 4.4, we found that it flows through the center of the channel and neither touches the top nor the bottom as evident from the inset. For the experiment described here, we rule out sticking of the thread

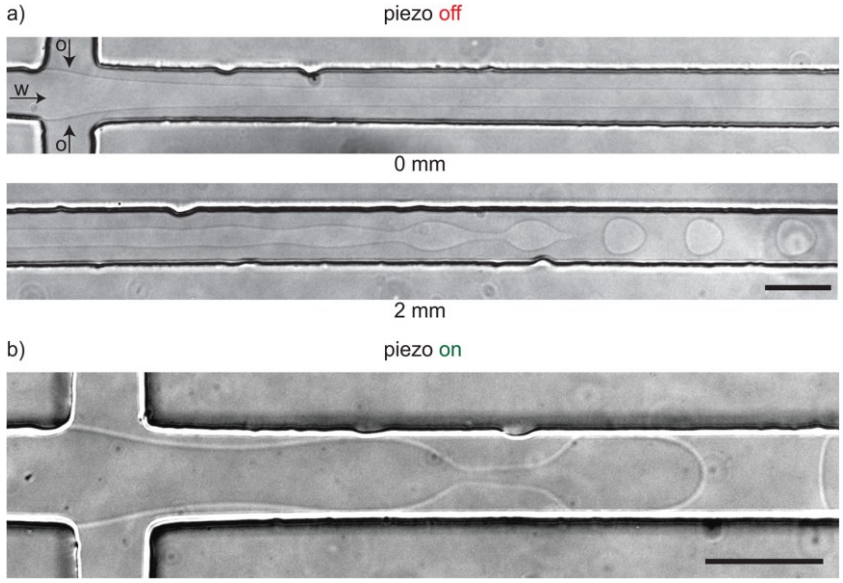

Fig. 4.3 *(a) Without forcing, a non-viscoelastic aqueous thread focused by an immiscible non-viscoelastic oil phase (hexadecane) breaks up into droplets 2 mm downstream of the cross junction in the channel with a square cross section of 80 x 80 µm². This breakup length corresponds well with the theoretical prediction for a confined thread that has an undisturbed radius $r_0 = 14$ µm and flows at a velocity of $U = 4.5$ mm/s). Fluid properties: $\eta_i = 22$ mPas; $\eta_i = 3.3$ mPas; $\gamma = 0.2$ mN/m. (b) The same experiment with the piezo-electric bending disc operating at 100 mV.*

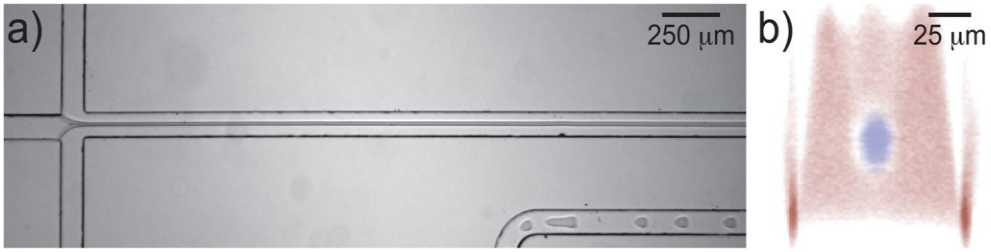

Fig. 4.4 *(a) Without forcing, threads of dextran in PEG are stable over significant lengths, which exceed the theoretically predicted break up lengths by an order of magnitude. Droplets are visible in the bottom right of the micrograph as the channel meanders as indicated in Fig. 4.2. (b) Cross sectional view of the channel taken 2 mm downstream of the cross junction showing that the thread is centered and does not touch the walls.*

to the wall as a stabilizing factor.

Another possible explanation for the enhanced stability would be the build up of elongational stresses during focusing of the thread. As we shall demonstrate below, the enhanced stability is not due to such stresses but is related to the lower growth rate of ATPS systems compared to oil/water systems.

4.3.3 Forced actuation of an ATPS thread

To better understand the observed stability for the ATPS threads, we study the evolution of the perturbations on the surface of the threads. Without applying any external forcing, the disturbances on the interface are not well defined leading to the breakup of droplets of different sizes as shown in Fig. 4.4. Applying a mechanical forcing to the thread such that the fastest growing wavenumber is excited leads to perturbations on the interface with a well-defined shape and wavelength that allows the measurement of growth rates.

Before we show measured values of growth rates, we first discuss the effect of mechanical forcing of the thread. Fig. 4.5(a) shows four frames during one period of a 100-fold more forceful actuation than that in Fig. 4.3(b). Clearly, the liquid-liquid interface moves in and out of the junction over considerable length. Fig. 4.5(b) shows the evolution of the thread downstream of the junction. In the first image, it is clear that the thread buckles a bit, similar in appearance to the buckling observed in expanding channels,[38] and such an overdamped response is not uncommon for threads with strong flow-modulation.[34]

In the first millimeter, the buckled thread straightens out and perturbations do not grow. We show now that this is due to tension in the thread. The tension directly at the junction can be estimated as the product of the extensional viscosity and the extension rate $T = \eta_{E;dex}\,\mathcal{E}$, where we estimate $\mathcal{E} \sim U\,(w-r)/\,w^2$, based on the observation that the thread thins from w to r over a length of order w inside the junction. We were unable to measure the extensional viscosity, which may well be 1000-fold the steady-shear value, leading to a tension at the junction on the order of 100 Pa. This tension relaxes as $T = T_0 \exp(-t/\tau_{r;dex})$. Growth of perturbations remains suppressed until $T \sim \gamma/r_0$, where the cross-over point L_T is given by

$$L_T = \tau_{r,dex} U \ln\left(\frac{\eta_{E,dex} U}{\gamma}\frac{r(w-r)}{w^2}\right) \qquad (4.2)$$

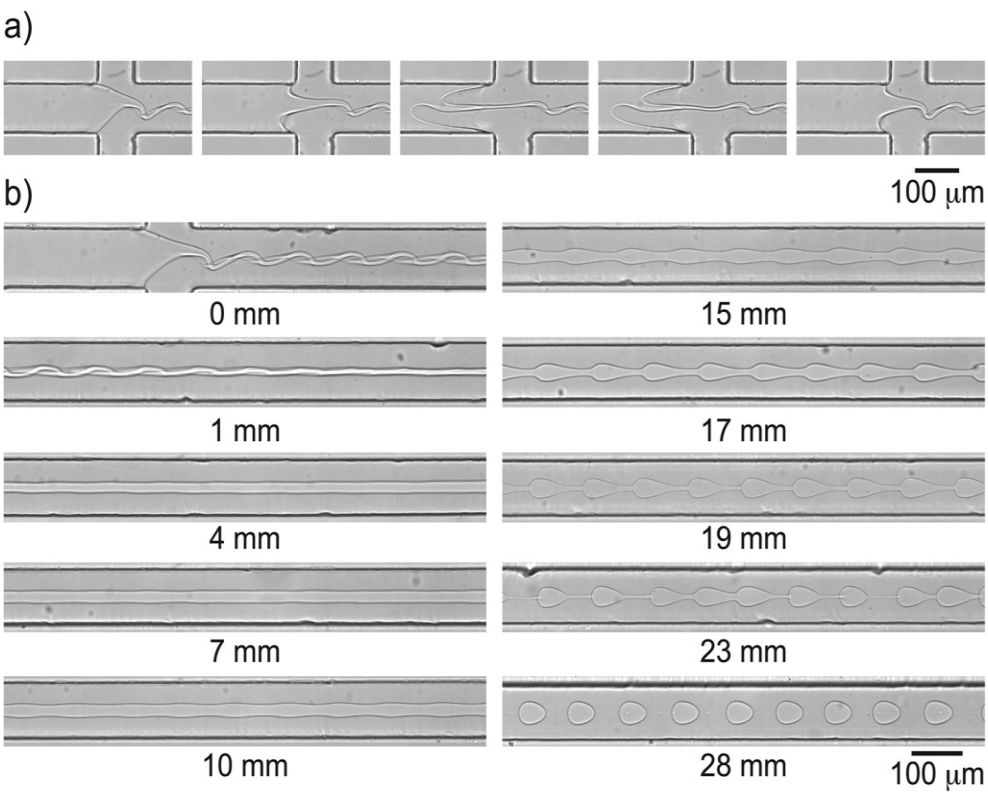

Fig. 4.5 *(a) Actuating the piezo-electric disc using an AC voltage (f = 54 Hz, V = 12.5 V) results in dextran solution being pushed out and pulled into the fluid reservoir underneath the disc, which introduces perturbations on the interface of the thread. (b) Perturbations initially dampen and subsequently grow as shown in the series of micrographs taken at different distances from the inlet. (r_0(4mm) = 12 μm;U = 5.8mm/s.)*

As the extensional viscosity only appears in the logarithm of a large number, it is not important to know the value very precisely. For typical experiments, we find that L_T is of the order of a millimeter. From the full dispersion relation of Ref. 12, we find that the transition from one regime to the next is quite abrupt, so we make little error by approximating that the upstream of L_T, the growth of perturbations is essentially suppressed, whereas for distances downstream larger than L_T, growth is unhindered by tension.

We now discuss the growth rate as determined from Fig. 4.5(b). We measured the amplitude $\delta r(t)$of the perturbation with $t = z/U$ from the distance from the junction and U the centerline velocity. The amplitude increased exponentially with time over the range in which dr was larger than one pixel and small enough do not exhibit the bead-string non-linear effects. From images recorded between 3 mm and 18 mm from the junction, the growth rate was directly calculated as $\omega = d\ln(\delta r/r_0)dt \approx 1 s^{-1}$. We compare this measured growth rate with the theoretical prediction based on Eq. (4.1), $\omega = 90\ s^{-1}$. The difference is almost two orders of magnitude and cannot be explained by experimental error. Elastic

tension in the line cannot explain the discrepancy between the theoretical value and the observed one. Indeed, previous account of the breakup of a viscoelastic jet in a Newtonian fluid shows that the growth rate is as predicted by linear theory after an initial delay.[39] We did observe the same delay for our ATPS system. Strikingly, theory consistently predicts a small increase in the growth rate,[4] whereas we observe the opposite.

One possible explanation for the observed slow growth is the thickness of the interface. Recent computational studies of free-boundary problems have proposed phase-field equations with diffuse interface models, based on the theory that goes back to van der Waals and Cahn and Hilliard.[40-42] For computational efficiency, numerical computations introduce a mesoscale interface thickness that is much larger than realistic for common fluid-fluid interfaces. The thicker interface invariably results in slower growth of interfacial instabilities, compared with sharp interface limits, and recent numerical schemes correct for this.[43,44] Here, however, we know that the diffuse interface of an ATPS is much larger than that of an oil/water interface, at least of the order of the radius of gyration of the polymers, and this thick diffuse interface may explain the slow growth. Such an explanation has the advantage of explaining the lower growth rate, in agreement with the experiments, not a slightly higher one. It also agrees with the observation that the dextran thread readily breaks in hexadecane, where the interface will be sharp, but not in an aqueous PEG solution, where the interface will be diffuse. However, this hypothesis remains untested and is offered here only as a tentative explanation for the observations.

We now describe the effect of actuation amplitude on the growth. The amplitude in Fig. 4.5 was 12.5 V, and the forced buckling died out under tension before it could grow. The decay of the perturbation occurs on a viscous time scale,[34] which we estimate as $\rho(U/f)^2/\eta_{dex}$, where the wavelength is based on the thread velocity U and actuation frequency f as (U/f). This actual decay time, by this estimate, is on the order of several microseconds for our experiments and increases with increasing voltage.
The decay time for tension, however, is longer, on the order of 10 or 100 ms. In other words, provided the perturbations are small, they die out before they can grow. Fig. 4.6(a) shows the amplitude $\delta r(t)$ of perturbations on the interface obtained by taking pictures at different distances from the inlets and measuring the amplitude as shown on the inset. Increasing the amplitude V of the voltage applied to the piezo disc yields larger perturbations at the mixing section such that the thread breaks closer to the inlet. Importantly, the growth rate is independent of voltage. Voltages smaller than those used in Fig. 4.5 moved the break-up further downstream by only 2–3 mm, indicating that the actuation is dissipated before the tension has relaxed. For higher voltages on the piezo-electric bending disc, however, the break-up occurs faster, but this is only due to a higher initial disturbance, not due to a faster growth.

The inset in Fig. 4.6 shows how the initial amplitude (obtained by extrapolating the growth curve to $t \approx 0.2$ s, i.e., to the end of the region under tension) increases linearly with applied voltage above a threshold value and has a minimum value of several tens of nanometers below that. It is striking that this length agrees with typical thicknesses of ATPS interfaces.[45] Clearly, provided that the amplitude at the junction is large enough, the perturbations can outlive the viscous decay while the thread is under tension. It is this regime that is most useful for the production of monodisperse droplets.

Finally, downstream of the linear growth range, we find the typical beads-on-string pattern for viscoelastic fluids with the slow ultimate stage of breakup, which happens in Fig. 4.5(b) 28 mm downstream of the junction.

4.3.4 Long-time fate of the thread: Gravitational effects

The growth rates recorded in Figs. 4.5 and 4.6 were measured under conditions that the thread did not touch the walls before break-up, as verified by confocal images similar to that in Fig. 4.4(b). In our ATPS, the density difference between the two dilute aqueous polymer solutions is small, $\Delta\rho = 25$ kg/m^3, such that the thread that was initially in the center of the channel does not sink quickly to the bottom of the channel. However, especially without actuation, the break-up time is so long that it competes with the settling time. In Fig. 4.7(a), we show a micrograph of such a thread that touches the bottom wall far downstream of the cross junction.

This stabilizes the thread, which runs from flow-focusing junction through the 160 mm long microfluidic channel all the way to the exit without breaking. We measured how fast the thread settles by taking confocal scans at different distances z from the inlet as shown in Fig. 4.7(b). From those scans, we could measure the height of the center of the thread h, which we plot as a function of the distance z in Fig. 4.7(c). The thread slowly settles and touches the bottom roughly $z = 76$ mm downstream of the inlet. The exact location where the thread touches the bottom depends on the thickness of the thread, as does the moment of breakup. For relatively thick threads ($x > 0.4$), we found that the thread always settled quicker than it breaks up, whereas for thin threads break up occurred before

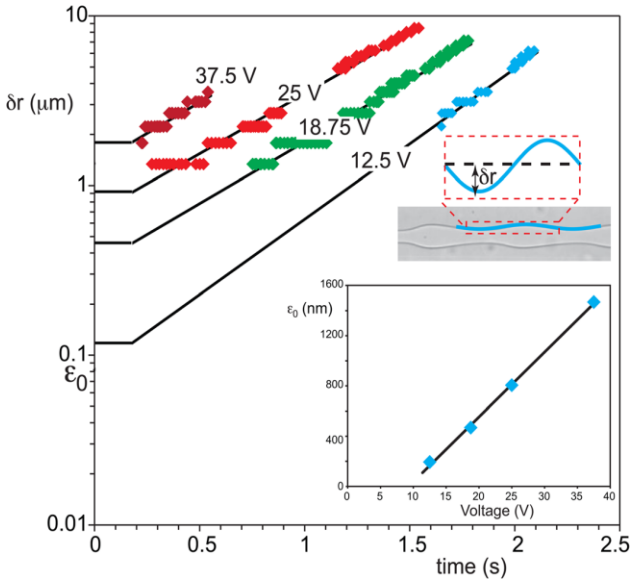

Fig. 4.6 *Amplitude of perturbations on the interface as a function of flow time for different actuation amplitudes. The lines are fitted to the experiments and are matched to horizontal lines that represent the zero-growth under tension immediately after the junction ($0 < t < 0.1$s). Inset: initial perturbation amplitude ε_0 as a function of the amplitude of the voltage applied to the piezo-electric disc. ($r_0 = 16$ μm; $U = 4.5$ mm/s; $f = 28$ Hz.)*

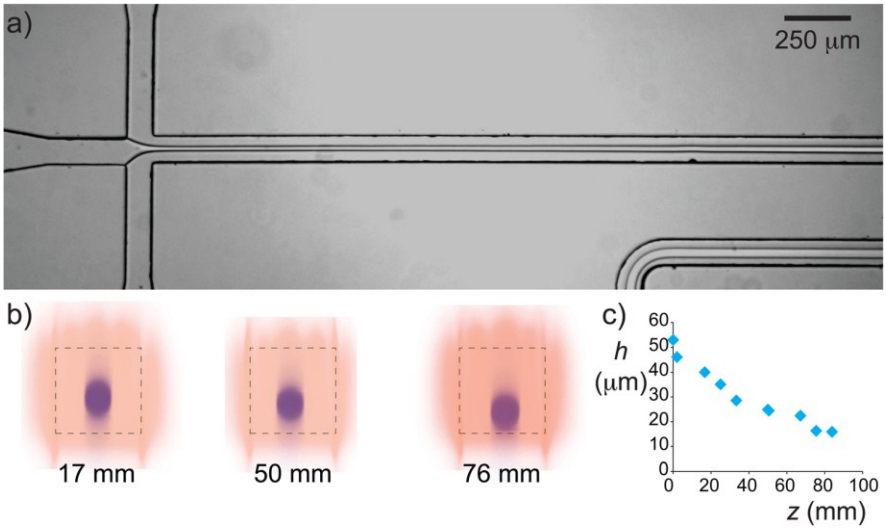

Fig. 4.7 *(a) Micrograph showing a stable thread of dextran in PEG. The slightly larger density of the dextran solution results in settling of the thread as shown in the confocal scans in (b), which were taken at different distances downstream of the cross junction. The plot of the center of the thread h as a function of the distance away from the inlet shows that the thread sticks to the bottom roughly 76 mm downstream of the mixing section.*

the thread touches the wall. From a practical point of view, the use of a mechanical actuator such as the piezo disc used in this work reduces the breakup length such that threads that would otherwise touch the walls can be broken up into droplets.

4.4 Conclusion

We have shown that aqueous two-phase systems have much slower interface dynamics in comparison with Newtonian oil/water mixtures. Careful vibration-free experiments with controlled actuation of the flow into a microfluidic flow focusing device allowed direct measurement of the growth of the Rayleigh-Plateau instability. Our experiments show that the growth rate of perturbations of a confined thread is two orders of magnitude smaller than predicted by theory. Experiments with all-Newtonian fluids of similar viscosity and interfacial tension show that this is not caused by fluid properties. The large discrepancy between theory and experiment, therefore, can only be explained by interfacial properties. Indeed, the interface of an ATPS is much more complex than the interface between oil and water and hence has a dynamic response on its own account that will require further theoretical analysis, for which the present work gives crucial experimental data. Comparison with experiments where a viscoelastic jet flows inside a hexadecane jet shows that viscoelasticity of the fluids also does not account for this difference, but viscoelasticity does explain the initial dampening of perturbations. From a more practical point of view, the results of this work are useful in the design of microfluidic devices that use parallel streams or droplet flows to exploit the separation possibilities of aqueous two-phase systems.

References

1 J. Plateau, Statique Experimentale et Theoretique des Liquides Soumis aux Forces Moleculaires (Gautier-Villars, Paris, 1873).

2 L. Rayleigh, *Proc. R. Soc. London, 1879,* **29**, 71.

3 L. Rayleigh, *Philos. Mag*., 1892, **34**, 145.

4 J. Eggers and E. Villermaux, *Rep. Prog. Phys*., 2008, **71**, 036601.

5 S. Tomotika, *Proc. R. Soc. London, Ser. A*, 1935, **150**, 322.

6 P. Guillot, A. Colin, A. S. Utada, and A. Ajdari, *Phys. Rev. Lett.*, 2007, **99**, 104502.

7 P. Guillot, A. Colin, and A. Ajdari, *Phys. Rev. E*, 2008, **78**, 016307.

8 M. A. Herrada, A. M. Gan˜a´n-Calvo, and P. Guillot, *Phys. Rev. E*, 2008, **78**, 046312.

9 K. J. Humphry, A. Ajdari, A. Fernandez-Nieves, H. A. Stone, and D. A. Weitz, *Phys. Rev. E*, 2009, **79**, 056310.

10 Y. Son, N. S. Martys, J. G. Hagedorn, and K. B. Migler, *Macromolecules, 2003,* **36**, 5825.

11 M. Goldin, J. Yerushalmi, R. Pfeffer, and R. Shinnar, *J. Fluid Mech*., 1969, **38**, 689

12 S. L. Goren and M. Gottlieb, *J. Fluid Mech*., 1982, **120**, 245.

13 S. Hardt and T. Hahn, *Lab Chip*, 2012, **12**, 434.

14 J. P. Frampton, D. Lai, H. Sriram, and S. Takayama, *Biomed. Microdevices*, 2011, **13**, 1043.

15 M. W. Beijerinck, *Zentralbl. Bakteriol*., 1896, **2**, 698.

16 P. A. Albertsson, *Nature(London)*, 1956, **177**, 771.

17 P. A. Albertsson, Partitioning of Cell Particles and Macromolecules (Wiley, New York, 1986).

18 K. Vijayakumar, S. Gulati, A. J. deMello, and J. B. Edel, *Chem. Sci*., 2010, **1**, 447.

19 M. Yasukawa, E. Kamio, and T. Ono, *ChemPhysChem* , 2011, **12**, 263.

20 I. Ziemecka, V. van Steijn, G. J. M. Koper, M. Rosso, A. M. Brizard, J. H. van Esch, and M. T. Kreutzer, *Lab Chip*, 2011, **11**, 620.

21 I. Ziemecka, V. van Steijn, G. J. M. Koper, M. T. Kreutzer, and J. H. van Esch, *Soft Matter* , 2011, **7**, 9878.

22 D. Lai, J. P. Frampton, H. Sriram, and S. Takayama, *Lab Chip,* 2011, **11**, 3551.

23 Y. S. Song, Y. H. Choi, and D. H. Kim, *J. Chromatogr. A*, 2007, **1162**, 180.

24 Y. H. Choi, Y. S. Song, and D. H. Kim, *J. Chromatogr. A*, 2010, **1217**, 3723.

25 J. Ryden and P. A. Albertsson, *J. Colloid Interface Sci*., 1971, **37**, 219.

26 D. Forciniti, C. K. Hall, and M. R. Kula, *J. Biotechnol*. 1990, **16**, 279.

27 M. R. Helfrich, M. El-Kouedi, M. R. Etherton, and C. D. Keating, *Langmuir* , 2005, **21**, 8478.

28 Y. Liu, R. Lipowsky, and R. Dimova, *Langmuir, 2012,* **28**, 3831.

29 R. G. Larson, *The Structure and Rheology of Complex Fluids* (Oxford University Press, USA, 1998).

30 M. Hashimoto, P. Garstecki, H. A. Stone, and G. M. Whitesides, *Soft Matter*, 2008, **4**, 1403.

31 J. R. Campanelli and X. Wang, *J. Colloid Interface Sci*., 1999, **213**, 340.

32 R. K. O. Apenten and Q.-H. Zhu, *Food Hydrocolloids*, 1996, **10**, 27.

33 S. Hansen, G. W. M. Peters, and H. E. H. Meijer, *J. Fluid Mech*., 1999, **382**, 331.
34 D. W. Bousfield and M. M. Denn, *Chem. Eng. Commun*., 1987, **53**, 61.
35 J. M. Montanero and A. M. Ganan-Calvo, *J. Fluid Mech*., 2008, **610**, 249.
36 P. E. Arratia, J. P. Gollub, and D. J. Durian, *Phys. Rev. E*, 2008, **77**, 036309.
37 E. Castro-Hernandez, W. van Hoeve, D. Lohse, and J. M. Gordillo, *Lab Chip*, 2011, **11**, 2023.
38 T. Cubaud, B. M. Jose, and S. Darvishi, *Phys. Fluids*, 2011, **23**, 042002.
39 D. W. Bousfield, R. Keunings, G. Marrucci, and M. M. Denn, *J. Non-Newtonian Fluid Mech*., 1986, **21**, 79.
40 J. Lowengrub and L. Truskinovsky, *Proc. R. Soc. London, Ser. A* , 1998, **454**, 2617.
41 H. Lee, J. Lowengrub, and J. Goodman, *Phys. Fluids*, 2002, **14**, 492.
42 H. Lee, J. Lowengrub, and J. Goodman, *Phys. Fluids* , 2002, **14**, 514.
43 R. Folch, J. Casademunt, A. Hernandez-Machado, and L. Ramirez-Piscina, *Phys. Rev. E*, 1999, **60**, 1724.
44 R. Folch, J. Casademunt, A. Hernandez-Machado, and L. Ramirez-Piscina, *Phys. Rev. E*, 1999, **60**, 1734.
45 S. H. S. Lee, P. Wang, S. K. Yap, T. A. Hatton and S. A. Khan, *Biomicrofluidics*, 2012, **6**, 022005.

All aqueous core-shell droplets produced in a microfluidic device*

5

Abstract

This chapter presents a microfluidic method to compartmentalize aqueous polymer solutions within water-in-water microdroplets, which are continuously generated without using organic solvents or surfactants. Phase separation inside the drops yields all-aqueous core-shell structures (water-in-water-in-water), as we demonstrate using the aqueous two phase system of polyethylene glycol and dextran.

* Published as: I. Ziemecka, V. van Steijn, G. J. M. Koper, M. T. Kreutzer and J. H. van Esch; All-aqueous core-shell droplets produced in a microfluidic device, Soft Matter, 2011, 7, 9878-9880

5.1 Introduction

Aqueous two phase systems (ATPS) are a biocompatible soft-matter in which all constituent phases share water as the common solvent, but differ in their dissolved components. These phases are immiscible due to the incompatibility of the components[1] and are separated by a diffuse interface that can be readily crossed by molecules without denaturation, whether they are charged or uncharged, large or small, hydrophobic or hydrophilic. This permeability combined with the low interfacial tension (typically in the μN/m-range) makes ATPS ideal for partitioning and separation of proteins, enzymes and cells.[1,2]

Recently, ATPS have been exploited for micro-compartmentation in synthetic cells with relevant biomimetic features. The phase separation of two immiscible aqueous polymer solutions inside liposomes and polymerosomes[3] led to different osmosensitive compartments with an uneven distribution of dissolved proteins. However, exchange between the inside and the outside of the vesicles is limited to water and small uncharged molecules because of the presence of a semipermeable bilayer membrane. The ability to extend the exchange to biomolecules and ions will greatly enhance the possibilities in synthetic cell studies. In microfluidics, ATPS have been limited to lamellar flows. Only recently, we and others succeeded in the controlled formation of ATPS microdroplets in a microfluidic device.[4–6] However, the microstructuring of such droplets remains an open challenge. In this work, we present a microfluidic method for the creation of all-aqueous core-shell droplets, i.e. a confined phase separated ATPS dispersed in an environment free of organic solvents and surrounded by no membrane at all.

Microfluidics offers the well-controlled environment that allows the precise formation of monodisperse microdroplets and double emulsions,[7] and subsequent manipulation and study thereof, e.g. as vehicles for high-throughput screening[8] or as templates for the synthesis of particles and capsules, notably hydrogels for drug delivery and tissue engineering.[9] For oil-based single and double emulsions, these microfluidic methods are robust and well-developed. In sharp contrast, the few first examples of ATPS (water-in-water) droplets and emulsions just appeared. Although the rheological and interfacial properties of ATPS that prevent facile emulsification are not properly understood, droplets can be generated using additional electrical or mechanical actuation of the fluids.[4,5] Without such actuation, drop formation is erratic, if it occurs at all, and does not resemble the monodisperse oil-based drops that spontaneously form at similar flow rates, viscosities and surface tension. With the aid of an oil phase, it is possible to generate water-in-water-in-oil (W/W/O) emulsions,[6] but without lipids, surfactants or an oil phase, it has not been possible to create more complex all-aqueous entities such as the W/W/W double emulsion that we demonstrate here.

5.2 Experimental

The method we used for the forced formation of all-aqueous double emulsions is illustrated in Fig. 5.1. The device (Fig 5.2) consists of a series of three flow focusing junctions,[10] in which four aqueous streams are injected, two solution of 10 w/w % dextran (MW = 500,000, from Leuconostoc spp., Sigma BioChemika) in water and two solutions of 7% polyethylene glycol (PEG, MW = 10,000, Aldrich) in water. These molecular weights

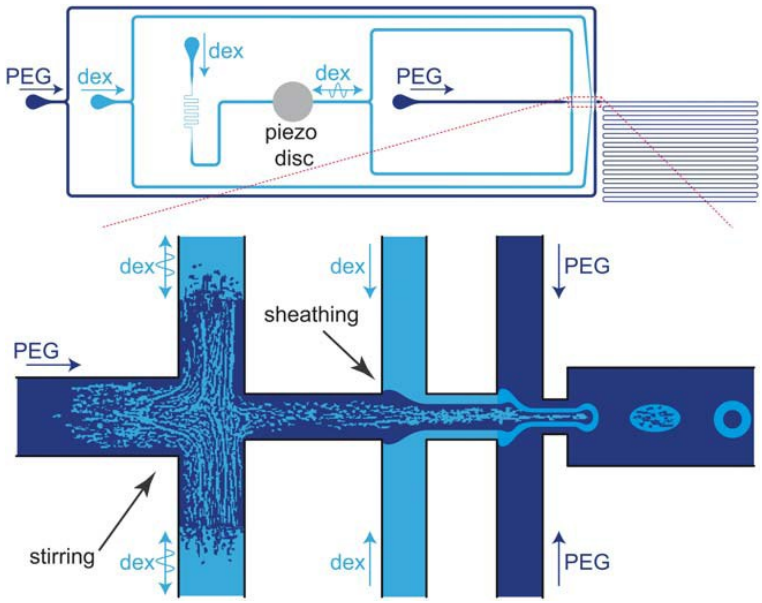

Fig. 5.1 *Microfluidic device used for the forced formation of water-in-water-in-water microdroplets. Aqueous drops containing a solution of PEG and dextran form at the downstream junction. Phase separation inside the drops yield double emulsion drops with a core of PEG and a shell of dextran. Actuation of the piezo electric bending disc causes pulsations in the flow, which are essential to release drops from the fluid thread as well as to stir PEG and dextran at the first junction.*

were chosen arbitrarily. Other combinations could have been used as well, as PEG and dextran are well known to phase separate over a wide range of molecular weights.[11]

The viscosities of the dextran-rich and PEG-rich phases are 22 mPas and 4.6 mPas, respectively, and the interfacial tension is $\gamma = 0.3$ mN/m.[12] The pH of the dextran-rich and PEG-rich solutions are 7.0 and 5.3 respectively and the ionic strengths of the solutions are relatively small. High-precision syringe pumps (Harvard Apparatus, 11 pico plus) are used to drive the fluids from 1 ml syringes (BD plastic) into the microfluidic device. Drops form at the most downstream junction by merging a stream of PEG with a stream that contains a mixture of PEG and dextran. This mixture phase-separates inside the drops a few cm downstream of the drop maker yielding double emulsion droplets with a core of PEG and a shell of dextran.

5.3 Results and discussions

Key to the method is the forcing we apply to one of the streams. Without this forcing, the immiscible streams flow in parallel without the formation of drops as shown in Fig. 5.3a. Due to uncontrolled disturbances in the system, the thread only sporadically breaks up into a short sequence of drops far from the inlet (> 0.5 mm) such that only roughly 10% of the volume of the fluids to-be-encapsulated ends up in droplets.

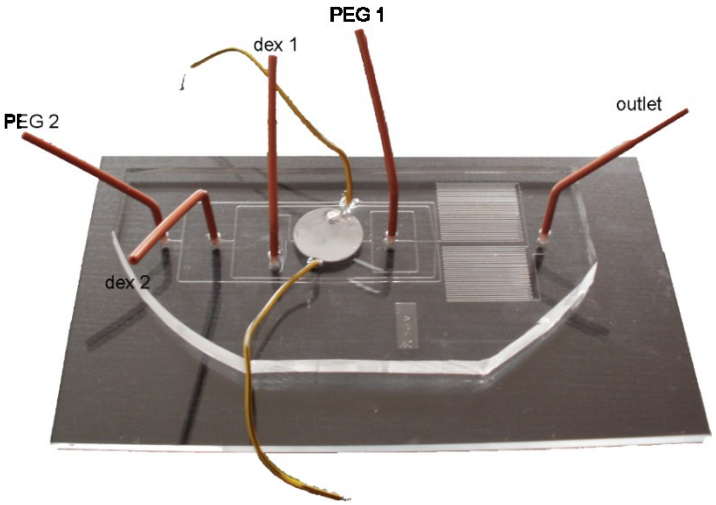

Fig. 5.2 *PDMS-on-glass chip used for the forced formation of core-shell double emulsions all aqueous microdrops. Solutions of PEG and dextran are fed into the four orange tubes on the left. Forced formation occurs by the contraction of a piezo electric bending disc embedded in the PDMS, which is actuated by applying a sinusoidal voltage to it through the two yellow wires. After their formation, drops flow through a channel with a length of 80 cm before leaving the device through the exit tube.*

To generate drops in a controlled way, we intentionally introduce fluctuations in the flow rate of one of the streams using a piezo electric bending disc (0.5 in. diameter, Piezo Systems, Cambridge, MA). The disc is embedded in our PDMS device and placed on top of a fluid reservoir, which connects the inlet of one of the two dextran stream to the first junction as shown in Fig. 5.1. Applying a sinusoidal voltage to the disc causes the disc to periodically contract, thereby pushing fluid out of the reservoir (Fig. 5.3b–d) and pulling it back in (Fig. 5.3e–g). This motion causes the threads running through the central channel with square cross section of 100 x 100 μm^2 to inflate (Fig. 5.3c) and thin out (Fig. 5.3f) at the second and third junction, which results in folding of the thread and the release of drops as shown in Fig. 5.3d and 5.3g. The frequency at which drops release closely resembles the actuation frequency of the piezo disc and we are able to produce drops at throughput between 12 and 45 drops per second in our device.The total volume of the drops, which consist of a core of PEG and a shell of dextran (see Fig. 5.4), follows from the actuation frequency f and the sum of the flow rates, q, at which PEG and dextran flow into the thread ($q = q_{PEG1} + q_{dex1} + q_{dex2}$) as $V=q/f$. Conversely, the diameter equals $d = (6q/f\pi)^{1/3}$. To verify this relation, we measured the diameter for several different flow rates q_{dex2}. As shown in Fig. 5.4, the experimental data agrees well with this simple description and teaches one that the total size of the droplets can be effectively tuned by tuning the rates of flow. The volume of the core can be estimated as $V_{core} = q_{PEG1}/f$. For all measurements in Fig. 5.4, this leads to a predicted value of 3 pl, or, equivalently, a diameter of 18 µm, which is close to the observed value of 15 µm.

The back-and-forth motion induced by the piezo disc not only forces the break up into drops. The oscillatory motion also folds separate streams of PEG and dextran into each other, thus mixing them on-chip. These streams are stirred at the first junction and

encapsulated into the drops at the third junction. The additional dextran stream introduced from the side at the second junction hereby acts as a sheath layer and prevents PEG in the central channel to merge with the PEG stream introduced at the third junction. The on-chip mixing of the polymer solutions is superior to injection of a single premixed PEG-dextran solution, because such premix solution would phase separate inside a syringe within 10 min. We emphasize here that stirring is most effective when perturbing the dextran stream that flows into the first junction – perturbing the first PEG stream resulted in much less mixing. The device produces a steady stream of droplets for hours, ending the experiments when the syringes are empty.

Immediately after formation at the third junction, drops consist of a mixture of PEG and dextran and appear as a single phase as shown in Fig. 5.5a. This mixture readily phase separates as evident from the micrograph in Fig. 5.5c, which was taken 2 cm downstream of the drop maker, or equivalently 7 s after formation. We stress that the drops only give the appearance of a single phase – it can be that the stirring has not mixed the phases all the way down to a molecular level. In any case, the later stages of growth of phase-separated volumes are visible.

The most likely mechanisms are Ostwald ripening and coalescence.[13] Ostwald ripening is slow due to the low surface tension and small diffusion coefficients of the polymers, and this effect is probably operative only in the early stages (Fig. 5.5a–c). The later stages exhibit a more rapid growth than the characteristic Lifshitz-Slyozov growth of Ostwald ripening. Coalescence of drops is prominent in these later stages (Fig. 5.5c–e). There is motion inside the drop and convection induced random walk drastically increases the likelihood that droplets meet and merge.[14] Without motion, the phase separation by coalescence occurs much slower: when we mixed our fluids and stored it without flow, it took several minutes to obtain phase separation.

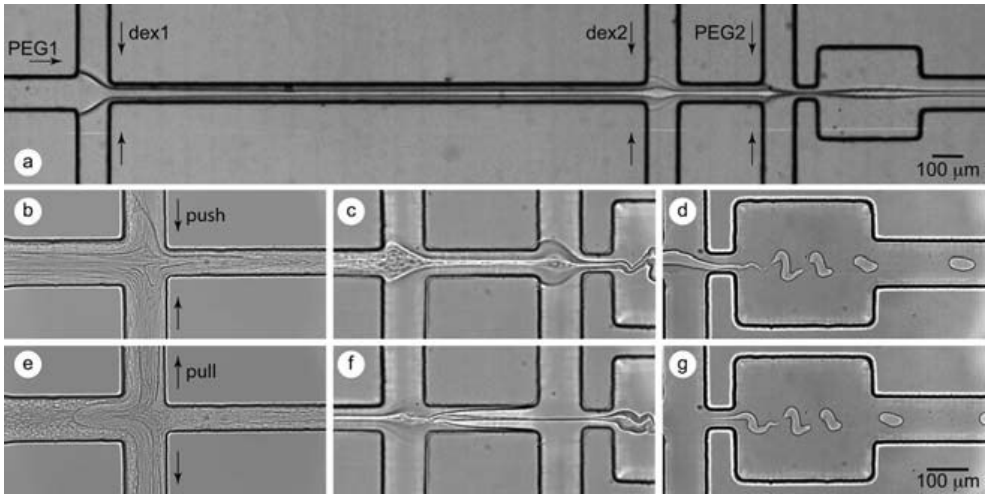

Fig. 5.3 *(a) Without forcing, the immiscible aqueous streams flow in parallel without the formation of drops. (b–g) High-speed camera snapshots at individual junctions: Actuating the piezo electric disc using a sinusoidal voltage with amplitude 93 V and frequency 16 Hz results in a pushing (b–d) and pulling (e–g) motion and the periodic break up of drops. Conditions:* $(q_{PEG1}, q_{dex1}, q_{dex2}, q_{PEG2}) = (0.18, 0.18, 4.2, 60)$ *µl/h.*

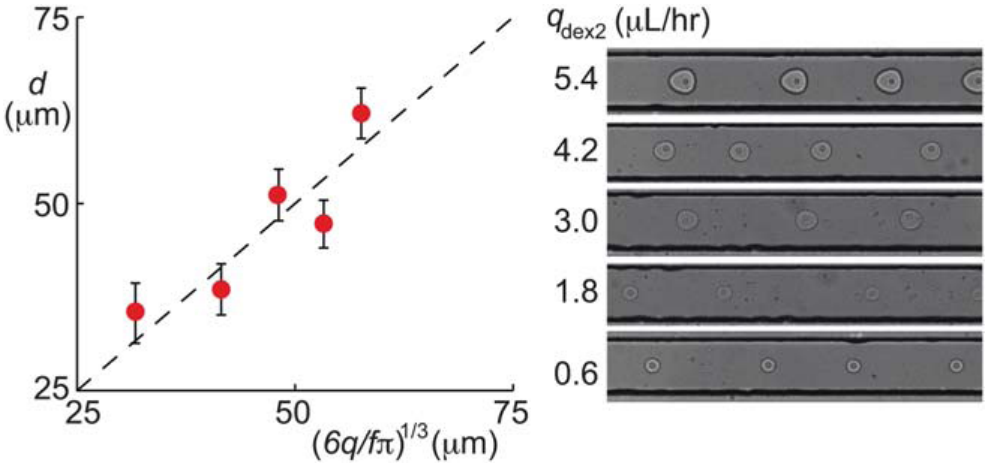

Fig. 5.4 *The diameter of double emulsion drops depends on the actuation frequency and the sum of the flow rates at which PEG and dextran flow into the thread as* $d = (6q/f\pi)^{1/3}$. *Symbols in the graph represent measurements of the diameter 4 cm from the inlet and the dashed line shows parity. The error bars represent the standard deviation of an ensemble of at least 100 drops as measured from micrographs shown on the right. Conditions:* $(q_{PEG1}, q_{dex1}, q_{dex2}, q_{PEG2}) = (0.18, 0.18, 0.6–5.4, 69)$ *μl/h. Actuation frequency: 16 Hz.*

Here, complete phase separation was observed 4 cm (14 s) downstream of the drop maker, see Fig. 5.5e. The aqueous polymer solutions inside the drops organized such that a PEG-rich core is surrounded by a dextran-rich shell. The average core diameter and shell thickness were 15 ± 1.5 μm and 17.5 ± 1.6 μm respectively.

Obviously, these core shell particles are thermodynamically unstable and return in time to their more stable microscopically phase-separated state. Nevertheless, the core-shell configurations were stable all the way up to the exit of the device, 80 cm (5 min) downstream of the drop maker. Only sporadically, droplets lost their core when merging with other droplets. To measure how long the double emulsion droplets kept their core-shell structure, we stopped the flow and observed their size and shape. After roughly 20 min, all droplets lost their PEG core, which escaped from the dextran shell and merged with the surrounding PEG solution. Importantly, we did not observe a notable change in size and shape of the double emulsion droplets during this period until the core escaped in agreement with the very slow Ostwald ripening for long chain polymers. The escape on the other hand is very fast and happens within a second upon contact between the PEG core and the surrounding PEG solution. The period over which the double emulsion drops are stable depends on the properties of the solution, such as the densities, the pH and the ionic strengths. For instance, we observed that adding large amounts of salt to the surrounding PEG phase resulted in an almost immediate collapse of the core-shell droplets. Being stable for at least ten minutes ensures a sufficiently long time window essential for downstream processing of the drops, for instance when using the double emulsion drops as template to form biocompatible capsules by online polymerization of the shell. We emphasize here that the production of hydrogel particles and capsules in an organic-solvent free environment has advantages over existing oil-based methods, as it reduces denaturation of encapsulated

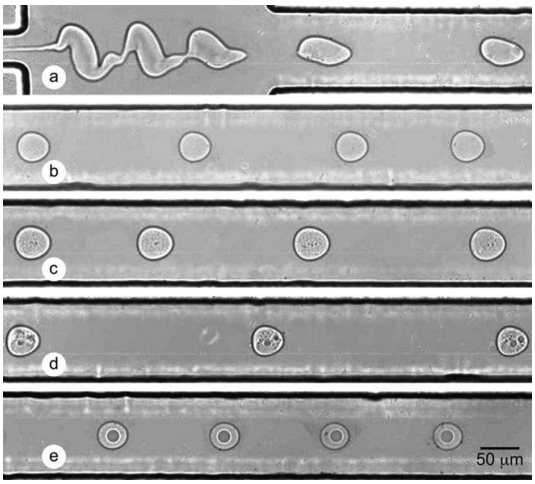

Fig. 5.5 *Drops contain a solution of PEG and dextran that phase separates while the drops flow through the channel resulting in drops with a core of PEG and a shell of dextran. a) 0 mm, b) 0.5 cm, c) 2 cm, d) 3 cm, e) 4 cm from the drop maker. Conditions as in Fig. 5.3b–g.*

biomaterial. It obviously also eliminates the need to transfer the particles from the organic phase to an aqueous phase after polymerization, which is known to affect the stability of the gel particles.[9]

5.4 Conclusion

In conclusion, we have demonstrated the continuous generation of water-in-water-in-water microdroplets from aqueous polymer solutions. This method allows the efficient encapsulation of biomaterial in a biofriendly environment, free of organic solvents. It also forms an excellent and versatile starting point for the fabrication of stable all-aqueous microstuctured systems by e.g. on-line crosslinking of the shell, and for the creation of more complex multicompartment microstructured phases. Without a physical barrier in the form of a lipid bilayer, we foresee that the core-shell structures offer the potential to impact on synthetic cell studies, as biomaterial can readily transfer from the core to the surroundings in these all-aqueous structured fluids.

References

1 H. Walter, G. Johansson and D. E. Brooks, *Anal. Biochem*., 1991, **197**, 1–18.

2 P. A. Albertsson, *Nature*, 1958, **182**, 709–711; A. M. Azevedo, P. A. J. Rosa, I. F. Ferreira and M. Aires-Barros, *Trends Biotechnol*., 2009, **27**, 240–247.

3 M. S. Long, A. S. Cans and C. D. Keating, *J. Am. Chem. Soc.*, 2008, **130**, 756–762; Y. Li, R. Lipowsky and R. Dimova, *J. Am. Chem. Soc*., 2008, **130**, 12252–12253.

4 I. Ziemecka, V. van Steijn, G. J. M. Koper, M. Rosso, A. M. Brizard, J. H. van Esch and M. T. Kreutzer, *Lab Chip*, 2011, **11**, 620–624.

5 Y. S. Song, Y. H. Choi and D. H. Kim, *J. Chromatogr. A*, 2007, **1162**, 180–186; Y. H. Choi, Y. S. Song and D. H. Kim, *J. Chromatogr. A*, 2010, **1217**, 3723–3728.

6 K. Vijayakumar, S. Gulati, A. J. deMello and J. B. Edel, *Chem. Sci*., 2010, **1**, 447–452; M. Yasukawa, E. Kamio and T. Ono, *Chem. Phys. Chem*, 2011, **12**, 263–266.

7 S. Okushima, T. Nisisako, T. Torii and T. T. Higuchi, *Langmuir*, 2004, **20**, 9905–9908; A. S. Utada, E. Lorenceau, D. R. Link, P. D. Kaplan, H. A. Stone and D. A. Weitz, *Science*, 2005, **308**, 537–541.

8 J. J. Agresti, E. Antipov, A. R. Abate, K. Ahn, A. C. Rowat, J.-C. Baret, M. Marquez, A. M. Klibanov, A. D. Griffiths and D. A. Weitz, Proc. Natl. Acad. Sci. U. S. A., 2010, **107**, 4004–4009; B. Zheng, L. S. Roach and R. F. Ismagilov, *J. Am. Chem. Soc*., 2003, **125**, 11170–11171.

9 P. Panda, S. Ali, E. Lo, B. G. Chung, T. A. Hatton, A. Khademhosseini and P. S. Doyle, *Lab Chip*, 2008, **8**, 1056–1061; E. Tumarkin and E. Kumacheva, *Chem. Soc. Rev*., 2009, **38**, 2161–2168.

10 S. L. Anna, N. Bontoux and H. A. Stone, *Appl. Phys. Lett*., 2003, **82**, 364–366.

11 H. O. Johansson, G. Karlstrom, F. Tjerneld and C. A. Haynes, *J. Chromatogr., Biomed. Appl*., 1998, **711**, 3–17.

12 D. Forciniti, C. K. Hall and M. R. Kula, *J. Biotechnol*., 1990, **16**, 279–296.

13 R. Jones, *Soft Condensed Matter*, Oxford University Press, Oxford, UK, 2002.

14 A. Acrivos, G. K. Batchelor, E. J. Hinch, D. Koch and R. Mauri, *J. Fluid Mech*., 1992, **240**, 651–657.

6

Stable particles composed of a permeable hydrogel shell and a liquid core produced by all-aqueous microfluidics*

Abstract

We report permeable microparticles composed of a hydrogel shell and a liquid core, rendered stable by controlled crosslinking of the shell of an all-aqueous double emulsion. Drying and rehydration experiments demonstrate the permeability of the shell, which enables the molecular-weight-dependent release and uptake of polar solutes.

* In preparation: I Ziemecka, A. G. L. Olive, V van Steijn, M. T Kreutzer and J. H. van Esch; Stable particles composed of a permeable hydrogel shell and a liquid core produced by all-aqueous microfluidics

6.1 Introduction

Encapsulation and compartmentalization are key to important functions in biological systems and technology, like controlled release and delivery,[1] storage and protection of incompatible components,[2] separation,[3] and catalyst control and recovery.[4] A highly useful strategy for the fabrication of microparticles with internal compartments is based on the encapsulation of different materials inside droplets. Microfluidics enables the continuous generation of droplets with an unsurpassed control over their size and their encapsulated content.[5] A wide variety of particles have been generated from microdroplets, including Janus particles,[6] macroporous polymer particles,[7] and particles with a core-shell structure.[8] These particles have in common that they are produced from aqueous solutions in combination with organic solvents, which are bioincompatible and potentially mangle the encapsulation. Lipid-based microparticles[9] form an alternative, but introduce another major limitation: the compartments are impermeable to most polar solutes, including many relevant biomolecules. Herein, we describe an organic-solvent free approach to produce all-aqueous compartmentalized microparticles with a cross-linked hydrogel shell, which enables the molecular-weight-dependent release and uptake of polar solutes.

Aqueous two-phase systems (ATPS) constitute a class of fluids especially relevant for the partitioning and the separation of polar constituents, biomolecules, and even living cells.[10] Particularly popular is the well-known and thoroughly characterized ATPS that forms after mixing aqueous solutions of dextran (DEX) and polyethylene glycol (PEG). At sufficiently large polymer concentrations, phase separation occurs by coacervation resulting in two immiscible phases: a phase rich in one polymer can exist in equilibrium with a phase low in that same polymer.[11] Recently, we and others explored ATPS for the continuous generation of single and double emulsion droplets in a microfluidic device.[12-15] In contrast to the formation of oil and water emulsions, the production of ATPS emulsions is complicated by the extremely low interfacial tension and the non-standard interface evolution of such complex fluid systems.[14] One strategy to produce ATPS emulsions is to encapsulate the two aqueous streams in a third stream of oil[16]. The alternative that completely omits the use of organic solvents is to force the formation of single and double emulsions.[12-14,17-19] Despite these first exploratory steps with ATPS in the field of droplet microfluidics, lack of methods to stabilize core-shell ATPS droplets precluded the production of all-aqueous capsules.

Here we introduce and detail compartmentalized microparticles from all-aqueous double emulsions based on free-radical polymerization and show that the resulting micro-containers are stable under a wide variety of conditions. We used the method previously developed in our lab[13] to produce double emulsions in the chip shown in Fig. 6.1a.

6.2 Production of particles

6.2.1 Microfluidic device

The device consisted of a series of three flow focusing junctions. At the first one, we merged a solution of glycidyl-methacrylated functionalized dextran (DEX-GMA) with a solution of PEG, both injected at a flow rate of 3 nL/min. Actuating the piezo-electric bending (16 Hz, 100 V, 0.5 in. diameter, Piezo Systems, Cambridge, MA) embedded in our

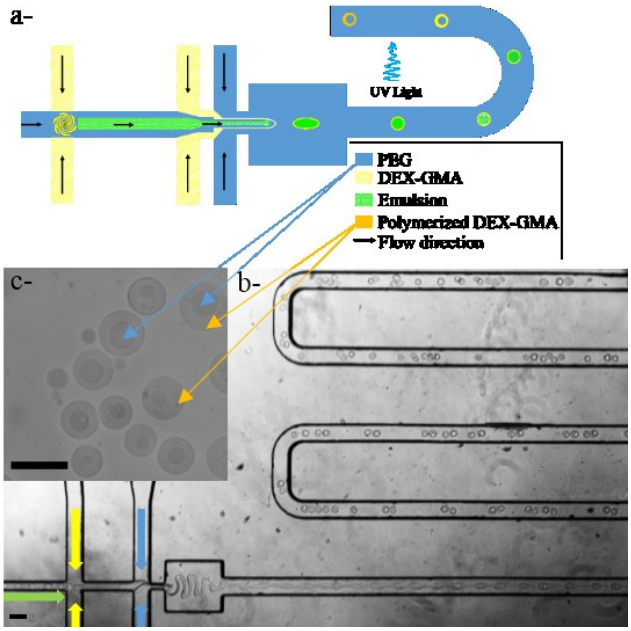

Fig. 6.1 *a- Production of particles with a permeable shell and a liquid core from aqueous solutions of PEG and DEX-GMA, which are injected at three consecutive flow focusing junctions. The resulting fluid thread breaks into droplets that contain a the mixture of PEG and DEX-GMA, which phase separates while the droplets travel through the channel resulting in droplets with a core-shell structure (b). Crosslinking the DEX-GMA in the shell by UV-irradiation result in stable core-shell particles (c). (scale bars 100 µm in b- and 50 µm in c-).*

device, we continuously mixed the streams at the first junction such that an emulsion formed. This emulsion was surrounded by another stream of DEX-GMA, introduced at the second junction at a flow rate of 70 nL/min. This flow created a protecting layer around the emulsion and prevented PEG in the central channel from merging with the PEG stream introduced at the third junction at a flow rate of 1.0 µL/min.

To maintain a reasonable volume fraction of DEX-GMA introduced at the second junction, we found that it was crucial to pre-saturate this outer PEG phase with DEX, because this limited partitioning of the DEX-GMA into this phase. Presaturation also has the advantage to reduce DEX-GMA polymerization in the outer phase, which caused rapid clogging of the microchannel, thereby limiting the operation time of the devices. The outer PEG stream introduced at the third junction served as the bulk phase and carried the droplets, which formed from the thread due to the periodic pulsations induced by the piezo disc. Although droplets appeared as a single phase, they contained a mixture of PEG and DEX-GMA. Phase separation of this mixture resulted in droplets consisting of a core of PEG and a shell of DEX-GMA (Fig. 6.1b). Stabilization of these double emulsion droplets was achieved by free-radical polymerization, which was initiated by irradiating the droplets with UV-light 16 cm downstream the inlet. This led to the crosslinking of the DEX-GMA phase by polymerization of the GMA moieties. Particles were collected directly at the exit of the 20 cm long microfluidic channel into a vitamin C solution. This rapidly quenched the

radical polymerization reaction and prevented coagulation of the particles. The stabilized particles shown in Fig. 6.1c had a 16 pL shell of DEX-GMA and a 2.6 pL liquid PEG core.

6.2.2 Preparation of the solutions

To create hydrogel shell particles, we synthesized a glycidyl methacrylate derivatized dextran (DEX-GMA) using the recipe of Van Dijk-Wolthuis *et al*.[1] The degree of substitution of dextran was 30. For the polymerization experiments we prepared the PEG phase by dissolving PEG (MW =10 000) in a 0.22 M KCl solution obtaining a 10 w/w % solution. For the DEX phase, we dissolved DEX-GMA (MW=500 000) in a 0.22 M KCl solution obtaining a 15 w/w % solution . The solutions were prepared in small volumes, typically 1 mL. We injected these solutions as prepared at the first flow-focusing junction shown in Fig. 6.1 of the communication. By contrast, the solutions injected at the second and third junction were pre-saturated by mixing the solutions and let them equilibrate overnight. The concentration of Irgacure® 2959 (2-Hydroxy-4'-(2-hydroxyethoxy)-2-methylpropiophenone) was 2 mg/mL for outer PEG solution and 4 mg/mL the other solutions. PDMS devices were created as described in Ziemecka *at al*.[2]

6.2.3 Photopolymerization

A critically important aspect of photo-polymerization in aqueous two phase systems is the partitioning of the different components over the different phases. Importantly, the photoinitiator (Irgacure®) partitioned over the PEG and DEX-GMA phase and could not be introduced solely in the phase that needed to be polymerized. Initial polymerization tests with Irgacure® only added to the DEX-GMA phase failed to produce stable particles, as noted from their immediate dissolution upon exposure to water. Absorbance measurements on bulk-phase separated samples showed that Irgacure® had a higher affinity for the PEG phase than for the DEX-GMA phase.

In initial experiments, we considered DEX-GMA with different degrees of substitution (DS), i.e. DS=15, 30. To determine the partitioning of Irgacure® for DEX-GMA and PEG, we added 5mg of Irgacure® to a 3 mL mixture of 15% DEX-GMA in water solution and a 10% PEG in water solution. Absorbance measurements showed that Irgacure® had a higher affinity for the PEG phase than for the DEX-GMA phase. More specifically, 20% partitions in DEX-GMA for DS=15, while 43% was found for DS=30 as shown in Fig. 6.2.

We therefore introduced Irgacure® in all solutions to prevent the depletion of the DEX-GMA phase by diffusion and maintain a sufficient level of Irgacure® in the DEX-GMA phase to induce complete photo-polymerization. The minimum required concentrations of Irgacure® to polymerize the shell was 2 mg/L for the outer PEG stream and 4 mg/L for all other streams.

Stabilization of the double emulsion droplets was achieved by free-radical polymerization, which was initiated by irradiating the droplets with UV-light. To this end, we coupled a UV-light source (Xcite® 120q, peak intensity at 368 nm) into the microscope with an optical fiber. Light first passed a band-pass filter (300-400) nm before it irradiated the microchannel through a 20x objective. A spot size of 2.5 mm was obtained by positioning the objective as close to the chip as possible. To further increase the intensity, we placed an aluminium foil on top of the device, which reflected light back onto the chip. We hereby considered the polymerization sufficient when particles remained stable in water

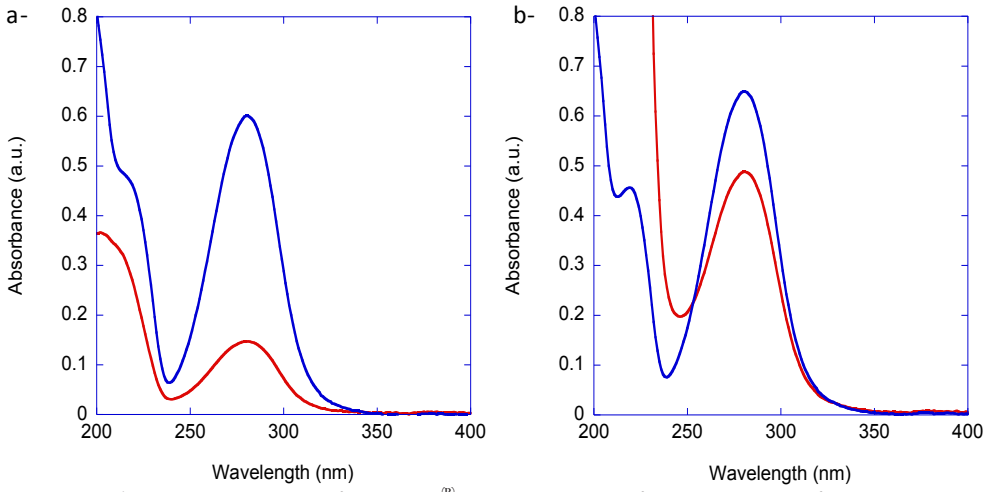

Fig 6.2 *Absorption spectra of Irgacure® 5 mg in 3 mL of a 1:1 mixture of PEG 10 KDa 10 % and DEX-GMA 500 KDa 15% (a- DS= 15, b- DS=30) after phase separation. Blue curve: DEX-GMA phase, red curve PEG phase.*

over several days, whereas incomplete or partial polymerization resulted in their dissociation or even their dissolution.

Interestingly, photo-polymerization enabled the arrest of the intermediate stages of phase separation shown in Fig. 6.3a. This is a clear indication that polymerization occured rapidly. Inducing polymerization before the droplets obtained their core-shell structure (<4 cm) enabled the production of particles with different shapes and microstructures, depending on the location of UV-exposure. Irradiating the droplets for example 3 cm downstream the inlet yielded particles with multiple compartments named as porous particles (Fig. 6.3c/d).

6.3 Characterization of the particles

6.3.1 Resistance to external stress

Particles were produced as mentioned earlier in the text and collected in a vitamin C solution. At the exit of the microchannels, 1 drop was pipetted out and diluted in an Eppendorf containing 0.5 mL of water, which was further centrifuged. Solution from the bottom of the tube was drop casted on a glass slide. Temperature was controlled by a mK1000 controller from Instec, Inc. Once the drop containing the particles on the microscope slide (glass watch, slightly curved), a volume of ~0.5 mL of the solution to study the effect was poured and after 15 min, a bright field microscopy image was recorded.

Core-shell particles displayed a great resistance to various external factors once the protective and stabilizing shell was formed. Isolated particles did not show any observable change in size and shape when heated up to 150 ^{o}C (see SI†). Submerging particles in acidic (2.5 M HCl), basic (2.5 M NaOH) or salt-saturated solutions also did not lead to any observable changes as shown in Fig. 6.4c-h. Comparing these values to some physiological values such as the salinity of blood (0.150 M of NaCl), gastric acid (pH ~ 1.5 to 3.5), and

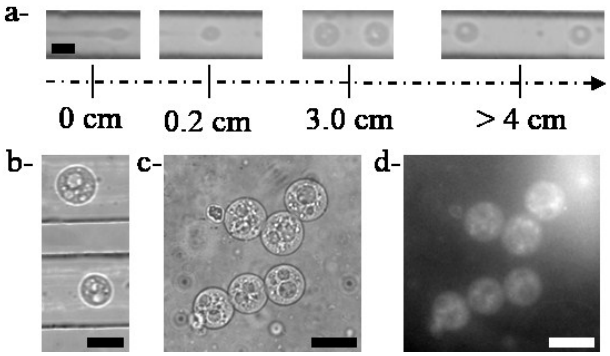

Fig. 6.3 *a- Phase separation inside droplets proceeds while the droplets flow through the microchannel such that their internal structure depends on their location. Droplets with incomplete phase separation 3 cm downstream the inlet before (b-) and after polymerization and collection (c/d) (scale bars: 50 µm)*

fluids in the small intestine (pH 7.0 to 9.0) underlines that the microparticles have a great stability in environments harsher than these physiological environments.

6.3.2 Resistance to drying

The stability of the particles towards repeated drying and rehydration was also excellent. Once collected and washed in water, it was possible to repeatedly dry and rehydrate the core-shell particles without any visible disintegration as shown in Fig. 6.6a. The diameter of the particles decreased upon drying and water was squeezed out of the core. Dried particles recovered their initial shape and size upon rehydrating, even after dry storage for two weeks.

6.4 Permeability of the shell

The successful drying and rehydration showed that the aqueous cross-linked dextran shell allows fast diffusion of water. We wondered to what extend other polar species are able to permeate through the aqueous cross-linked dextran shell. To study the possible diffusion of encapsulated polar species through the shell, a fluorescein-labelled PEG (PEG-FL, 5000 Da) was introduced at a concentration of 15 mg per mL to the PEG phase injected at the first flow-focusing junction (Fig. 6.1a).

6.4.1 Partitinioning of PEG-Fluorescein

To study the partitioning of PEG-FL, we measured absorption spectra of the compound in bulk solutions of PEG 10 KDa 12.5 % in 0.22 M KCl solution and in DEX-GMA 500 KDa 15 % in 0.22M KCl solutions to determine the molar extinction coefficient. In parallel, a solution containing 1mL of PEG solution, 1 mL of the DEX-GMA solution and 50 µL of PEG-FL (100 mg/mL) was shaken and left for phase separation. After phase separation, each phase was carefully collected, and absorption spectra recorded (Fig. 6.5). From the spectra and the molar extinction coefficient, the amount of PEG-FL in each phase was calculated. Emission spectra of two solutions with the same concentration of PEG-FL

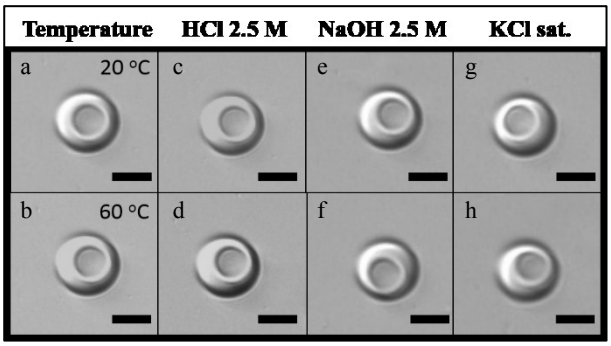

Fig. 6.4 *Resistance of the particle to temperature (a,b) acid (c,d), base (e,f) and saturated salt solution (g,h). Top row represents the initial stage, bottom row the final stage. (scale bars 20 µm).*

in PEG and in DEX-GMA were recorded in the same conditions. The intensity of emission was compared and we deducted that PEG-FL was 10 times more emissive in DEX-GMA than in PEG(see Fig. 6.5). PEG-FL partitioned in a 14/86 ratio over DEX-GMA and PEG such that both the core and the shell showed fluorescence (Fig. 6.6bi). It should be noted that the polymerized DEX-GMA shell of the fully hydrated particles was more emissive than the liquid PEG core, whereas the reverse situation might be expected based on the partitioning.

6.4.2 Release of PEG-Fluorescein

Upon drying, the shell shrinked, which triggered the release of PEG-FL from the shell to the particle's surrounding and to the core. This is clearly seen from the sharp increased emission of the outer fluid and the core, which lighted up more brightly than the shell (Fig. 6.6bii). This observation indicated that the partitioning of PEG-FL into the

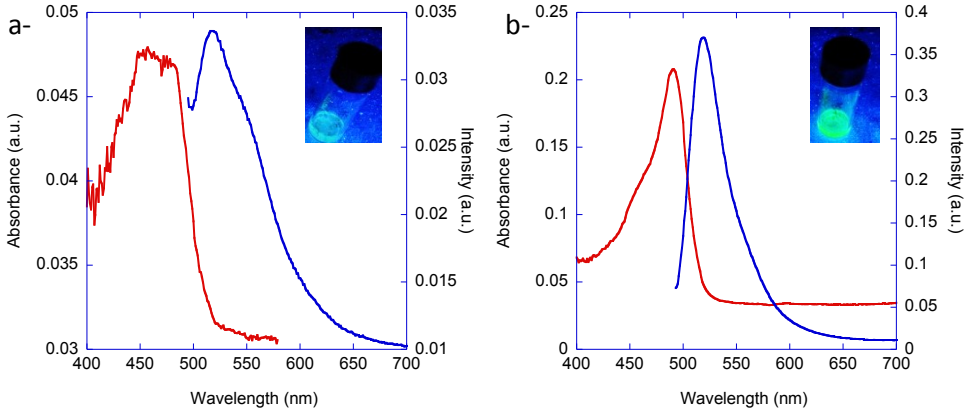

Fig. 6.5 *Absorption spectra (red) and emission spectra (blue, λ_{ex} 468 nm) of 20 µL of PEG-FL solution (100 mg/mL) in a- PEG 10 kDa 10 % in 0.22 M KCl solution, and b: DEX-GMA 500 kDa 15.0 % in 0.22 M KCl solution. Insets: photography of the solution used under UV-light irradiation.*

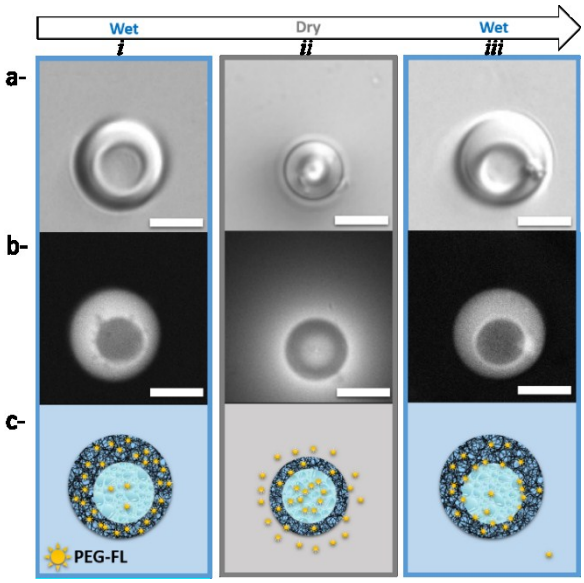

Fig. 6.6 *Core-shell particles in the wet (i and iii) and dry state (ii) observed via a- bright field microscopy and b- confocal fluorescence microscopy; c- illustration of the diffusion of PEG-FL upon drying and rehydration (scale bars 20 µm)*

polymerized DEX-GMA shell changed as the water content in the shell reduced. This repartitioning was reversible upon rehydration. Now the shell swelled again with water and returned to its initial shape as shown in Fig. 6.6a/biii.

The PEG-FL previously expelled from the shell to the outside was dispersed in the bulk solution and not seen in the fluorescent image. In contrast, the PEG-FL in the core first diffused rapidly to the core-shell interface, and then slowly diffused back into the shell, as evident from the dark core and the bright emissive ring at the core-shell interface in Fig. 6.6biii. The initial intensity of the shell is most likely caused by the PEG-FL that did not partition out of the shell during drying.

Altogether, these observations showed that the aqueous polymerized dextran shell was permeable to water molecules, which equilibrated the system with fast diffusion out (upon drying) and in (upon hydrating), expressed by the size recovery of the particles. Diffusion of PEG-FL from the core to the interface with the shell was fast and such a large polar molecule as PEG-FL even permeated and diffused through the aqueous cross-linked dextran shell. However, the diffusion and the redistribution within the aqueous cross-linked dextran shell were very slow (several hours) compared to small water molecules. Future work aims at controlling molecular weight release cut-off from the core to the outer PEG environment by changing the degree of the substitution of DEX-GMA.

6.5 Harvesting of particles

Particles were collected in a vitamin C solution (5 mg/mL). During careful optimization of the photo-polymerization process, we found that it is essential to collect the freshly polymerized particles in an aqueous solution of vitamin C, because this prevents the

particles from sticking together (Fig. 6.7a). We tentatively suggest that this sticky behaviour is caused by residual free radicals at the surface of the particles. Harvesting particles in pure water or directly on the glass of the chip such that these radicals are still present enables the assembly of core-shell particles into larger structure by partly fusing the shells (Fig. 6.7b).

6.6 Microchannel clogging

As mentioned earlier in this chapter, DEX-GMA as well as Irgacure® partion with the outer PEG phase. Therefore, after 5 s of irradiation and the production of 100-200 core-shell particles, the microchannel clogs due to the polymerization of the outer phase. To overcome this issue, studies of the partitioning of DEX-GMA in PEG as a function of the degree of substitution (DS) have been undertaken.

To study the effect of the DS on its partitioning between a PEG rich phase and a DEX-GMA phase a chromophore (fluorescein) has been introduced to DEX-GMA. The amount of DEX-GMA-Fluorescein present can then be quantified by absorption spectroscopy.

In a first time calibration curves for each DS are obtained by measuring absorption spectra for known percentage of DEX-GMA-Fluorescein. Typically a 20 % DEX-GMA-fluorescein solution w/w in 0.22 M KCl is prepared. Then aliquots of 20 µL of this solution are added to 2.8 mL of a 0.22 M KCl solution and the spectra recorded (Fig. 6.8). Calibration curves are plotted by reporting the absorbance at 493nm as a function of the percentage of DEX-GMA-Fluorescein present.

Next, 1 mL of a 20 % DEX-GMA-Fluorescein solution in 0.22 M KCl and 1 mL of a 10 % PEG solution in 0.22 M KCl were vigorously checked and left for phase separation. Once complete, 20 µL of the PEG phase are diluted into 2.0 mL of 0.22 M KCl solution and the spectrum recorded. This step is repeated 2 more times with aliquots added to the same solution. From the values of absorption at 493 nm and the calibration curves, the percentage of DEX-GMA-Fluorescein in the PEG rich phase can be determined.

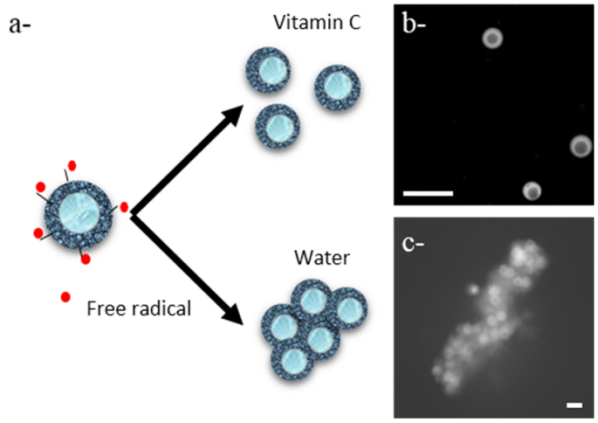

Fig. 6.7 *a- scheme representing the behavior during their collection in medium with a different acidity; Confocal microscopy images of the particles collected in b- vitamin C and c- pure water (scale bars 50 µm).*

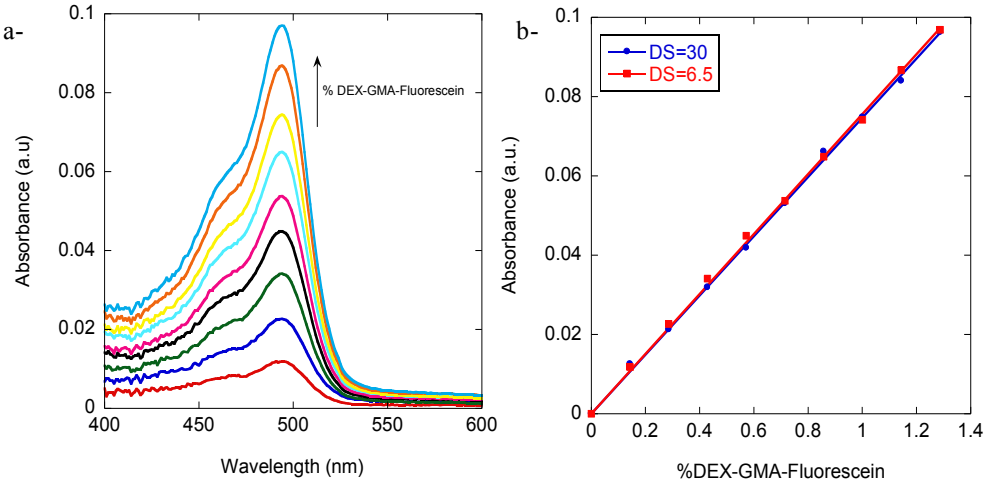

Fig. 6.8: *a- Absorption spectra of DEX-GMA-Fluorescein (DS=6.5) after addition of 20 µL aliquots of a 20 % solution to a 2.8 mL solution. b- Absorbance at 493 nm as a function of the percentage of DEX-GMA-Fluorescein DS=6.5 red, DS=30 blue (lines represent fitting curves).*

For DS=6.5, < 1% of DEX-GMA are present after phase separation where as 22 % are present for DS=30.

For DS=6.5, partitioning experiments have been repeated with Irgacure added to both phases. The PEG phase is then impossible to polymerize upon long irradiation time. In contrast it is still possible to polymerize DEX-GMA after long irradiation time (30 s).

These preliminary results are extremely promising and offer a solution to prevent clogging of the microchannel and to allow the continuous production of core-shell particles. At the time the present thesis is being printed, experiments were still undergoing in this direction, the key point being now to increase the irradiation time of core-shell emulsion (made of DEX-GMA DS=6.5) in the microchanel.

6.7 Conclusion

In summary, we have demonstrated the production of stable and permeable particles from all-aqueous compartmentalized microdroplets. The release and uptake upon drying and rehydration depends on the molecular weight of the solutes and is fast for water and slow for larger solutes. The large number of known aqueous two-phase systems provides access to the continuous water-based production of a wide variety of compartmentalized water-permeable microparticles.

References

1. S. Mitragotri and J. Lahann, *Adv Mater*, 2012, **24**, 3717-3723.
2. D. T. Nguyen, M. Smit, B. Dunn and J. I. Zink, *Chem. Mater.*, 2002, **14**, 4300-4306.
3. K. Huang and J. Rzayev, *J. Am. Chem. Soc.*, 2011, **133**, 16726-16729.
4. S. H. S. Lee, P. Z. Wang, S. K. Yap, T. A. Hatton and S. A. Khan, *Biomicrofluidics*, 2012, **6**.
5. Y. Wei, S. Soh, M. M. Apodaca, J. Kim and B. A. Grzybowski, *Small*, 2010, **6**, 857-863.
6. A. R. Abate and D. A. Weitz, *Small*, 2009, **5**, 2030-2032.
7. Y. Song and H. C. Shum, *Langmuir*, 2012, **28**, 12054-12059.
8. S. Lone, S. H. Kim, S. W. Nam, S. Park, J. Joo and I. W. Cheong, *Chem. Comm.*, 2011, **47**, 2634-2636.
9. S. Dubinsky, H. Zhang, Z. Nie, I. Gourevich, D. Voicu, M. Deetz and E. Kumacheva, *Macromol.*, 2008, **41**, 3555-3561.
10. S. Okushima, T. Nisisako, T. Torii and T. Higuchi, *Langmuir*, 2004, **20**, 9905-9908.
11. A. S. Utada, E. Lorenceau, D. R. Link, P. D. Kaplan, H. A. Stone and D. A. Weitz, *Science*, 2005, **308**, 537-541.
12. J. Kovacs-Nolan and Y. Mine, *J. Immunol. Methods*, 2005, **296**, 199-209.
13. M. Shimizu and Y. Nakane, *Biosci., Biotechnol., Biochem.*, 1995, **59**, 492-496.
14. M. Yasukawa, E. Kamio and T. Ono, *Chemphyschem*, 2011, **12**, 263-266.
15. M. Nasseau, Y. Boublik, W. Meier, M. Winterhalter and D. Fournier, *Biotechnol. Bioeng.*, 2001, **75**, 615-618.
16. H. Walter and G. Johansson, *Anal Biochem*, 1986, **155**, 215-242.
17. M. W. Beijerinck, *Colloid. Polym. Sci.*, 1910, **7**, 16-20.
18. H. G. Bungenberg de Jong and H. R. Kruyt, *Colloid. Polym. Sci.*, 1930, **50**, 39-48.
19. R. Arshady, *Polym. Eng. Sci.*, 1990, **30**, 915-924.
20. D. Forciniti, C. K. Hall and M. R. Kula, *J. Biotechnol.*, 1990, **16**, 279-296.
21. S. D. Geschiere, I. Ziemecka, V. van Steijn, G. J. M. Koper, J. H. van Esch and M. T. Kreutzer, *Biomicrofluidics*, 2012, **6**.
22. S. Hardt and T. Hahn, *Lab Chip*, 2012, **12**, 434-442.
23. I. Ziemecka, V. van Steijn, G. J. M. Koper, M. Rosso, A. M. Brizard, J. H. van Esch and M. T. Kreutzer, *Lab Chip*, 2011, **11**, 620-624.
24. I. Ziemecka, V. van Steijn, G. J. M. Koper, M. T. Kreutzer and J. H. van Esch, *Soft Matter*, 2011, **7**, 9878-9880.

Chemical-gradient directed self-assembly of hydrogel fibers *

7

Abstract

In this chapter, we demonstrate and investigate how a propagating acidic wave in a solution of dibenzoyl-L-cystine (DBC) can lead to the orientation and alignment of self-assembled fibers constituting a hydrogel. Taking advantage of its pH-induced self-assembly, a hydrogel composed of parallel fibers can be formed by propagating a pH gradient front from one part of a cell to the other. The diffusing species (typically the ion pair H^+/Cl^-) control the velocity of the pH-gradient front and, therefore, their diffusion rate should match the gelation rate so as to attain complete orientation.

* Published as: I. Ziemecka, G. J. M. Koper, A. G. L. Olive and J. H. van Esch, Chemical-Gradient Directed Self-Assembly of Hydrogel Fibers, Soft Matter, 2013, 9, 1556-1561.

7.1 Introduction

The ability to create directed self-assembled nano-structures,[1] in-situ, through non-invasive processes and without template[2-5] or pre-treatment, such as lithography,[6] is an essential step towards the easy access of nano-meter scale featured materials. Directed self-assembly implies total control over the orientation of superstructured materials. Novel properties can be realized from materials displaying oriented nanostructures,[7-9] they can be applied to various fields of research such as electronic (semi-conductors,[10,11] wires),[12] optic (thin films)[13], opto-electronic (photovoltaic,[14-17] liquid crystals)[18,19] or biochemistry (artificial muscles,[20] synthetic membranes,[21] cell growth).[22] They also offer the possibility in some cases to organize the nanostructures hierarchically.[23,24] The nature of the self-assembling entities can be manifold; examples are inorganic[25-27] or polymeric particles,[28] block copolymers,[29,30] carbon nanotubes,[31,32] biomolecules (DNA,[33] phospholipids,[34] peptides),[35] and supramolecular structures.[36-38]

The classical method to induce directed self-assembly is by solvent evaporation[39-41] during which spontaneous self-assembly is induced by increasing the concentration, even though convection and flow instabilities might deteriorate the targeted architectures. Other techniques involve the use of an external force such as mechanical stress,[42,43] temperature[44] or electric,[45-48] magnetic,[49-53] or optical[54,55] field gradients to align the self-assembled structures either during their formation[56-58] or once formed.[59] Combination of several triggers has also been shown in an elegant example reported by Zhang *et al.*[60] where stretching is combined with temperature to direct the self-assembly. However, chemical gradients[61,62] are considered to be more suitable for studies and for applications as they can be precisely controlled spatially. Inspired by nature where reaction-diffusion processes are often involved in the building of precise ordered structures,[63] Stupp *et al.*[64] described a system where chemical gradients at the interface of two aqueous solutions led to the directional self-assembly of aligned fibrous membranes. Depending on the type of reaction involved (self-assembly, complexation), the orientation of the resulting structures can be parallel (most common) or perpendicular[65] to the flow of diffusing species.

Our research group already extensively investigated the gelation properties of the low molecular weight hydrogelator dibenzoyl-L-cystine (DBC, Fig. 7.1),[66,67] which can self-assemble into fibers to form a gel under acidic conditions.[68-71] Here we focus on the directionality of fiber self-assembly to obtain a gel composed of parallel fibers. To accomplish the alignment, a sharp acidic wave is propagated in a cell containing a basic solution of DBC. The resulting pH gradient does not only induce the fiber formation by self-assembly but also ensures that the out coming nanostructures are parallel.

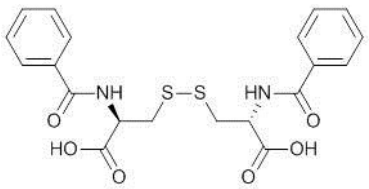

Fig. 7.1 *Structure of dibenzoyl-L-cystine, DBC hydrogelator molecule.*

With the aim of fully characterizing the system, we first analyse, quantify and describe the model assumed and used for the pH gradient and the diffusing species. Directed self-assembly has been studied with microscopic techniques (bright field, AFM) and visualized using polarized light, leading to information on the degree of alignment and spacing of the fibers among the hydrogel. Finally, we show how these oriented hydrogel can be used as a template to create a polymeric nano-porous membrane.

7.2 Materials and Methods

7.2.1 Preparation of an oriented hydrogel by pH-gradient

Aqueous solutions from 10 to 30 mM of DBC (Fluka Analytical) were prepared by dissolving the powder under sonication in an adequate amount of water while simultaneously adjusting the pH to 12-13, with a 5mM NaOH solution. To visualize the pH-gradient during gelation, a universal indicator solution (Fluka Analytical, pH range 0-5 or pH range 3-10) was added to the DBC solution, at a final concentration of 4 % v/v. A high precision quartz flow-through measurement cell (SUPRASIL®, 137-QS, Hellma) with a transverse optical light path of 1 mm was filled with DBC solution (~ 0.3 mL) in such a way that both cell entrances were filled halfway. Two droplets of highly concentrated hydrochloric acid, 1 – 5 M, with a volume of about 3 µL were added into one of the entrances by means of a flat ended, not sharp, needle. The drops were added on the top of the meniscus and care was taken to not introduce air into the cell.

7.2.2 Bright field and birefringence measurements

Bright field as well as birefringence mode pictures were taken with an inverted microscope Zeiss Axiovert 100M. Rotating birefringence mode pictures were captured with the use of a polarizing microscope Nikon Eclipse E600 POL.

Image analysis was done off line with the Scanning Probe Image Processing software package (SPIP, version 2.000, Image Metrology A/S, Lungby, Denmark) and with Matlab® (Mathworks, U.S.A.).

7.2.3 Atomic force microscopy (AFM)

The surface structure of the oriented gels was imaged by means of AFM (Ntegra, NT-MDT Co., Russia) with a lateral resolution in the nanometer range. The sample surface was scanned in tapping mode, and a rectangular ($100 \pm 5 \times 35 \pm 5$ µm^2) cantilever (NSG01, NT-MDT Co., Russia) was used with a nominal force constant of 0.3 N/m with a resonance frequency of around 150 kHz and a probe tip radius of 10 nm. All images (256 × 256 pixels) were recorded in air. The Scanning Probe Image Processor software Nova Software, NT-MDT Co. was used for the analysis of the images.

7.2.4 Fixation of the oriented gel

For fixation of the oriented gel, we added acryl amide with bis-acrylamide cross linker to a DBC solution, followed by formation of the oriented gel, after which the sample was polymerized. The solution was prepared by mixing one part of a 30 mM DBC solution at pH 12 prepared as described above, with one part a 30 % (by mass) acrylamide/bis-acrylamide solution, (acryl amide : bis-acrylamide is 37.5:1, Sigma Aldrich), and one part of water. For these experiments, a home built cell was used consisting of a standard

microscope glass slide, a PDMS slab (1.0 mm thick), and a microscope cover slip. In the PDMS slab an elongated hexagon (65 by 4 mm) was cut out by means of a sharp knife. The PDMS slab was covalently bonded to the microscope glass slide by plasma treatment. The microscope cover slip was put over the long edges of the hexagon in the PDMS slab and slightly pressed. Two tips of the hexagon were left free as liquid inlets. The cover slip adhered to the PDMS slab by van der Waals forces. Cells were filled with the solution (~ 0.3 mL) by means of a needle into one of the inlets and gelation was initiated with the addition of droplets of 3 M hydrochloric acid (~ 1.0 µL), as described above. Typically, the concentration of hydrochloric acid was lower than used for gelation of DBC in water to prevent the degradation of the acylamide/bis-acrylamide monomer. After gelation of DBC, polymerization of acylamide/bis-acrylamide monomers was achieved by irradiation with gamma rays for 10 minutes. We used a Co-60 gamma source, and the dose rate was 2.5 kGy/h. This resulted in a total dose of 0.4 kGy for 10 min. The polymerized sample was removed from the cell and placed in 2 M NaOH solution for 5 weeks to dissolve and extract the DBC gel. The sample was then placed in water, which was refreshed until neutral. In order to visualize the channels in the polyacrylamide matrix, samples were placed for few weeks in a water solution containing fluorescent styrene beads of 400 nm and in a water solution containing fluorescent vesicles of 30 nm. After rinsing with water, microscope pictures of the samples were taken, using a Zeiss Axiovert 100M microscope in the fluorescence image capture mode.

7.3 Results and Discussion

DBC is known to gel if the pH is below 5. It is therefore not a surprise that when to a cell filled up with a basic DBC solution a drop of a highly concentrated HCl solution is added, the liquid near the entrance immediately gels. As the acid diffuses into the cell the gelled region increases until the cell is completely gelled. This has the advantage that convection inside the cell is largely prohibited and that only diffusion controls the distribution of acid.

7.3.1 pH-gradient

The picture of Fig. 7.2a represents a cell containing a solution of DBC where the pH profile is visualized by means of a pH-indicator; note that the acidic drop has been

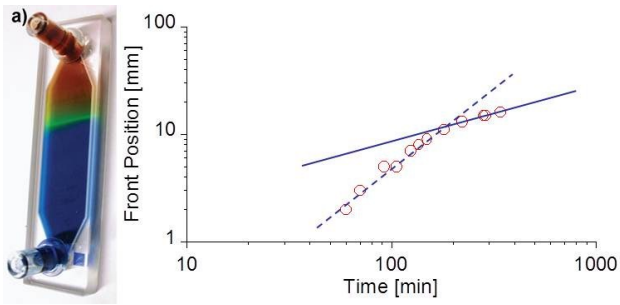

Fig. 7.2 *Gelation of a DBC 30 mM solution at 25 ^{O}C a) pH gradient visualized by indicator b) change of the position of front of the gel in time.*

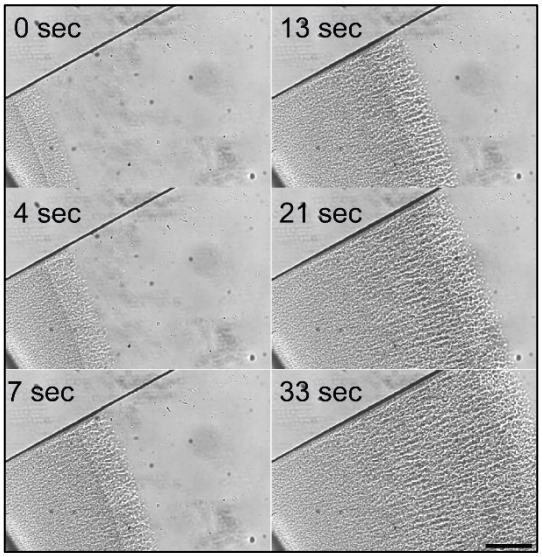

Fig. 7.3 *Bundles of fibers of DBC (30 mM in basic solution) growing due to pH gradient from a 1 µL solution of 5 M HCl, at 25 ^{O}C (bright field mode), scale bar 500 µm.*

introduced on the upper part of the cell and that the blue colour indicates the region where the pH is 5 or higher, the greenish colour covers a range from 3.5 to 2 and the reddish colour below 2. At the beginning of the experiment the pH-profile is relatively sharp so that with time the progression of the concentration profile appears as a green front travelling away from the entrance, see Fig. 7.2b where the front position is plotted versus time. Although the situation is more complex, for the discussion of the experimental findings, we invoke the simple model of the development of a concentration profile of a single species by diffusion after an initial injection. We also assume that the gel does not significantly hinder the diffusion of the small ions. The resulting concentration profile has a Gaussian shape with a maximum at the entrance that decays as $t^{-1/2}$ and where the width increases proportional to $t^{1/2}$, where t stands for time. The first part of the graph in Fig. 7.2b is almost linear with a slope of 1.5 due to the triangular inlet shape of the cell. The second part has a slope of 0.5, as predicted by the simple model described above. From a linear regression of the front position versus time we found an effective diffusion coefficient of $3 \cdot 10^{-9}$ $m^2 \cdot s^{-1}$. This value is quite comparable to the value of $2.0 \cdot 10^{-9}$ $m^2 \cdot s^{-1}$ for the self-diffusion coefficient of the chlorine ion, which is the limiting diffusing specie for the ion pair H^+,Cl^-, at infinite dilution. These results indicate that acid transport is only diffusive and convection does not play a role, most likely due to the blockage of the inlet by the gel formation nearby the entrance. It should be noted that with time the slope of the concentration profile becomes less steep, as it was apparent from broadening of the green region.

7.3.2 Gelation

Gelation sets in for pH-values below 5 and hence occurs just at the foot of the above described concentration profile where the colour becomes greenish, see Fig. 7.2a.

This process can also be followed by microscopy in bright mode or birefringence mode, (see Fig. 7.3). From the onset, the growth of DBC fibers appears to be oriented in the direction of the pH-gradient as it is visible from the structured birefringence. The ghost front following the first front at a distance of about 500 µm in the pictures in Fig. 7.3 roughly demarcates the end of the concentration profile and hence the orientating effect of the gradient ends there.

The degree of alignment has been quantified by analysing 2D Fourier transforms (FFT) of 6 slabs of 316 µm x 1065 µm (158 x 530 pixels) from the overall picture in Fig. 7.4a. An example of the transformed image is depicted in Fig. 7.4b, where the amplitudes are represented on a logarithmic colour scale. The blue regime is a global peak with a maximum at zero frequency in the middle corresponding to the random frequencies occurring in the image. In light blue there are two small peaks, superimposed on the main global peak (dark blue), denoting the most significantly and recurrently occurring spatial frequencies in the image, corresponding to a regular spacing of about 50 µm. To quantify the fiber alignment in a given location, an empirical parameter, the texture direction index S, was calculated from a weighted average of A_{max} (amplitude of the radial Fourier spectrum for each orientation in the plane), such that

$$S = \frac{\sum_{t=0}^{M-1} A(\frac{t\pi}{M})}{M A_{max}} \qquad (7.1)$$

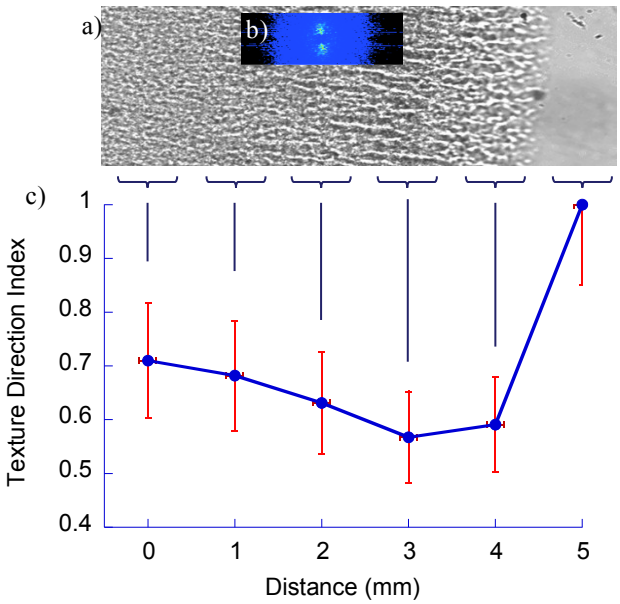

Fig. 7.4 *Texture direction index of 6 areas of 316 µm x 1065 µm (158 x 530 pixels) of a) the picture at 33 s Fig. 7.3, were analysed by FFT as shown in graph b) resulting in data points separated by 1 mm in graph c) where the guide line shows the trend of the alignment in the sample.*

where t is an index running through all angles on the surface. S approaches zero for perfectly aligned structures, and S tends to 1 for an isotropic distribution.[72]

On the graph Fig. 7.4c, representing the mapping of the orientation after gelation, the texture direction index decreases from 0.7 at the inlet where the diffusive wave starts to 0.57, 3 mm further, at the front of the ghost wave. In between 3 mm from the inlet to 4 mm where the front of the pH-gradient wave is, the alignment does not significantly vary (S = 0.59). Additionally, no directionality is observed in the area where the acid did not diffuse (S = 1). This graph clearly shows that the onset of alignment and the region of maximum alignment are in a range of 3 - 4 mm (where the pH gradient is sharp), closer to the inlet fiber alignment slightly fades away due to the continued gelation process while the pH-gradient is dissipated ($\Delta S_{\Delta t\ =\ 33\ s} = +\ 0.05$, Fig 7.5). These results clearly show that the formation of aligned gel fibers can be achieved by a propagating pH gradient. Further research is necessary to improve fiber alignment or extend alignment over larger areas, e.g. by optimization of pH gradient and gelator concentration, and cell geometry.

Polarization microscopy near the front of the concentration gradient reveals a colour pattern as presented in Fig. 7.6. Using the Michel-Levy birefringence chart we find an optical path difference of about 500 nm. Taking for the optical path length the thickness of the cell, 1 mm, this implies a birefringence of $5 \cdot 10^{-4}$. The relation between the induced birefringence Δn and the polarizability anisotropy $\Delta\alpha$ is given by

$$\Delta n = \frac{1}{2} nc\Delta\alpha F \qquad (7.2)$$

where c is the concentration in molecules per m^3, and n the average refractive index for which we shall take the value for water of 1.33. The factor F describes the orientation due to the concentration gradient, it is maximally 1. Assuming nearly perfect orientation, the polarizability anisotropy is estimated to be about $40 \cdot 10^{-30}$ m^3 which compares well with values found for aromatic molecules.

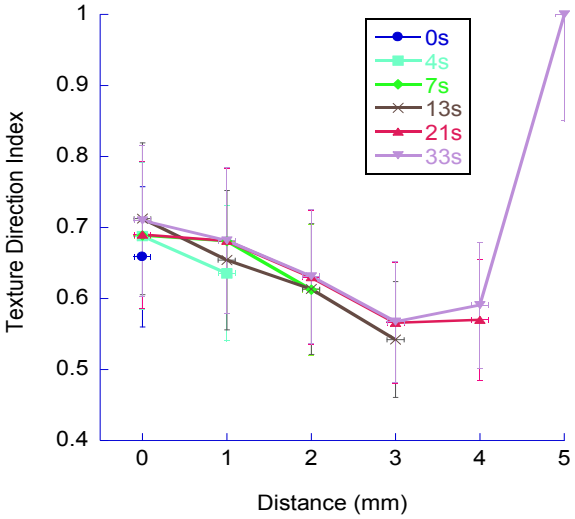

Fig. 7.5: *Texture Direction Index as a function of the distance from the inlet at different time.*

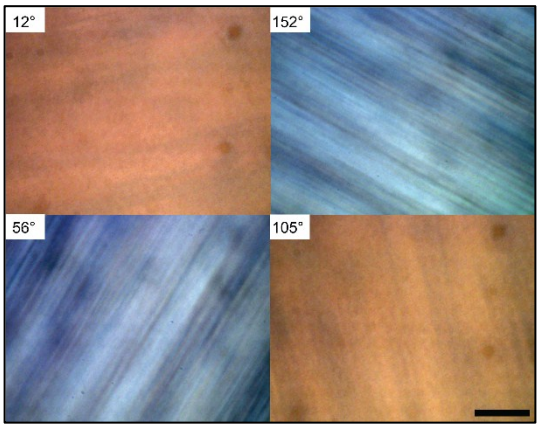

Fig. 7.6 *Pictures of a sample of aligned fibers of DBC rotated in birefringence mode,*

The alignment of the hydrogel fibers has been further verified by AFM on dried oriented gels, see Fig. 7.7. The orientation is visible over a variety of length scales with only few strong deviations as can for instance be seen from Fig. 7.7c. These deviations are probably due to the fact that gelation still continues after the passing by of the concentration gradient. From Fig. 7.7c one would deduce a fiber diameter of about 100 nm which is larger than the value of 20-60 nm obtained in a recent electron microscopy analysis. The structures that are revealed by AFM are therefore probably fiber bundles that could be formed during sample drying or may already have developed during the directed growth. The texture direction index calculated for AFM images is 0.48. The degree of alignment is higher at the nanometer scale than micrometer scale (S = 0.59).

In summary, the above experimental results confirm that directional growth of hydrogel fibers can be induced by means of a sufficiently steep concentration gradient. The process is controlled by the velocity and the increase in width of the concentration front through the sample and the rate at which gelation proceeds. Because convection does not play a role, the wave front velocity and its broadening are controlled by the diffusion of the acid and cannot easily be influenced otherwise, whereas the gelation rate is also controlled

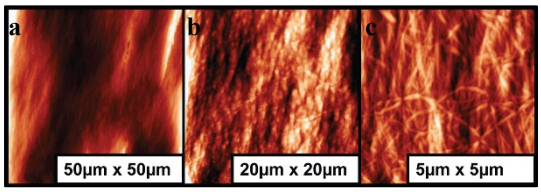

Fig. 7.7 *Semi-contact topography AFM images of dried 30 mM DBC fibers (pH before gelation 12.13) obtained by the diffusion of acid from a drop of 5 M HCl. a), b) being two different areas, c) new image from b), resolution 512 x 512 pixels*

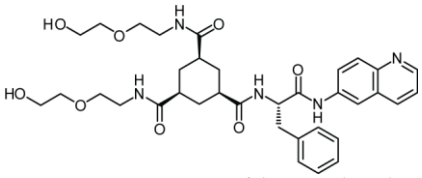

Fig. 7.8 *Structure of low-molecular-weight hydrogelator molecule based on 1,3,5-cyclohexyltricarboxamide,* ***1****.*

by the concentration of DBC. The partial destruction of the oriented structure that is visible when the concentration front has passed by is due to still proceeding gelation, suggesting that fiber alignment can be improved by balancing the pH wave front velocity and rate of gelation. The directed growth of gel fibers is not specific for the DBC hydrogelator. We were also able to grow oriented fibers of another low molecular mass hydrogelator based on 1,3,5-cyclohexyltricarboxamide, for the structure see Fig. 7.8. This hydrogelator is soluble in acidic solution and forms a gel in neutral-basic solution. Similar experiment in a quartz cuvette as described above using a steep base concentration profile resulted in oriented fibers which also exhibit birefringence, see Fig. 7.9.

7.3.3 Fixation of gelated structures

Aligned gel fibers can be used as a template for the creation of porous materials such as membranes. To demonstrate this we have conducted experiments where directed growth of hydrogel fibers was done in an acrylamide/bis-acrylamide solution that was subsequently polymerized, leading to fixed aligned fibers similarly to the work done by Wu *et al*.[73]

Afterwards, DBC gel has been removed by dipping the obtained polymer in a basic solution, to leave behind aqueous channels without hydrogel. The resulting material was submitted to colloidal solutions containing fluorescent beads of about 400 nm and of fluorescent vesicles of about 30 nm, the results are displayed in Fig. 7.10. The porous structure is well visible and shows channel sizes of various diameters. The channels visualized in Fig. 7.10a are filled with the fluorescent beads and hence have a diameter of 400 nm or more whereas those in Fig.7.10b are at least 30 nm in diameter. This shows that a wide range of DBC fibers diameter is obtained mainly due to bundling of the smallest DBC fibers. S values are respectively 0.86 and 0.83 for the Fig. 7.10a and 7.10b, suggesting that bundles of fibers are less oriented than small fibers although few channels are present on the images rendering the statistical analysis less accurate.

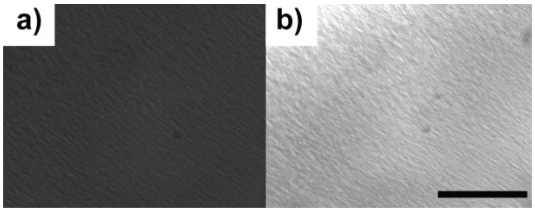

Fig. 7.9 *A sample of aligned fibers of hydrogelator* ***1*** *a) bright field b) birefringence mode; scale bar 200µm.*

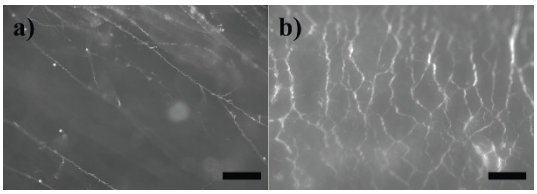

Fig. 7.10 *Channels in polyacrylamide visualized via a) fluorescent styrene beads, scale bar 200 μm b) fluorescent vesicles [scale bar 100 μm].*

7.4 Conclusion

Whereas directed self-assembly is usually done by means of physical gradients, we here demonstrated a simple method to attain aligned fibers by means of a chemical gradient. The system was particularly suitable for this type of study as convection was surpassed and diffusion was the only mechanism involved in the propagating acidic wave. In order to achieve directed self-assembly of hydrogel fibers by means of a pH-gradient, as described in the present paper, a few requirements are to be fulfilled. In the first place, the pH-gradient has to be large enough. In the present experiments we found 2 pH units per mm as a lower limit. In the second place, the time scale at which the pH gradient persists should match the one of gelation. Analysis of bright field microscopy and AFM images of the parallel fibers allowed us to quantify the degree of alignment. The highest degree of alignment (from the texture direction index values) was achieved at a distance of 3 mm from the inlet where the diffusive acidic wave is the sharpest. Interestingly, alignment of small fibers depends on the scale and is higher at nanometer scale (S=0.48 from AFM images) than at micrometer scale (S=0.57 from bright field microscopy images) than for bundles of fibers (S=0.83 from fluorescent microscopy images). The process is relatively fast and complete gelation is achieved within the order of a minute in our experiments. The thus created oriented fibrous systems can be applied in various kinds of materials. Here we demonstrate their use as a template for the synthesis of polymeric porous membranes. Other applications could be orthogonal self-assembly based materials and structures such as gellosomes.[64]

References

1. P. Kumar, *Nanoscale Res. Lett.*, 2010, **5**, 1367-1376.
2. Y. Lei, S. K. Yang, M. H. Wu and G. Wilde, *Chem. Soc. Rev.*, 2011, **40**, 1247-1258.
3. R. Baati, D. Ihiawakrim, R. R. Mafouana, O. Ersen, C. Dietlin and G. Duportail, *Adv. Funct. Mater.*, 2012, **22**, 4009-4015.
4. K. A. Arpin, J. H. Pikul, W. P. King, H. Y. Fan and P. V. Braun, *Soft Matter*, 2011, **7**, 10252-10257.
5. Y. Chen, H. P. Liu, T. Ye, J. Kim and C. D. Mao, *J. Am. Chem. Soc.*, 2007, **129**, 8696-8697.
6. D. Wouters and U. S. Schubert, *Angew. Chem. Int. Edit.*, 2004, **43**, 2480-2495.
7. A. M. Schwartzberg and J. Z. Zhang, *J. Phys. Chem. C*, 2008, **112**, 10323-10337.
8. F. S. Kim, G. Q. Ren and S. A. Jenekhe, *Chem. Mater.*, 2011, **23**, 682-732.
9. Y. Lei, W. P. Cai and G. Wilde, *Prog. Mater. Sci.*, 2007, **52**, 465-539.
10. J. Stangl, V. Holy and G. Bauer, *Rev. Mod. Phys.*, 2004, **76**, 725-783.
11. H. Hlaing, X. H. Lu, T. Hofmann, K. G. Yager, C. T. Black and B. M. Ocko, *Acs Nano*, 2011, **5**, 7532-7538.
12. G. R. Dholakia, W. Fan, J. Koehne, J. Han and M. Meyyappan, *Phys. Rev. B*, 2004, **69,** 1534021-4.
13. L. N. Wong, C. H. Hu, R. Paradise, Z. N. Zhu, A. Shtukenberg and B. Kahr, *J. Am. Chem. Soc.*, 2012, **134**, 12245-12251.
14. P. V. Kamat, *J. Phys. Chem. C*, 2007, **111**, 2834-2860.
15. J. Peet, A. J. Heeger and G. C. Bazan, *Accounts Chem. Res.*, 2009, **42**, 1700-1708.
16. S. E. Gledhill, B. Scott and B. A. Gregg, *J. Mater. Res.*, 2005, **20**, 3167-3179.
17. D. Dalacu, M. E. Reimer, S. Frederick, D. Kun, J. Lapointe, P. J. Poole, G. C. Aers, R. L. Williams, W. R. McKinnon, M. Korkusinski and P. Hawrylak, *Laser Photonics Rev.*, 2010, **4**, 283-299.
18. H. E. Romeo, C. E. Hoppe, M. A. Lopez-Quintela, R. J. J. Williams, Y. Minaberry and M. Jobbagy, *J. Mater. Chem.*, 2012, **22**, 9195-9201.
19. M. Prehm, G. Gotz, P. Bauerle, F. Liu, X. B. Zeng, G. Ungar and C. Tschierske, *Angew. Chem. Int. Edit.*, 2007, **46**, 7856-7859.
20. Y. Liu, A. H. Flood, P. A. Bonvallett, S. A. Vignon, B. H. Northrop, H. R. Tseng, J. O. Jeppesen, T. J. Huang, B. Brough, M. Baller, S. Magonov, S. D. Solares, W. A. Goddard, C. M. Ho and J. F. Stoddart, *J. Am. Chem. Soc.*, 2005, **127**, 9745-9759.
21. R. H. Sui and P. Charpentier, *Chem. Rev.*, 2012, **112**, 3057-3082.
22. L. Richert, F. Vetrone, J. H. Yi, S. F. Zalzal, J. D. Wuest, F. Rosei and A. Nanci, *Adv. Mater.*, 2008, **20**, 1488-1492.
23. A. H. Groschel, F. H. Schacher, H. Schmalz, O. V. Borisov, E. B. Zhulina, A. Walther and A. H. E. Muller, *Nat. Commun.*, 2012, **3**, 710.
24. H. Xu, R. Hong, T. X. Lu, O. Uzun and V. M. Rotello, *J. Am. Chem. Soc.*, 2006, **128**, 3162-3163.
25. J. D. Carter and T. H. LaBean, *Acs Nano*, 2011, **5**, 2200-2205.
26. J. Strle, D. Vengust and D. Mihailovic, *Nano Lett.*, 2009, **9**, 1091-1095.
27. O. Kotova, R. Daly, C. M. G. dos Santos, M. Boese, P. E. Kruger, J. J. Boland and T. Gunnlaugsson, *Angew. Chem. Int. Edit.*, 2012, **51**, 7208-7212.

28. R. M. Capito, H. S. Azevedo, Y. S. Velichko, A. Mata and S. I. Stupp, *Science*, 2008, **319**, 1812-1816.

29. B. A. Grzybowski and G. M. Whitesides, *J. Chem. Phys.*, 2002, **116**, 8571-8577.

30. J. W. Jeong, W. I. Park, L. M. Do, J. H. Park, T. H. Kim, G. Chae and Y. S. Jung, *Adv. Mater.*, 2012, **24**, 3526-3531.

31. R. R. Bao, C. Y. Zhang, Z. L. Wang, X. J. Zhang, X. M. Ou, C. S. Lee, J. S. Jie and X. H. Zhang, *Chem.-Eur. J.*, 2012, **18**, 975-980.

32. A. Huczko, *Appl. Phys. a-Mater.*, 2002, **74**, 617-638.

33. R. Amin, S. Kim, S. H. Park and T. H. Labean, *Nano*, 2009, **4**, 119-139.

34. I. G. Denisov, Y. V. Grinkova, A. A. Lazarides and S. G. Sligar, *J. Am. Chem. Soc.*, 2004, **126**, 3477-3487.

35. E. K. Johnson, D. J. Adams and P. J. Cameron, *J. Am. Chem. Soc.*, 2010, **132**, 5130-5136.

36. C. Y. Zhang, X. J. Zhang, X. H. Zhang, X. M. Ou, W. F. Zhang, J. S. Jie, J. C. Chang, C. S. Lee and S. T. Lee, *Adv. Mater.*, 2009, **21**, 4172-4175.

37. J. Q. Sun, M. Y. Gao and J. Feldmann, *J. Nanosci. Nanotechno.*, 2001, **1**, 133-136.

38. J. R. Kumpfer and S. J. Rowan, *Acs Macro Lett.*, 2012, **1**, 882-887.

39. L. B. Sun, J. R. Li, J. Park and H. C. Zhou, *J. Am. Chem. Soc.*, 2012, **134**, 126-129.

40. J. B. Fan, F. Long, M. P. Aldred, Y. J. Li, Z. W. Liang and M. Q. Zhu, *Macromol. Chem. Phys.*, 2012, **213**, 1499-1508.

41. M. Byun, W. Han, F. Qiu, N. B. Bowden and Z. Q. Lin, *Small*, 2010, **6**, 2250-2255.

42. M. Lescanne, A. Colin, O. Mondain-Monval, K. Heuze, F. Fages and J. L. Pozzo, *Langmuir*, 2002, **18**, 7151-7153.

43. B. D. Wall, S. R. Diegelmann, S. M. Zhang, T. J. Dawidczyk, W. L. Wilson, H. E. Katz, H. Q. Mao and J. D. Tovar, *Adv. Mater.*, 2011, **23**, 5009-5014.

44. M. P. Valignat, O. Theodoly, J. C. Crocker, W. B. Russel and P. M. Chaikin, *P. Natl. Acad. Sci. USA*, 2005, **102**, 4225-4229.

45. M. E. Leunissen, H. R. Vutukuri and A. van Blaaderen, *Adv. Mater.*, 2009, **21**, 3116-3120.

46. M. Yang, C. S. Ozkan and H. Gao, *J. Assoc. Lab. Autom.*, 2003, **8**, 86-89.

47. A. Winkleman, B. D. Gates, L. S. McCarty and G. M. Whitesides, *Adv. Mater.*, 2005, **17**, 1507-1511.

48. I. O. Shklyarevskiy, P. Jonkheijm, P. C. M. Christianen, A. P. H. J. Schenning, A. Del Guerzo, J. P. Desvergne, E. W. Meijer and J. C. Maan, *Langmuir*, 2005, **21**, 2108-2112.

49. S. Sahoo, S. Husale, B. Colwill, T. M. Lu, S. Nayak and P. M. Ajayan, *Acs Nano*, 2009, **3**, 3935-3944.

50. M. Motornov, S. Z. Malynych, D. S. Pippalla, B. Zdyrko, H. Royter, Y. Roiter, M. Kahabka, A. Tokarev, I. Tokarev, E. Zhulina, K. G. Kornev, I. Luzinov and S. Minko, *Nano Lett.*, 2012, **12**, 3814-3820.

51. Y. Sahoo, M. Cheon, S. Wang, H. Luo, E. P. Furlani and P. N. Prasad, *J. Phys. Chem. B*, 2004, **108**, 3380-3383.

52. H. L. Niu, Q. W. Chen, H. F. Zhu, Y. S. Lin and X. Zhang, *J. Mater. Chem.*, 2003, **13**, 1803-1805.

53. A. Shalit, D. E. Lucchetta, V. Piazza, F. Simoni, R. Bizzarri and R. Castagna, *Mater. Lett.*, 2012, **81**, 232-234.

54. L. Jiang and D. Erickson, *Langmuir*, 2011, **27**, 11259-11264.
55. K. C. Gersh, K. E. Edmondson and J. W. Weisel, *J. Thromb. Haemost.*, 2010, **8**, 2826-2828.
56. A. Kureshi, U. Cheema, T. Alekseeva, A. Cambrey and R. Brown, *J. R. Soc. Interface*, 2010, **7**, S707-S716.
57. A. Mata, L. Hsu, R. Capito, C. Aparicio, K. Henrikson and S. I. Stupp, *Soft Matter*, 2009, **5**, 1228-1236.
58. A. Michelman-Ribeiro, R. Nossal, R. Morris, S. Lange, C. S. Kuo and R. Bansil, *Phys. Rev. E*, 2006, **73**, 0114101-10.
59. Z. K. Zhang, P. Pfleiderer, A. B. Schofield, C. Clasen and J. Vermant, *J. Am. Chem. Soc.*, 2011, **133**, 392-395.
60. R. R. Bhat, J. Genzer, B. N. Chaney, H. W. Sugg and A. Liebmann-Vinson, *Nanotechnology*, 2003, **14**, 1145-1152.
61. B. H. Clare, K. Efimenko, D. A. Fischer, J. Genzer and N. L. Abbott, *Chem. Mater.*, 2006, **18**, 2357-2363.
62. B. A. Grzybowski, K. J. M. Bishop, C. J. Campbell, M. Fialkowski and S. K. Smoukov, *Soft Matter*, 2005, **1**, 114-128.
63. Q. Yan, Y. Xin, R. Zhou, Y. Yin and J. Yuan, *Chem. Comm.*, 2011, **47**, 9594-9596.
64. A. Heeres, C. van der Pol, M. C. A. Stuart, A. Friggeri, B. L. Feringa and J. van Esch, *J. Am. Chem. Soc.*, 2003, **125**, 14252-14253.
65. A. Brizard, M. Stuart, K. van Bommel, A. Friggeri, M. de Jong and J. van Esch, *Angew. Chem. Int. Edit.*, 2008, **47**, 2063-2066.
66. C. G. Wolf and E. K. Rideal, *Biochem. J.*, 1922, **16**, 548-555.
67. E. Ruel-Gariepy and J. C. Leroux, *Eur. J. Pharm. Biopharm.*, 2004, **58**, 409-426.
68. A. Totosaus, J. G. Montejano, J. A. Salazar and I. Guerrero, *Int. J. Food Sci. Tech.*, 2002, **37**, 589-601.
69. J. H. van Esch, *Langmuir*, 2009, **25**, 8392-8394.
70. *I. M. Scanning Probe Image Processor (SPIP) v2.000, A/S, Lyngby, Denmark*.
71. Z. L. Wu, D. Sawada, T. Kurokawa, A. Kakugo, W. Yang, H. Furukawa and J. P. Gong, *Macromolecules*, 2011, **44**, 3542-3547.

Summary

Aqueous two-phase systems (ATPS) consist of two immiscible aqueous solutions of incompatible polymers or of one polymer solution and a salt solution. Phase separation occurs in these systems when the polymer concentration exceeds a threshold value. They display a very low interfacial tension; typically less than 0.1 mN/m. The combination of an all-aqueous environment and a low interfacial tension makes these systems ideal for partitioning and separation of biomolecules, such as proteins and enzymes as well as living cells, since they provide the mild conditions that do not denature or destabilize these biomaterials.

In this thesis we pioneered the use of microfluidics to produce all-aqueous microstructures such as "water-in-water" droplets and "water-in-water-in-water" droplets. We enforced the formation of droplets by perturbing an otherwise stable jet that forms at the junction where the two aqueous streams meet using a piezo electric element. Depending on the frequency, monodisperse droplets or droplets with accompanying satellites were produced. Increasing the frequency reduces the number of satellites. In the range 20-50 Hz the jet breaks into monodisperse droplets. Droplets size can be tuned based on flow rates and actuation frequency. We were able to produce droplets between 30 and 60 µm. Droplets outside the chip were not stable, as the collected emulsion phase separate. Rapid on-chip polymerization of dextran derivatives inside the droplets created monodisperse hydrogel particles (chapter 3 and Fig S1).

We observed that perturbation in ATPS threads do not develop according to the Rayleigh-Plateau theory which describes the growth of instabilities of analogous organic-aqueous systems with matched viscosities and interfacial tension (chapter 4). We excluded visco-elastic properties of the fluids as the explanation of that interesting behavior. We suggest that interfacial properties of ATPS are important. The interface of an ATPS is much more complex than the interface between oil and water. We also showed long-time fate of the thread. When, especially without actuation, the breakup time is very long, the thread touches the bottom of the channels which enhances the stability of the thread.

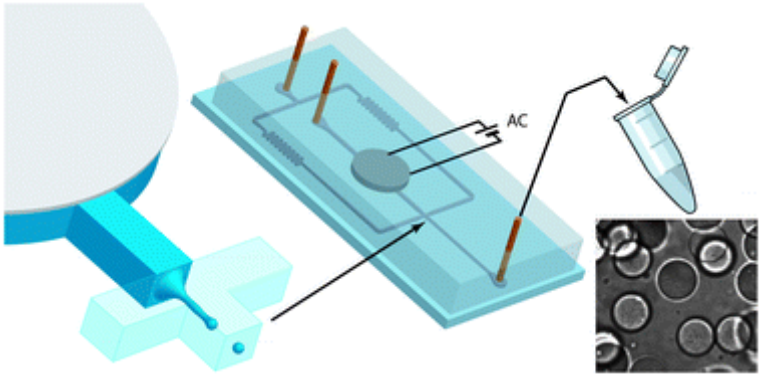

Fig. S1 *Hydrogel microsphere formation from aqueous two-phase droplets.*

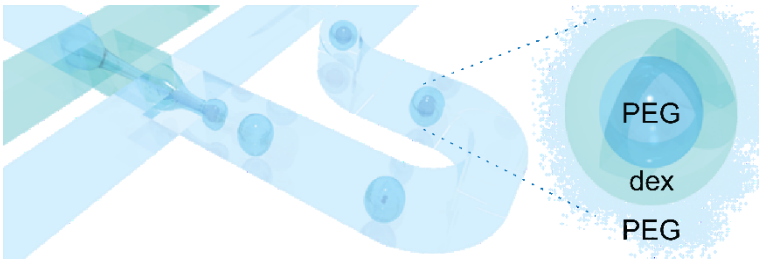

Fig. S2 *All-aqueous core-shell emulsions by microfluidics..*

Monodisperse core-shell droplets can be produced upon suitable actuation frequency and high amplitude of the piezo electric disc. The diameters of the double emulsion drops and shell thickness depend on the actuation frequency and the flow rates (chapter 5). Obviously, these core-shell particles (Fig. S2) were thermodynamically unstable and returned in time to phase separated state. To overcome this issue, we used DEX functionalized with GMA, which, in combination with a photo-initiator, allowed the polymerization of the shell, rendering the obtained core-shell particles stable (Chapter 6).

In the last chapter, we presented a completely different approach of ATPS system. A microfluidic channel was filled with an aqueous solution of dibenzoyl-L-cystine (DBC). A sharp diffusing acidic pH wave is then propagated through the channel. This resulted not only in phase separation of DBC which self-assemble into fibrillar structures but also in inducing directionality to the aforementioned structures. These gel fibers can be grown aligned in different aqueous polymer solution. The medium can then be polymerized and the fibers removed by dipping the formed polymer in a basic solution. This shows further possibilities to use aligned fibers as a template for micro channel creation, since self-assembly process is reversible upon pH change.

The systems presented in this thesis open-up APTS-microfluidic to many fields of research and the development of new medical delivery systems, cosmetics, and low-fat and non-fat products.

Samenvatting

Waterhoudende tweefase systemen (Aqueous Two-Phase Systems ATPS) bestaan uit twee niet mengbare waterige polymeeroplossingen of uit een polymeeroplossing en een zoutoplossing, die faseschеiden wanneer de concentratie van het polymeer een specifieke drempelwaarde overschrijdt. Zij vertonen een zeer lage grensvlakspanning die typisch kleiner is dan 0.1 mN/m. De combinatie van een geheel waterhoudende omgeving en een lage grensvlakspanning maakt dat deze systemen ideaal zijn voor deling en scheiding van biomoleculen, zoals proteïnen en enzymen, maar ook levende cellen, omdat deze biomaterialen niet denatureren of destabiliseren bij deze condities.

In dit proefschrift verkennen we het gebruik van microfluidische chips voor de creatie van volledig water gebaseerde structuren, zoals “water-in-water” druppels en zelfs “water-in-water-in-water” druppels. We forceren de formatie van “water-in-water” druppels door een anders stabiele vloeistofdraad, die ontstaat op de plaats waar de twee waterstromen samenkomen, te verstoren door middel van een piëzo-electrisch element. Afhankelijk van de frequentie worden monodisperse druppels of druppels met satellietdruppels gevormd. Toename van de frequentie vermindert het aantal satellieten. In het bereik van 20-50 Hz breekt de stroom op in monodisperse druppels. De diameter van de druppels wordt bepaald door de stroomsnelheid en ingestelde frequentie. Wij zijn in staat druppels te produceren met een diameter tussen 30 en 60 µm. Druppels buiten de chip zijn niet stabiel. Door gebruik te maken van dextraan derivaten kunnen de druppels gepolymeriseerd worden tijdens hun reis door de chip om zo monodisperse hydrogel deeltjes te produceren (hoofdstuk 3 en Fig S1).

Wij hebben waargenomen dat verstoring op het oppervlak van ATPS jets zich niet ontwikkelen volgens de welbekende Rayleigh-Plateau theorie welke de groei beschrijft van de instabiliteit van analoge organisch-waterige systemen met overeenkomende viscositeit en grensvlakspanning (hoofdstuk 4). Wij sluiten de visco-elastische eigenschappen van de vloeistoffen uit als de verklaring van dit interessante gedrag. Wij stellen dat de

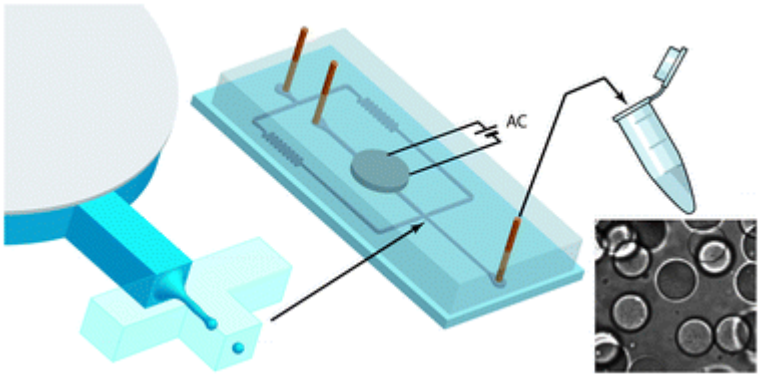

Fig. S1 *Hydrogel microsfeer formatie van water-in-water droppels*

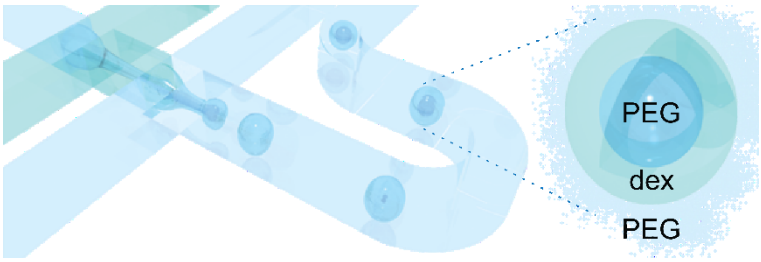

Fig. S2 *Totaal water kern-schil emulsies door een microfluid.*

eigenschappen van het ATPS grensvlak, dat veel complexer is dan het grensvlak tussen olie en water, hierbij een belangrijke rol spelen. Wij laten ook het lange termijn gedrag van de jets zien. Wanneer, in het bijzonder zonder activering, de opbreektijd erg lang is, zinkt de draad naar de bodem van het kanaal, waardoor de draad stabieler wordt.

Monodisperse “core-shell” druppels kunnen worden geproduceerd met een geschikte activeringsfrequentie en hoge amplitude van het piëzo-electrische element. De diameter van de kern en de dikte van de schil hangen af van de activeringsfrequentie en de stroomsnelheden (hoofdstuk 5). Deze “core-shell” deeltjes zijn duidelijk thermodynamisch onstabiel en keren na verloop van tijd terug naar de toestand van faseschеiding. Stabilisering van deze deeltjes was bewerkstelligd door gebruik te maken van een photoinitiator in combinatie met dextraan dat gefunctionaliseerd is met GMA. Blootstelling van deze deeltjes aan UV licht terwijl ze door de chip heen stromen resulteerde in deeltjes met een gepolymeriseerde schil en een vloeibare PEG kern (hoofdstuk 6).
In het laatste hoofdstuk presenteren wij een compleet andere benadering van een ATPS systeem. Een microfluidisch kanaal wordt gevuld met een oplossing in water van dibenzoyl-L-cystine (DBC). Een scherpe diffuse zuur pH golf wordt dan verspreid door het kanaal. Dit resulteert niet alleen in faseschеiding van DBC die bij elkaar komt in gevezelde structuren, maar ook in het induceren van het richten van de hiervoor genoemde structuren. Deze gel vezels kunnen gericht aangroeien in verschillende water-polymeer oplossingen. Het medium kan dan worden gepolymeriseerd en de vezels worden verwijderd door het dopen van het gevormde polymeer in een basische oplossing. Dit laat de verdere mogelijkheden zien om de gerichte vezels te gebruiken als een model voor microkanaal creatie, daar een self-assembly proces omkeerbaar is in pH verandering.

De systemen gepresenteerd in dit proefschrift openen de weg naar het gebruik van volledige water gebaseerde microstructuren in veel verschillende onderzoeksgebieden en maken onder meer de ontwikkeling mogelijk van nieuwe medische afgiftesystemen, cosmetica en vetvrije voedingsproducten.

Acknowledgements

Doing PhD is not only performing high quality research, having fun with creating or exploring unknown areas but it is also a period during which personality of the researcher is built up. I wish to thank all the people who made my PhD journey an important step in my life.

I would like to start by acknowledging the people who had the biggest influence on my research project:

●My promoter Jan van Esch who believed I will be a good material for a doctor and offered me the possibility to join his group. Without his critical and demanding judgment of my research this thesis would not be of such good quality, would not look like how it is now and I would not be as proud of it as I am now. We sometimes had different point of view about which direction my research should take, where it should go, but he gave me the scientific freedom for which I am extremely grateful, because this is the way of creating independent researcher, which is a goal for PhD studies.

● My promoter Michiel Kreutzer for his extremely big enthusiasm in my research and his support in engineering which was for me an attractive but unexplored area. I am grateful that he opened the door of his lab for me and for giving me the motivation to not give up during hard times.

● My copromoter Volkert van Steijn for the great support which I got from him, for all these years with never ending patience. I would like to thank him for all the time he found for helping me and for the nice pictures which found place on Lab Chip cover and cover of this thesis.

● Ger Koper for valuable help in my thesis. I have been fortunate to receive tips and inspiration from him and time for discussions on scientific and non-scientific related topics.

● Alexandre Olive for the great interest in my research and his support with my latest experiments and papers and for the corrections of this thesis.

I would like to thank the doctoral committee for accepting to review my work. I hope he found this research as much interesting as I did.

I should not omit acknowledging all co-authors of my publications. Today's research including this one, would not be possible without cross-boundary cooperation with such great professionals as them. Words of special appreciation go to the all TUD technical staff, especially to Piet Droppert and Ben Norder for technical support I was getting during all my PhD. Particular thanks go to my officemates. I got a pleasure to be always in the office with them, at their last months in the group. I am sure that looking at their stress in the last period when they were completing papers and thesis was a great motivation for me to work efficiently every year of my PhD journey such as I could prevent big stress in the last year. I would like to thank SAS, PPE, NOC, BOC and other TUD group members who made my PhD life less terrible, either by scientific discussions or non-scientific discussions, inside and outside working hours! I hope our contact will last! I would like to thank my Polish friends I met during my time in the Netherlands. It was a pleasure to get to know them. Finally I would like to thank my family members and nearest friends. Thank you for believing in me and support! I realize that many of you read this chapter hoping to find their name and some personal note associated with it. Definitely, they all deserve it! However they must be satisfied with what they have just read. I promise to thank them personally, when we meet each other next time!

About the Author

Iwona Ziemecka was born on November the 12th, 1984 in Łódź (Poland). She obtained her secondary school diploma in 2003 at the I LO im. M. Kopernika in Łódź (Top 3 Secondary School in Poland that period). Between 2003 and 2008 she studied at the University of Łódź (UL). From the first year of Interdisciplinary Science Studies, she followed an individual program under supervision of Prof. G. Mlostoń during which she did full program of chemistry enriched of courses in field of: genetics, microbiology, biotechnology and cell biology. In the third year of her study (2005-2006) she gained her first international research experience and studied at Rijksuniversiteit Groningen (The Netherlands) at the Faculty of Biology and the Faculty of Chemistry as Erasmus-Socrates fellow. She spent seven months in the group of Prof. Cees Hummelen (Chemistry of (Bio)organic Materials and Devices - Stratingh Institute for Chemistry). Her M.Sc. project was done at the Polish Academy of Science as a collaboration with the University of Łódź under supervision of Prof. G. Mlostoń and Prof L. Woźniak. She obtained her M.Sc. degree in Chemistry with honors (summa cum laude equivalent) in 2008. During her studies Iwona Ziemecka got one scholarship (2005) two scholarships from the Minister of Sport and Education (2005, 2006) and one scholarship from the Rector of the UL (2007).

She was vice-president of Scientific Biotechnology-Microbiological Students Association UL (2004-2005) and Member of Self Government of Chemistry Students of UL (2007-2008).

After M.Sc. Iwona started her Ph.D. with Prof. Jan van Esch at Delft University of Technology in the Self-Assembling Systems group, funded by a NWO-VICI grant. During her Ph.D. Iwona collaborated extensively with the Product and Process Engineering group of Prof. Michiel Kreutzer.

List of publications

[1] **I. Ziemecka**, V. van Steijn, G. J. M. Koper, M. Rosso, A. M. Brizard, J. H. van Esch and M. T. Kreutzer, Monodisperse hydrogel microspheres by forced droplet formation in aqueous two-phase systems, *Lab on a Chip*, 2011, 11, 620-624 (IF = 6,3) [Front cover]

[2] **I. Ziemecka**, V. van Steijn, G. J. M. Koper, M. T. Kreutzer and J. H. van Esch, All-aqueous core-shell droplets produced in a microfluidic device, *Soft Matter*, 2011, 7, 9878-9880 (IF=4,4) [Top 10 most read Soft Matter paper Sept. 2011]

[3] **I. Ziemecka,** S. D. Geschiere (co-first author), V. van Steijn, G. J. M. Koper, J. H. van Esch and M. T. Kreutzer, Slow Growth of the Rayleigh-Plateau Instability in Aqueous Two Phase Systems, *Biomicrofluidics*, 2012, 6, 022007 (IF=3,9)

[4] **I. Ziemecka**, G. J. M. Koper, A. G. L. Olive and J. H. van Esch, Chemical-Gradient Directed Self-Assembly of Hydrogel Fibers, *Soft Matter*, 2013, 9, 1556-1561 (IF=4,4)

[5] **I. Ziemecka**, A. G. L. Olive , V. van Steijn, M. T. Kreutzer and J. H. van Esch,Stable particles composed of a permeable hydrogel shell and a liquid core produced by all-aqueous microfluidics, in preparation

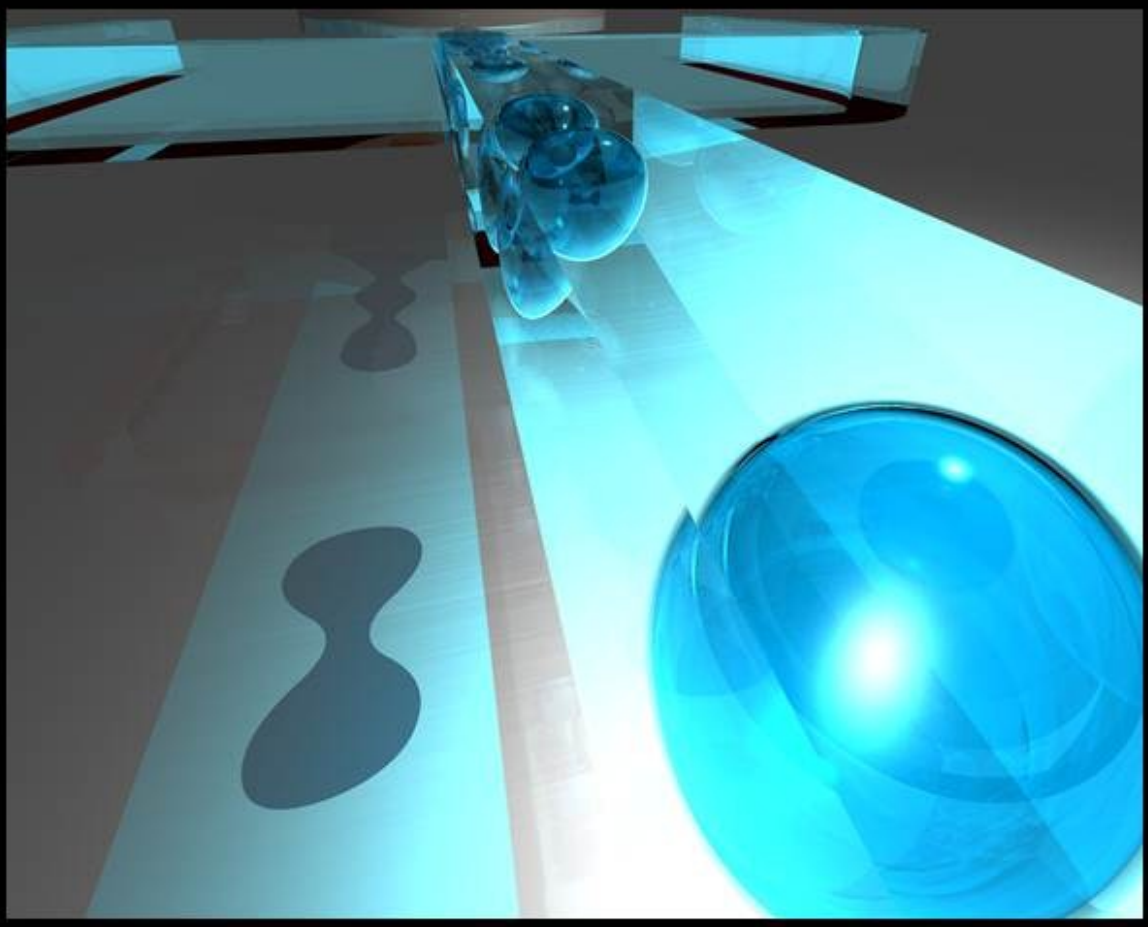

ISBN: 978-94-6191-593-1